



Martin, Benjamin Thomas (2019) *Predictive Fluvial Facies Models: Huesca Distributive Fluvial System, Spain*. MSc(R) thesis.

<http://theses.gla.ac.uk/76789/>

Copyright and moral rights for this work are retained by the author

A copy can be downloaded for personal non-commercial research or study, without prior permission or charge

This work cannot be reproduced or quoted extensively from without first obtaining permission in writing from the author

The content must not be changed in any way or sold commercially in any format or medium without the formal permission of the author

When referring to this work, full bibliographic details including the author, title, awarding institution and date of the thesis must be given

Enlighten: Theses

<https://theses.gla.ac.uk/>
research-enlighten@glasgow.ac.uk



PREDICTIVE FLUVIAL FACIES MODELS: HUESCA DISTRIBUTIVE FLUVIAL SYSTEM, SPAIN

Ben Martin

Supervisors: Dr. Amanda Owen & Dr. Richard
Williams

Submitted in fulfilment of the requirements of the
Degree of MSc by Research

School of Geographical and Earth Sciences,
University of Glasgow

SUBMITTED:22/09/2019

Abstract

Recent research of modern aggradational continental sedimentary basins has highlighted that sedimentation is dominated by distributive fluvial systems (DFSs). Only one outcrop-based, fully quantified rock record example is currently available within literature (Salt Wash Member of The Jurassic Morrison Formation) which highlights expected trends within conceptual DFS models. This study based on the Oligocene-Miocene Huesca Fluvial System within the Ebro Basin, northern Spain aims to characterise facies across the system, analyse predicted trends using a conceptual DFS model and determine whether these expected trends are scalable across both system and basin-scale studies. The results of this study will be compared with other DFS studies, namely with the Late Jurassic Salt Wash. Proximal-to-distal trends show that channel thicknesses across the system decrease from 20.2 m to 0.4 m alongside channel percentage decreases from 66% at the most proximal region to 4% in the most distal locality. Storey thicknesses also decrease downstream from 11.4 m proximally to 0.4 m in the most distal locality with storey frequency at a maximum of 4 in the proximal region. Downstream shifts in architecture are also noted across the system from massive, highly amalgamated channel-body sandstones dominating the proximal regions to isolated or offset-stacked, lesser amalgamated channel-body dominating distal region. This data compares well with that of the Salt Wash study which is directly comparable despite differences in the size of these systems. This study provides quantified data for an ancient DFS on a system scale that is directly comparable with other quantified DFSs from both previous and future works, regardless of scale. The data from this study will also aid resource exploration in the future alongside help to create a more accurate, quantified, conceptual DFS model.

Contents

List of tables	7
List of Figures	7
List of accompanying material preface	11
Acknowledgement.....	11
Chapter 1	13
1.0) Introduction.....	13
1.2) DFS Concept.....	13
1.4) Huesca DFS.....	15
1.5) Research Methods	18
1.5.1) Lidar	19
1.5.2) Drone	19
1.5.3) Fieldwork	20
Chapter 2.....	22
2.0) Facies Descriptions.....	22
2.1) Facies Overview	23
2.1.1) Sg	23
2.1.2) Sm Facies	24
2.1.3) Sx Facies.....	27

2.1.4) Sr Facies	29
2.1.5) Sh Facies	30
2.1.6) Mm Facies.....	32
2.1.7) Mh Facies.....	33
2.1.8) Mp Facies.....	34
2.2) Facies Geometries	36
2.2.1) Sm Bed Geometry	36
2.2.2) Sx Bed Geometry.....	36
2.2.3) Sr Bed Geometry	36
2.2.4) Sh Bed Geometry	36
2.2.5) Mm and Mh Bed Geometry	36
2.2.6) Mp Bed Geometry.....	37
2.3) Facies Associations	37
2.3.1) Channel Facies Associations.....	37
2.3.2) Floodplain Facies Associations	41
2.4) Sandstone body architecture.....	42
2.4A) Massive Channel Body Geometry	43
2.4B) Semi-Amalgamated Channel Body Geometry	45
2.4C) Internally-Amalgamated Channel Body Geometry.....	47

2.4D) Offset-Stacking Channel Body Geometry.....	49
2.4E) Isolated Channel Geometry (I)	51
2.5) Summary	52
Chapter 3.....	53
3.0) Vertical Trend Analyses	53
3.1A) Overview	54
3.2 Discussion.....	56
3.2A) Weighted Grain Size Analysis	57
3.2B) Paleocurrent Analyses.....	60
3.2C) Channel-body Percentages	61
3.2D) Channel-body thickness trends.....	63
3.3 Architecture Panels	65
3.3A) Pertusa	66
3.3B) Monzon.....	67
3.3C) Piraces	68
3.3D) Torrollon.....	69
3.3E) Castleflorite.....	70
3.3F) Monte Aragon	71
3.3G) Bolea	72

3.4) Summary	72
Chapter 4.....	73
4.0) Lateral Variation within Outcrops.....	73
4.1A) Pertusa.....	74
4.1B) Piraces.....	75
4.1C) Torrollon.....	78
4.1D) Bolea – 7 Logs.....	82
4.1E) Sigena - 14 Logs.....	83
4.2) Discussion – Channel Percentage.....	84
4.2B) Storey Thickness.....	87
4.3) Summary.....	88
Chapter 5.....	91
5.0) Discussion: Summary.....	91
5.1A) Apex location.....	93
5.1B) Spatial Trend Analyses.....	94
5.1C) Basin margin localities.....	95
5.2) Case Study Comparison: Salt Wash DFS.....	96
5.3) Implications.....	102
6.0 Conclusions.....	103

References.....	104
Accompanying Material.....	119

List of tables

Table 1: Sandstone Facies Geometry Percentages.....	35
Table 2: Mudstone Facies Geometry Percentages.....	37
Table 3: Pseudo-log average channel percentage comparison with field log data.....	85
Table 4: Pseudo-log average channel thickness comparison with field log data.....	86
Table 5: Pseudo-log average storey thickness comparison with field log data.....	87

List of Figures

Figure. 1: Google maps image showing the extent of the Huesca DFS in relation to the Ebro Basin and its position within Spain.....	15
Figure. 2: Location map of the Huesca DFS and the adjacent Luna DFS.....	16
Figure. 3: A brief stratigraphic column containing the relevant lithology.....	18
Figure. 4: Location map of all localities studied.....	21
Figure. 5: Bedform stability diagram after Southard & Boguchwal (1990).....	22
Figure. 6: Erosive gravel lags observed within channel sandstones.....	23
Figure. 7: Massive sandstone facies within channel sandstones.....	26
Figure. 8: Burrowing and bioturbation within channel sandstones.....	27
Figure. 9: Cross-bedding and cross-sets observed within channel sandstones.....	27
Figure. 10: Fully preserved, uni-directional current ripple within a splay deposit.....	29
Figure. 11: Horizontal laminations within channel sandstones.....	30

Figure. 12: Massive mudstone facies within floodplain deposits.....	32
Figure. 13: Horizontal laminations within floodplain deposits.....	33
Figure. 14: Palaeosol deposits within floodplain sequence.....	34
Figure. 15: Lateral accretion packages observed whilst logging.....	38
Figure. 16: Channel plug and lateral accretions providing full channel depth observed whilst logging.....	40
Figure. 17: Compensationally stacked splay sheets observed whilst logging.....	41
Figure. 18: Massive channel body geometries observed within the Pertusa outcrop.....	44
Figure. 19: Semi-amalgamated channel body geometry observed within the Monzon outcrop.....	46
Figure. 20: Internally-amalgamated channel body geometry observed within the Torrollon outcrop.....	48
Figure. 21: Offset-stacked channel body geometries observed at Tramaced.....	50
Figure. 22: Isolated channel body geometry observed at the Bolea outcrop.....	51
Figure. 23: Comparison between the Hirst apex and the suggested apex position of Naval using elevation data.....	53
Figure. 24: Moving average plots showing channel body thickness vs log height with individual channel bodies indicated.....	55
Figure. 25: Grain size comparison with distance from suggested apex.....	58
Figure. 26: Location map of all logged locations including channel body thickness data.....	59
Figure 27: Location map of all logged locations showing paleocurrent data.....	60

Figure. 28: Channel body percentage comparison with distance from suggested apex.....	61
Figure. 29: Estimated temporal groupings of successions plotting elevation data against the distance from the estimated apex.....	62
Figure. 30: Average channel body thickness data taken from field logs.....	64
Figure. 31: Channel body thickness variations downstream.....	64
Figure. 32: Storey thickness variations downstream.....	64
Figure. 33: Channel body geometry scheme of Owen et al. (2015).....	65
Figure. 34: Pertusa outcrop panel including channel body geometry indication.....	66
Figure. 35: Monzon outcrop panel including channel body geometry indication.....	67
Figure. 36: Piraces outcrop panel including channel body geometry indication.....	68
Figure. 37: Torrollon outcrop panel including channel body geometry indication.....	69
Figure. 38: Castleflorite outcrop panel including channel body geometry indication.....	70
Figure. 39: Monte Aragon outcrop panel including channel body geometry indication.....	71
Figure. 40: Bolea outcrop panel including channel body geometry indication.....	72
Figure. 41: Location map detailing the amount of pseudo-logs taken at each location where digital outcrop data was available.....	73
Figure. 42: Pertusa pseudo-log channel body thickness distribution and storey proportions.....	74
Figure. 43: Piraces pseudo-log channel percentage and channel thickness distribution.....	76

Figure. 44: Piraces pseudo-log storey proportion and storey thickness distribution.....	76
Figure. 45: Piraces pseudo-log fence panel detailing channel body and floodplain interaction.....	77
Figure. 46: Bird's eye view schematic of the Piraces outcrop and where pseudo-logs were taken.....	77
Figure. 47: Torrollon pseudo-log channel percentage distribution and channel thickness distribution.....	79
Figure. 48: Torrollon pseudo-log storey proportion and storey thickness distribution.....	79
Figure. 49: Torrollon pseudo-log fence panel detailing channel body and floodplain interaction alongside a bird's eye view schematic of the outcrop and where pseudo-logs were taken.....	81
Figure. 50: 3D screen-grab of the Bolea outcrop within the LIME VOG software and where logs were taken.....	82
Figure. 51: Bolea pseudo-log channel body thickness distribution.....	83
Figure. 52: Sigena pseudo-log channel body thickness and storey distribution.....	83
Figure. 53: Pseudo-log channel percentage data plotted against field data.....	84
Figure. 54: Pseudo-log channel thickness data plotted against field data.....	86
Figure. 55: Pseudo-log storey thickness data comparison downstream.....	87
Figure. 56: Location map detailing the difference between the estimated apex positions of this paper and of Hirst (1991).....	93
Figure. 57: Grain size data comparison between the Salt Wash and Huesca DFS localities with distance downstream as a percentage.....	99

Figure. 58: Channel percentage comparison between the Salt Wash and Huesca DFS localities with distance downstream as a percentage.....99

Figure. 59: Average channel body thickness comparison between the Salt Wash and Huesca DFS localities with distance downstream as a percentage.....99

Figure. 60: Schematic diagram of proposed depositional model for the Huseca DFS.....101

List of accompanying material preface

Pertusa Field Log.....119

Monzon Field Log.....120

Piraces Field Log.....121

Torrollon Field Log.....122

Castle Florite Field Log.....123

Monte Aragon Field Log.....124

Bolea Field Log.....125

Acknowledgement

First and foremost, I would like to thank my supervisor Dr. Amanda Owen for all of her support, patience and advice throughout this project alongside her company on one of the most memorable field trips I have ever undertaken. I would also like to thank Dr Richard Williams and the University of Glasgow's support through the Stressed Environments grant, alongside allowing me to study from afar. I would like to thank my family for their unfaltering support over the past year and a half, I could not have done it without them. Finally, to my partner who was there start to finish and has been a constant driving force in helping me achieve my goals over the past 18 months.

Declaration

“I declare that, except where explicit reference is made to the contribution of others, that this dissertation is the result of my own work and has not been submitted for any other degree at the University of Glasgow or any other institution.”

Printed Name: _____

Signature: _____

Chapter 1

1.0) Introduction

A global remote-sensing study on over 700 modern aggrading continental sedimentary basins has shown that fluvial sedimentation patterns in continental basins are dominated by distributive fluvial systems (DFS) (Weissman et al. 2010, 2011; Hartley et al., 2010). Distributive fluvial systems have been noted in both the modern and ancient (Owen et al., 2015). Key modern examples include the Okavango DFS (Stanistreet and McCarthy, 1993); the Taquari DFS, Brazil (Assine, 2005; Buehler et al., 2011); Buyunda DFS, Siberia (Weissman et al., 2010); alongside systems in the Andean foreland basin (Weissman et al., 2010). Ancient examples include the Devonian systems of Greenland and Ireland (Kelly & Olsen, 1993) through to the Late Jurassic Salt Wash Member of the Morrison formation (Craig et al., 1955; Mullens & Freeman, 1957; Owen et al., 2015, 2017a, 2017b) and the focus of this study, the Oligocene-Miocene deposits of the Huesca DFS. Although without controversy (e.g. Sambrook-Smith et al., 2010; Fielding et al., 2012), and debate ensues as to whether alluvial fans should be treated differently to DFS (see Ventra and Clarke, 2018 for discussion) the terminology and concept has been widely accepted (Ventra and Clarke, 2018).

1.2) DFS Concept

The distributive fluvial system (DFS) concept has been discussed in previous works (Hirst, 1991; Nichols & Fisher, 2007; Weissman et al., 2010; Hartley et al., 2010; Owen et al. 2015; Owen et al. 2017a/b). DFSs form within sedimentary basins where confined, terminal systems become unconfined and disperse across a basin floor (Nichols & Fisher, 2007; Hartley et al., 2010). They are characterized by a radial distribution of channels through avulsion and/or bifurcation of both singular and/or coevally active channels (Hartley, 2010). DFS exhibit systematic downstream trends such as decreasing sandstone:mudstone ratios; grain size and channel width:depth ratios with increasing distance from the system apex (Hirst, 1991; Nichols and Hirst, 2007). DFS profiles are characteristically concave-upwards downstream and convex-upwards laterally across the system thought to relate to compensational stacking of fluvial-depositional lobes (Mackay & Bridge, 1995; Straub et al., 2009; Huerta et al., 2011). The above trends have been noted in both modern systems and ancient analogues (Hirst, 1991; Nichols & Fisher, 2007; Cain & Mountney, 2009; Weissman et al., 2010; Hartley et al., 2010; Weissman et al., 2013).

At current, very few DFSs have been extensively examined in the geologic record, though examples include the Salt Wash DFS (Owen et al., 2015; Owen et al., 2017); the Organ Rock Formation, Paradox basin (Cain and Mountney, 2009); the Luna and Huesca DFSs (Hirst and Nichols, 1986; Hirst, 1991; Hamer et al., 2007; Nichols, 2017). Only one fully quantified study of a DFS exists (Owen et al., 2015; Owen et al., 2017b) alongside the partially quantified study of Hirst (1991). Quantified studies should be considered as studies that have collected, compiled and presented quantified measurements of: net:gross; channel body thickness; storey thicknesses; storey frequency and grain-size data. Partially quantified studies may contain some of this data however findings may be predominantly described rather than using quantified data.

The recent studies of Weissman et al. (2010) and Hartley et al. (2010) indicate that DFSs dominate continental sedimentary basins worldwide in a range of climatic and tectonic settings, the largest of which are found within foreland basins under tropical; sub-tropical and dryland climatic conditions (Hartley et al., 2010; Weissman et al., 2010). Distributive fluvial systems typically have high preservation potential within the geologic record due to their commonly aggradational/progradational properties (Weissman et al., 2010; Hartley et al., 2010; Nichols, 2017) in comparison with tributary systems that experience degradation with brief aggradational phases which become preserved that facies models are typically based on (Bristow et al., 1999; Weissman et al., 2010). The dominance of DFSs throughout the continental record means we must seek to further develop quantified DFS models if we are to understand how they behave in the modern. Many DFS can contain a wealth of resources in the form of oil and gas (Moscariello, 2005; Kukulski et al., 2013); mineral deposits (Peterson, 1977; Turner-Peterson, 1986) and aquifers (Weissman et al., 1999, 2002, 2004). Currently, outcrop analogues are being used to aid sub-surface exploration and to understand the distribution and connectivity of reservoir bodies, however studied analogues rarely provide quantitative data. Through quantification of DFS within the rock record, we may begin to construct predictive facies models that can be applied to sub-surface deposits, aiding exploration, alongside improving our understanding of modern DFS such as the Okavango (Stanistreet & McCarthy, 1993). This project aims to build on the prior work of Hirst (1991) through the use of adapted facies schemes (Miall, 1985) and sandstone body classification schemes (Owen et al., 2017) to fully quantify the Huesca DFS. Very few studies have taken a quantitative approach in assessing and providing extensive numerical information on: spatial (downstream), temporal (vertical) and lateral (depositional strike)

variations within a single DFS, such has been done on a portion of the Sunnyside fluvial system by Wang and Plink-Björklund (2019).

1.3) Study Aims

1. Provide quantitative facies analysis of the Oligocene-Miocene Huesca DFS measuring: net:gross; channel body thicknesses and geometries; storey thicknesses and occurrence frequency.
2. Document proximal-distal changes in facies associations alongside net:gross, channel and storey thicknesses. Lateral changes across the system will also be documented to improve conceptual DFS models using quantitative data.
3. Identify and construct a quantified facies model for distributive fluvial systems and compare results with those of the Late Jurassic Salt Wash DFS study (Owen et al., 2015).

1.4) Huesca DFS

The Oligocene-Miocene Huesca Fluvial System resides within the Ebro basin, Spain, which covers 45,000km² on the Iberian Peninsula and sat at 37°N, 3° below its current position (Puidegáfabregas et al., 1992; Van der Voo, 1993; Barberá et al., 2001). The basin formed through flexural subsidence that began during the Paleocene as a result of shortening within the Pyrenean orogenic belt in the North.

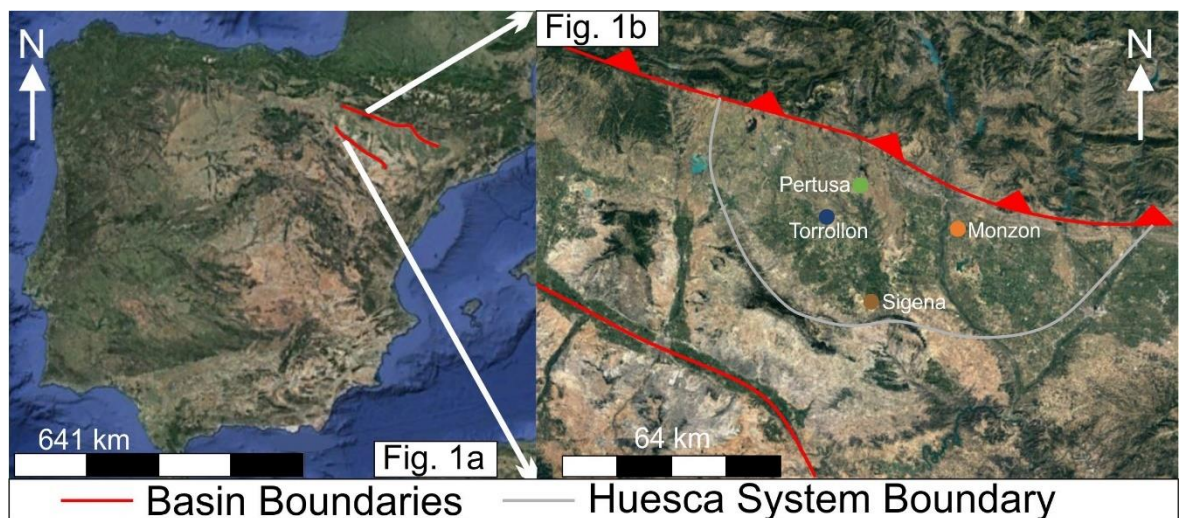


Figure 1: Location map showing the position of the Ebro basin within Spain. Figure. 1b details the position of the Huesca system within the Ebro Basin with some key localities shown.

The emergence of the External Sierras to create the Northern basin margin was a result of movement on the Guarga thrust (Nichols & Hirst, 1998; Nichols, 2004; Hamer et al., 2007). It is believed that the stacking of thrusts along the southern Pyrenean margin also resulted in the differential subsidence rates experienced within the basin (Nichols, 1987). Later convergence of the Iberian and European plates in the Late Eocene tied with tectonic shortening shut down the connection to the Atlantic Ocean until the Late Miocene (García-Castellanos et al., 2003). Meanwhile, the emergence of the Catalan Coastal Range blocked connection to the Mediterranean. Therefore during this period, the basin was endorheic and disconnected to the sea allowing for no influence from eustatic sea level change (ultimate base level) (Riba et al., 1983; Coney et al., 1996; Hamer et al., 2007). Over time, the depositional basin floor rose above ultimate base-level through continued accumulation of sediments with an approximated 2000m of sediment deposited proximal to the thrust belt and roughly 800m within the basin centre (Coney et al., 1996). Whilst the tectonic setting of the system is relatively well understood, there has been debate around the climatic conditions experienced within the basin (Nichols & Hirst, 1998; Hirst, 1991; García-Castellanos et al., 2003; Hamer et al. 2007). The modern basin experiences a dry, semi-arid climate with low annual rainfall, around 300mm/yr (Hamer et al., 2007). Early studies suggested that the basin experienced a semi-arid climate however palaeosol studies have suggested a shift from a warm and dry climate in the Early Oligocene to a humid, seasonal climate in the Late Miocene with micromammal assemblages suggesting a humid, seasonal environment in the Late Oligocene-Miocene (Álvarez Sierra et al., 1990; Cavagnetto & Anadón, 1996; Alonso-Zarza & Calvo, 2000; Hamer et al. 2007). The above data is further supported by a paleo-

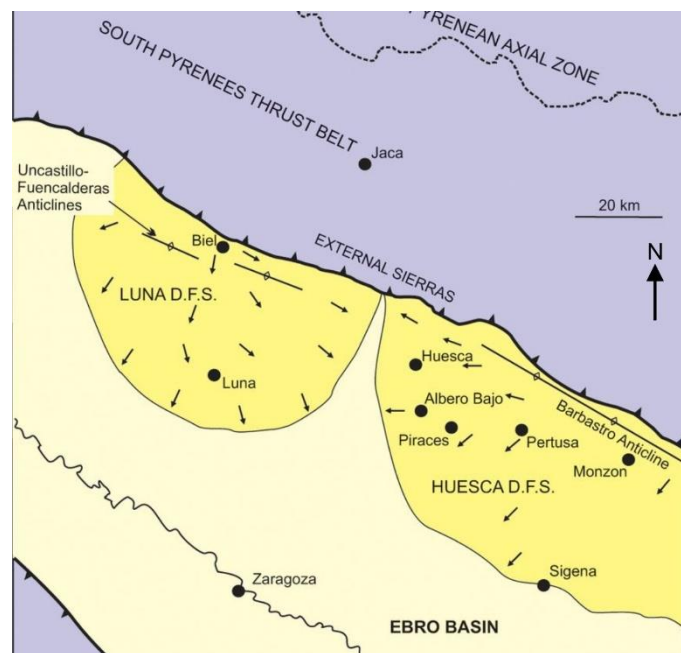


Figure 2. Location map of the Huesca DFS and the adjacent Luna DFS (Fisher & Nichols, 2013).

reconstruction of the system which suggests a mosaic of open woodland consisting of shrubs and small trees in the distal areas whilst a general lack of palaeosols across the system suggests paleoprecipitation in excess of 500mm/yr. Temperatures ranged between 10-14°C ±4°C with annual precipitation ranging between 450-830 mm ±200 mm, much wetter than present day (Hamer et al. 2007). Stable isotope analysis of lacustrine sediments from the central basin lake recorded a slight decrease in aridity during the Early Miocene, further suggesting that initial interpretations of a semi-arid environment may have been incorrect (Hirst, 1991; Arena & Pardo, 2000; García-Castellanos et al., 2003; Hamer et al., 2007).

Two major fluvial systems prograded into the Ebro basin, forming fan-shaped, terminal systems that transitioned distally towards ephemeral lacustrine environments (Hirst & Nichols, 1986). The Huesca Distributary System is the focus of this study (Hirst & Nichols, 1986; Hamer et al, 2007, Nichols, 2017). The Huesca system has been interpreted as a fan-shaped fluvial system with a radius of 60 km and South/South-Westerly radial distribution of paleocurrents (Hirst, 1991). Deposits are composed of the Sarinena Fm. fluvial channel sandstones and their associated fine-grained floodplain facies. Facies changes occur both laterally and proximal-distally with localised variations common across the system (Hirst, 1991). Jupp et al., (1987) used a model based on the von Mises distribution of paleocurrent data to estimate the apex location in the Huesca, however, due to deformation resulting from the formation of the Eocene, gypsum-cored Barbastro anticline (Hirst, 1991), no apex could accurately be identified, it is however believed to be located to the North of the current basin margin. Hirst (1991) suggested that input may have been from multiple sources which is supported by the works of Reynolds (1989) whereby several potential feeder paleovalleys were identified using paleocurrent data.

The termination of this system appears to be well understood as a switching fluvial/alluvial-lacustrine environment identified within the palaeosol study of Hamer et al. (2007) and facies analysis that highlights interfingering of lacustrine deposits with distal deposits (Nichols, 1987; Hirst, 1991; Nichols & Hirst, 1998; Hamer et al, 2007; Nichols & Fisher, 2007; Nichols, 2017). A low-relief lacustrine delta formed as distal channels terminated in a central lake during periods of lake highstand (Nichols & Fisher, 2007). The interfingering of lacustrine and distal fluvial deposits is interpreted as seasonal alternations of lake level due to climatic changes, resulting in net evaporation higher than input (Nichols & Fisher, 2007). Gypsum and carbonates present within the central areas of the basin supports this inference suggesting periodic drying out of the lake (Nichols, 1987; Arenas & Pardo, 1999).

Quaternary Deposits		
Lower Miocene/ Upper Oligocene	Uncastillo/ Sarinena Fm. Fluvial and alluvial-fan deposits (N Basin)	Alcubierre/ Zaragoza Fm. Lacustrine and alluvial-plain deposits (Central Basin)
Lower Oligocene/ Upper Eocene	Campodarbe Group Fluvial and lacustrine deposits of the Jaca Basin (Ebro Basin Subsurface)	

Figure 3: Brief stratigraphic column detailing underlying deposits within the study area (Nichols & Hirst, 1998)

At current, multiple outcrops span proximally-distally across the system with good exposure. The collection of data will consist of sedimentary logs collected via field work and digital outcrop panels. Logs will include thickness, grain-size and net:gross data whilst documenting sedimentary structures, facies associations and channel geometries.

1.5) Research Methods

Data collection for the project was undertaken using both 3D virtual outcrop data provided by the SAFARI consortium and using the LIME VOG software provided by the University of Bergen to analyse, alongside a later 9-day field excursion to the Huesca DFS. Initial data sourced from the SAFARI consortium was collected using both LIDAR scans and drone-capture images. The use of the LIME VOG software package and the datasets provided by the SAFARI consortium allowed for the creation of digital pseudo-logs before fieldwork could take place which aided in assessing sites of interest prior to the field research. This software also aided the creation of a vast digital dataset rapidly which allowed for field research to be carried out efficiently and to be complimented by digital data.

1.5.1) Lidar

Two LIDAR models were used within the preliminary study: the locations of Pertusa and Piraces. LIDAR was developed in the 1960s however only recently began use within the field of sedimentology (Calvo et al., 2015). LIDAR allows for photorealistic 3D data visualisation and avoids using a point cloud mesh which prevents the creation of extra “false” geometries (Kreylos et al., 2013). The technology fires laser pulses and records two-way-travel time, signal intensity and the distance travelled which creates point clouds. These point clouds are then textured with high resolution images, merged in a singular point cloud to later be georeferenced. At current, the collected models provide high-resolution data with the majority of the outcrop, however the lower reaches of Piraces or where overhangs exist at Pertusa, data is often poor or missing entirely.

1.5.2) Drone

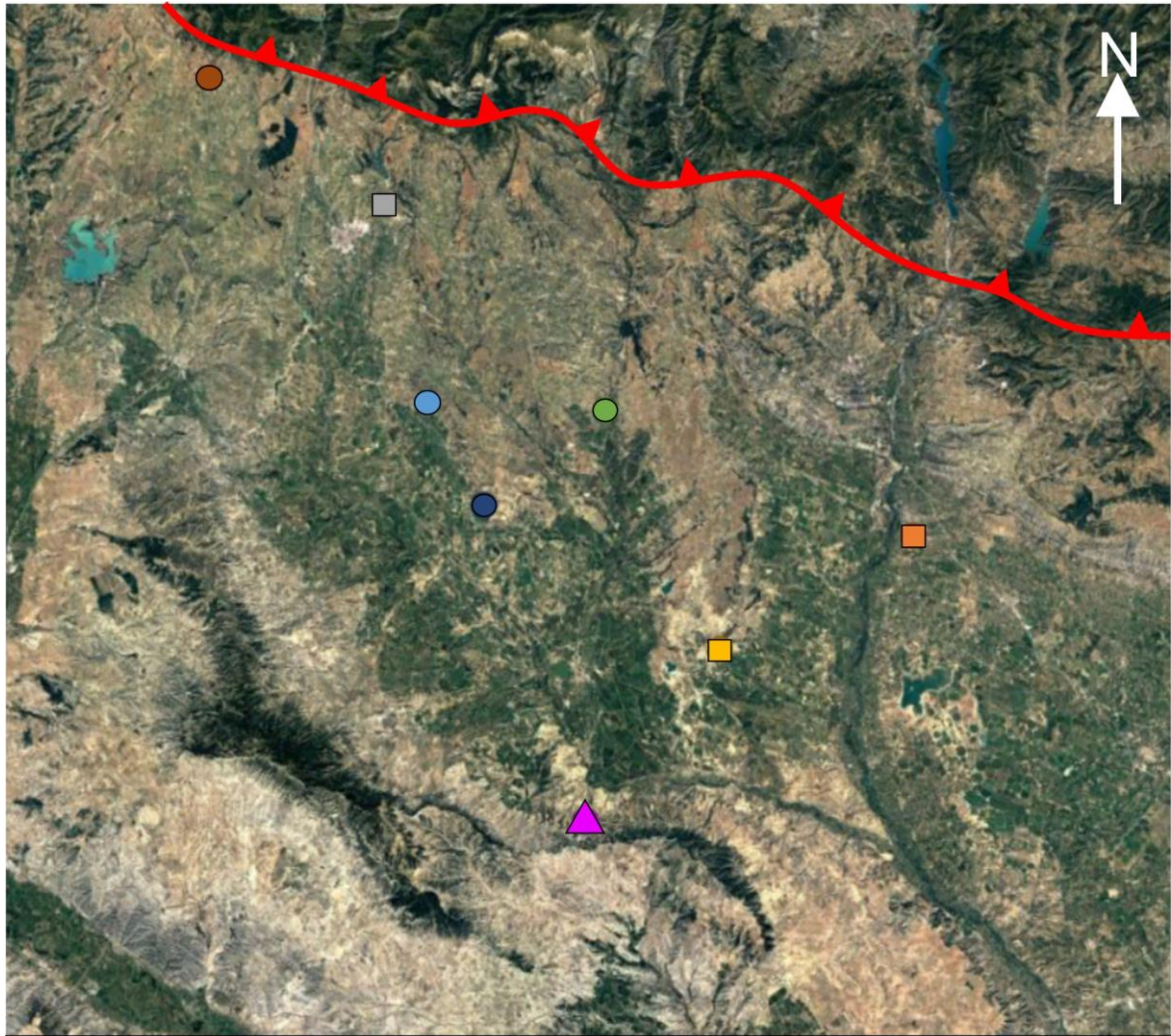
Three models created using drone technology were used in initial data collection at the outcrops of Torrollon, Sigena and Bolea. The use of drone technology is becoming increasingly more frequent within stratigraphic and geomorphological studies (Watts et al., 2012; Gallik & Bolešová, 2016; Madjid et al., 2018) due to their mobility; speed of data capture and the high resolutions of acquired data (Watts et al., 2012; Gallik & Bolešová, 2016). Due to the mobility drones provide, overhangs provide little issue and do not impact upon data quality unlike LIDAR. Drones allow for much higher resolution images to be collected as, dependent on the skill of the pilot, drones can get within metres of outcrops, rather than being shot at 10s to 100s of metres away.

These outcrop models covered the Medial and Distal reaches of the system however no proximal models exist at present. The preliminary database constructed enabled quantification of crude net:gross through vertical log sections alongside channel body thickness, storey surface frequency (where observable) and the identification of channel body geometries using the classification scheme of Owen et al. (2017). Storey surfaces could be mapped across large lateral sections and traced through channel bodies whilst changes in channel body geometry can also be observed both laterally and vertically through the succession, highlighted through the use of barcode logs.

1.5.3) Fieldwork

Fieldwork took place between the 27th of February and the 9th of March, 2018 and allowed for primary data collection at all of the virtual outcrop model sites apart from Sigena. Further localities were included within the study: Castleflorite; Monté Aragon and Monzon where virtual outcrop models were not available. Sedimentary logs were taken through each section in a single location at the outcrop however due to terrain and exposure, logs should not be taken as truly vertical representations of the succession. Logs were created at decimetre scale and include paleocurrent data, sedimentary structures present, channel geometry and stacking relationships and general facies descriptions.

Outcrop photo-panels were used allowing for channel body geometry analysis away from the field, especially at locations where 3D outcrop models do not exist. The geometry data has been analysed with an aim to identify lateral and vertical trends within each locality and determine the temporal change within system deposits.



Key - Locations
 ● Pertusa ● Monzon ● Piraces ● Torrollon ● Castleflorite
 ● Monte Aragon ● Bolea ▲ Sigena —▲— Basin Margin

Key - Data Type
 ● Field and Virtual Outcrop Data ■ Field Data Only
 ▲ Virtual Outcrop Data Only

Figure 4: Location map detailing all studied outcrop sections in the Huesca Fluvial System.

Chapter 2

2.0 Facies Descriptions

Walker (1984) states that the primary purpose of facies models is to create “a general summary of a specific sedimentary environment” through the observation and interrogation of sedimentary structures and features. Facies models have been employed throughout the field of sedimentology as a tool to characterise sedimentary environments by considering the interplay between different sedimentary structures, through both vertical and lateral successions within outcrops. One of the major issues that we currently experience when using these models is that often, they are created in relation to either specific case studies, often singular (Miall, 1996; Lunt et al., 2004; Fielding et al., 2009; Horn et al., 2012), or highly specialised systems that have little applicability to other systems which therefore limits their use (Colombera et al., 2012). This chapter aims to describe and interpret facies and their associated sub-facies, build paleoenvironmental interpretations and understand depositional processes alongside discuss channel body geometries. The chapter will apply and adapt the facies scheme described by Miall (1985) accompanied by the bedform stability diagram (Figure. 3) of Southard & Boguchwal (1990) to describe and interpret facies deposited under various conditions across the system. In order to describe the channel body geometries observed within the system, the scheme of Owen et al. (2017) will be used as it

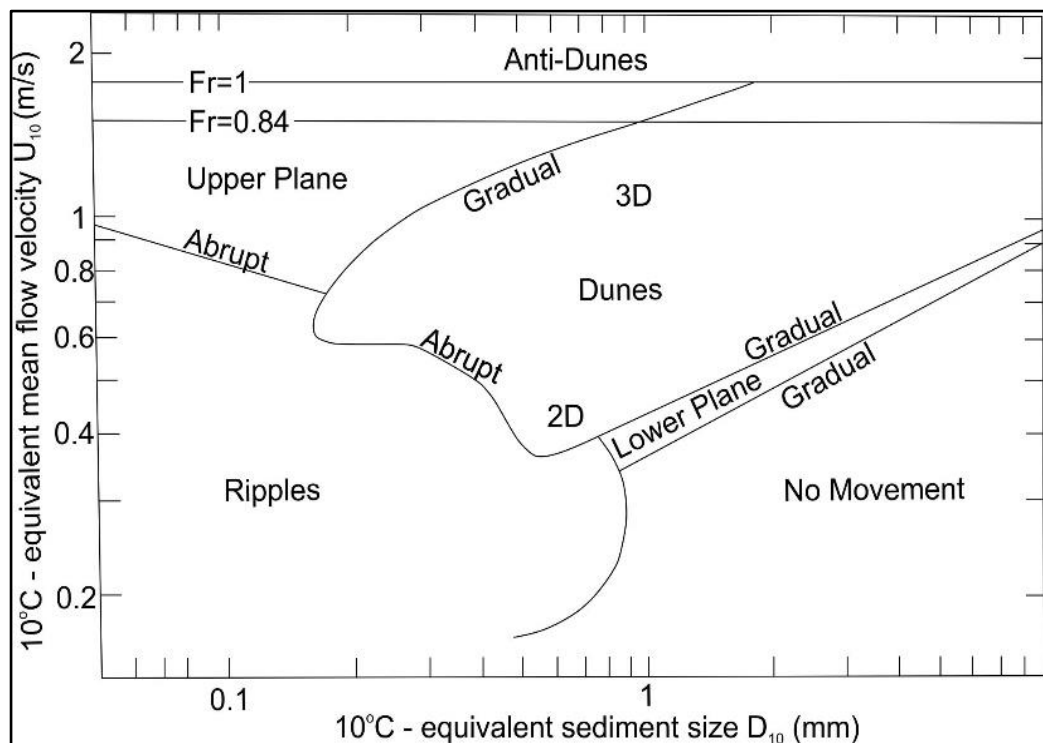


Figure. 5: Bedform stability diagram after Southard & Boguchwal (1990). The flow depth shown is 0.33m if $U = 1.8$; $Fr=1$ and $g=9.81$.

accurately splits channel sheets into well described internal and external geometries that can be applied across systems.

2.1) Facies Overview

The decision was taken to separate facies into Channel (S) and Overbank (M) categories to ease interpretation. Facies are determined using the dominant facies within beds, however this was done in order to allow for mass data extraction from a large database of field data collected from 7 localities across the Huesca DFS. Facies may contain other notable secondary facies or may be overprinted by a secondary modification feature; however this will be addressed within each description. Therefore, we must consider that all of the below facies will have, at some point within the system, displayed mottling as the result of pedogenic alteration and vegetation; the development of gravel lags within beds or the formation of vertical and horizontal burrowing and bioturbation. All of these features provide insight into the conditions of the system and will be considered when constructing paleoenvironmental interpretations.

2.1.1) Sg

Gravel lag facies often occur just above erosional surfaces or as major cross bedding. Some gravel lags observed are very coarse, up to pebble-sized clasts with a clear erosive surface existing between successions (Figure. 4) The facies is grain-supported with angular to sub-angular grains poorly-moderately sorted and typically consists of up to 0.2 m of basal bed boundaries to several grains high when entrained within cross beds. Lags may form localised deposits or completely line erosional surfaces.

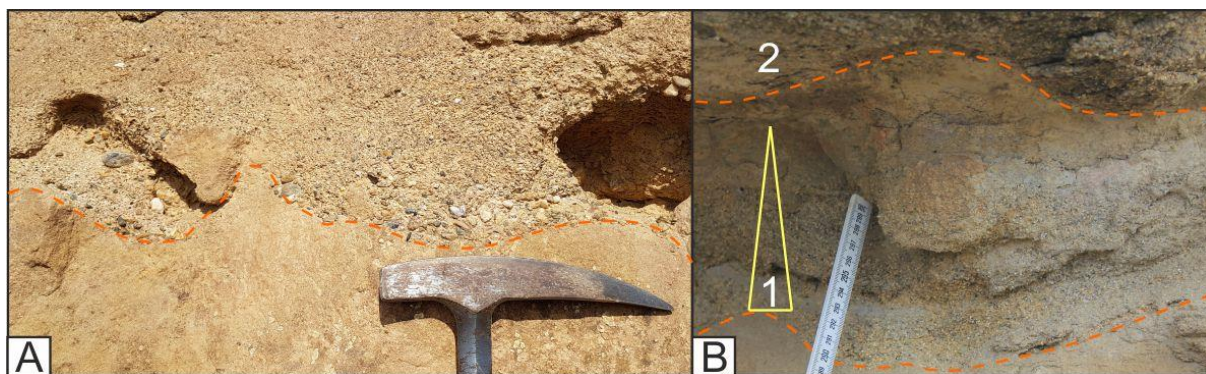


Figure. 6: A) Highly erosive gravel lags containing mature, pebble-sized clasts; B) Two coarse gravel lags can be observed with lag 1 showing minor normal grading before erosion via lag 2.

Interpretation

Gravel lags are often present within the base of cross-sets which is potentially related to slower gravel transport along dunes resulting in deposition of gravel first within dune formation sequences, overlain by a fining upward succession (Hein & Walker, 1977). Overpassing of gravel lags may occur where gravel is transported within flows and act as on a smooth surface under similar conditions to sand, allowing for it to form on the topsets rather than slipfaces (Allen, 1983). Gravel lags show internal variations in texture, believed to be a result of sorting on avalanche slopes of dunes shown by the modelling of Carling & Glaister (1987) and Carling (1990). Miall (1985) suggests that the matrix-filled and matrix supported gravel that forms the base of cross-sets results from the simultaneous deposition of gravel clasts that avalanche down the foreset slope and the settling of sand deposited from the separation eddy at the dune crest. It should be noted that diurnal and seasonal variations in discharge and climate all influence water velocity and sediment loads which can lead to localised and temporally isolated changes in sediment deposition however this is unlikely to have been represented in successions of this scale.

2.1.2) Sm Facies

The Sm facies consists of sandstones ranging from very fine to very coarse sands, averaging as fine-medium sands. Massive beds are generally moderately sorted, typically with angular to sub-rounded grains however granules may be present. Beds are yellow to pale yellow in colour generally. Lower bounding surfaces may be erosional or planar with upper bounding surfaces undulating or planar also. Burrows may be observed on the base of deposits, potentially from burrowing aquatic worms.

The Sm facies has been identified when no sedimentary structures can be observed (Figure. 5). Some beds may exhibit a colour change towards bed tops or burrows (Figure. 6) may be observed towards the base of deposits. Mottling may also be present as a secondary sedimentary feature.

Interpretation

Miall (1977; 1985) did not include a massive sandstone facies within his comprehensive fluvial lithofacies descriptions however they have been noted by others especially in braided river deposits (e.g. Brierley, 1989; Martin, 1995; Hjellbakk, 1997). Massive sandstones have

multiple features in common with deposits resulting from highly concentrated sediment:water flows, indicated by the lack of any identifiable structures (Lowe, 1982; Martin & Turner, 1998). Reduced turbulence leads to the inhibition of dune formation, alongside other bedforms (Harms et al. 1982). It is likely that where cross-sets are present at the base of Sm beds, initial flow conditions allowed turbulent flow and dune formation before localised influx of suspended sediment caused laminar flow to take over, resulting in the juxtaposition of structureless sands above the initial cross-sets. Experimental works of Arnott & Hand (1989) showed that when aggradation rates exceed 6.7×10^{-4} m/s, no structures can form in fine sandstones. This provides an insight into the high rates of sediment deposition that are required for the Sm facies to develop. Rapid deposition may occur through suspended sediment fallout although it has also been noted that the collapse of banks and bars may also result in the formation of massive-type sandstones (Martin & Turner, 1998). Rapid deposition is the likely method of formation for the observed deposits with a lack of dewatering structures or deformation features present as flows were likely not deposited fast enough. It should also be noted that secondary processes, such as diagenesis, weathering and/or pedogenesis alongside bioturbation may lead to the destruction of primary sedimentary structures, leading beds to appear structureless (Martin & Turner, 1998).

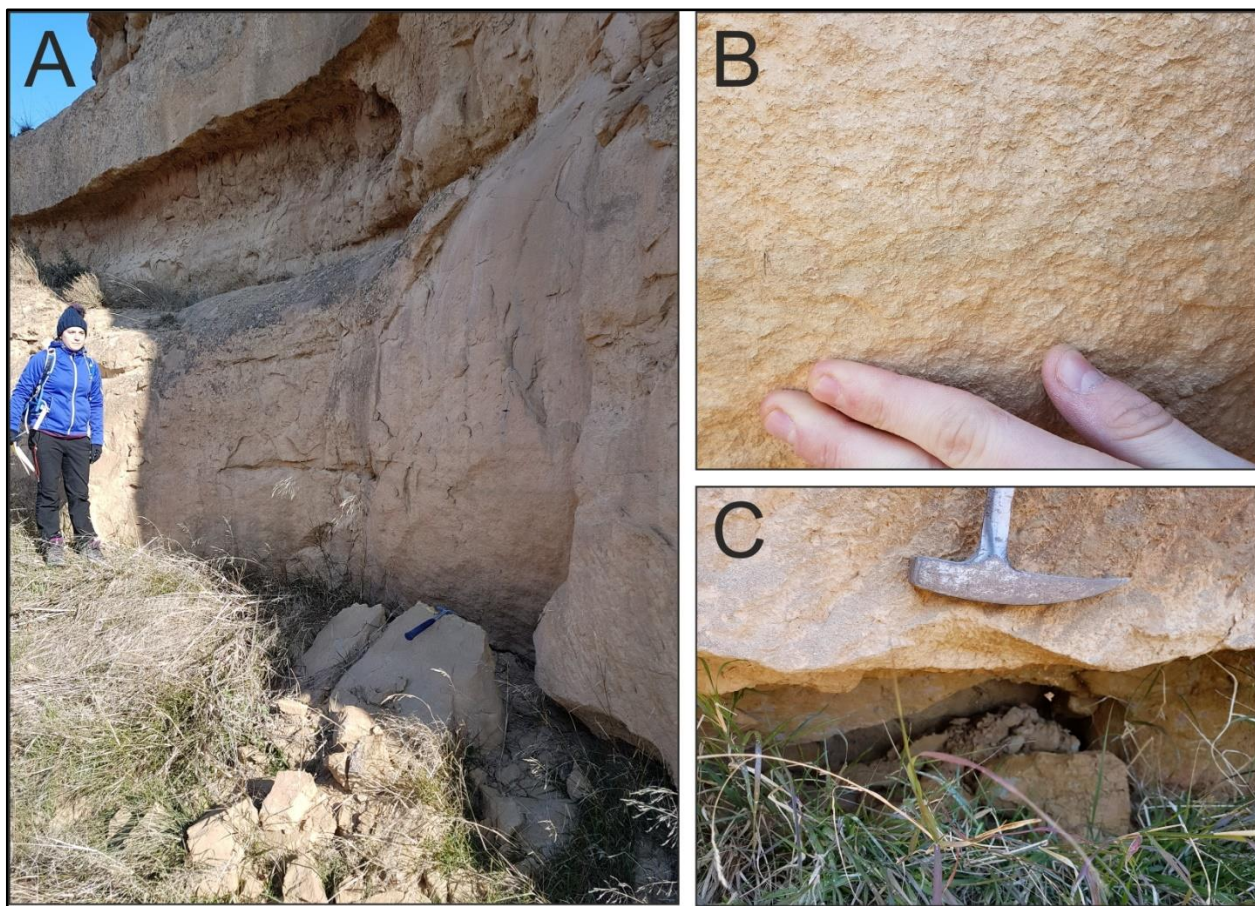


Figure. 7: A) Massive sandstone facies bed with erosional base split by a lower amalgamation surface, Dr.Amanda Owen for scale (1.57m); B: massive, medium-grained matrix with no discernible features present; C: lower erosional surface of the bed cutting into the underlying, mottled siltstone

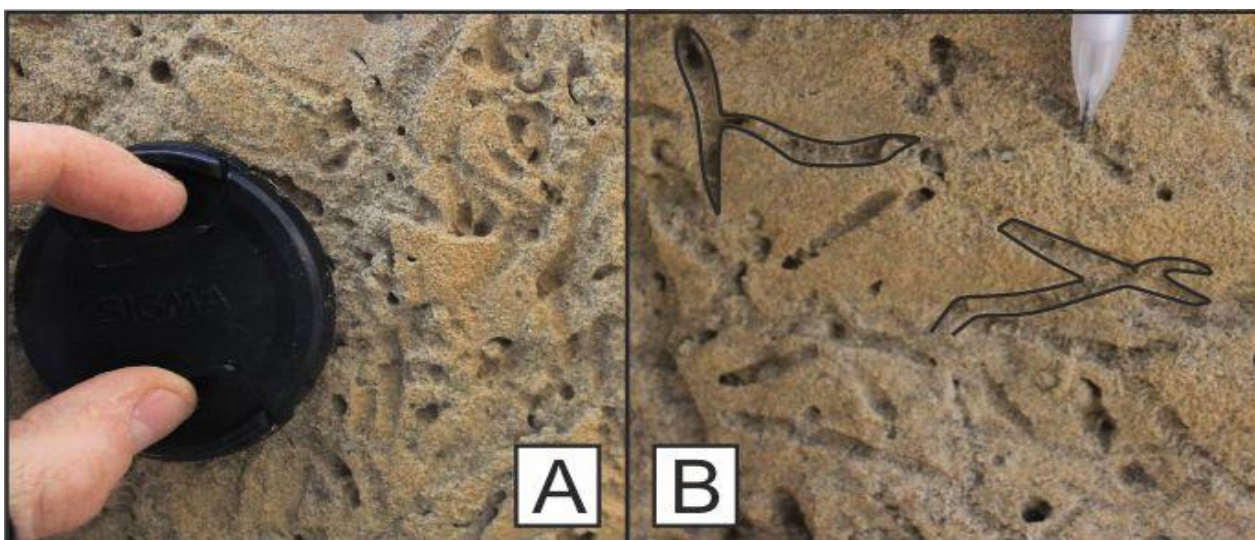


Figure. 8: Burrowing observed on the base of a medium-fine sandstone. Branching of burrows can be identified in image B.

2.1.3) Sx Facies

The Sx facies consists of sandstones ranging from fine to coarse grains, averaging as medium grained. Gravel lags are present and typically pick out cross-sets. Beds consist of typically normally graded sets that show fining upwards successions with the inclusions of intermittent gravel lags in some beds. Sediments are moderately sorted with grains ranging from sub-angular to sub-rounded. Beds are often pale yellow to grey in colour with occasional mottling ranging from red/burgundy in colour to white.

Trough and planar cross-bedding dominates these facies as solitary features within beds or as continuous trains (Figure. 7). Faint cross-bedding may be observed due to weathering of exposed surfaces, in others, gravel lags help to identify the lower parts of cross beds. Cross set thicknesses range from 0.1 m to 1.1 m, typically being 0.5 m in thickness. Cross set angles vary between low (15°) and high (45°). Deposits may form solitary sets or stacked co-sets several metres high (2-3m). Some cross beds may form trains that can be observed for several metres laterally though the deposits.

Interpretation

The bedform stability diagram (Figure. 3) illustrates that large dunes can form under a range of conditions in uni-directional flow, from fine sands through to gravel clasts. Dunes form under subcritical flow conditions (Froude <1) and are observed forming on the base of fluvial channels. Flume-tank research has shown

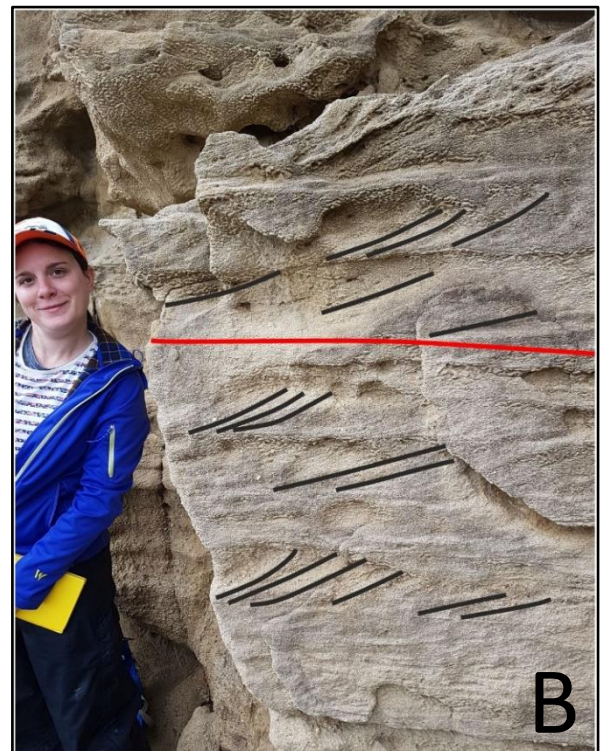
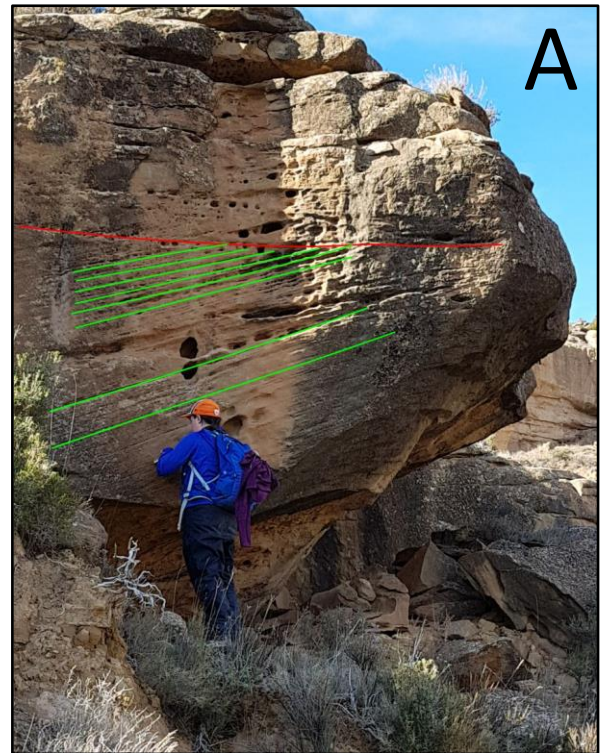


Figure. 9: A) Large, bar-scale, high angle cross-sets. B) Cross-bed trains trending SE, stacking upon each other. Angles of cross-sets tend to vary, within this image, most are low-mid angle.

dunes are considered as steady-state bed configurations (Coleman & Nikora, 2011). The development of dunes occurs as the result of seed waves forming through general planar granular motion (Coleman & Nikora, 2011). As ripple bedforms transition into dune bedforms, wave coalescence begins to occur whereby seed waves migrating at different speeds coalesce (Jain & Kennedy, 1974; McLean, 1990; Raudkivi and Witte, 1990; Coleman, 1991; Ditchfield and Best, 1992; Coleman and Melville, 1994). Periods of accelerated growth of dunes occur due to instability of the fluid-sediment flow system, often paralleled by increased rates of bedform coalescences with the potential for multiple coalescence events occurring during this stage of development (Coleman and Melville, 1994; Coleman and Fenton, 2000). This results in dune growth whilst wave numbers decrease until steady-state equilibrium is reached (Hino, 1968; Nakagawa and Tsujimoto, 1984; Nikora et al., 1997). Once steady-state equilibrium is reached, dune migration begins whereby dunes may begin to amalgamate, cannibalise, and/or superimpose on one another within the channel (Leeder, 2011). It is this migration of dunes that results in the formation of cross-sets within deposits. Grains are transported up the stoss before later avalanching down the lee slope to be preserved as cross sets, similarly to ripples (Leeder, 2011). However, dunes also have the addition of large scale advected eddys, rich in suspended sediment that rise at low angles from separation flows which erupt at the river surface (Leeder, 2011). This results from a combination of shear instability and vortex interactions between separating free stream and the lee-side fluid found closer to the bed downstream from the dune crest (Leeder, 2011). Dunes with low angle lee slopes can allow for the downflow of superimposed dune-like forms down the lee slope, generating down-dipping sets of high angle, cross-stratification further separated by low angle surfaces (Leeder, 2011).

Trough cross sets develop due to sinuous dune planforms whereas planar cross sets are the result of straight crested dunes. The normal grading observed within many of these deposits is indicative of a waning flow over time allowing for the settlement of coarser grains at the base of the dune forming gravel lags that pick out cross sets. These lags may also be indicative of individual flow events as in many cases, deposits may be interspersed with multiple lags within stacked co-sets which may indicate periods of increased flow velocity or influx of coarser sediments into the system. The appearance of mottling amongst cross-sets suggests that at periods of low-stand, dunes may have been exposed sub-aerially where they became vegetated as part of early pedogenic processes before later being re-submerged (Retallack, 2001). Erosional bases of deposits suggest that initial periods of flow were powerful enough to cut into underlying deposits.

2.1.4) Sr Facies

The Sr facies consists of sandstones ranging from very fine to medium sand grains, averaging as very fine to fine. Sediments are well sorted ranging from sub-angular to sub-rounded. Beds are pale yellow to grey in colour, often light grey towards the tops of beds. Normal grading is common. Ripple forms are predominantly asymmetric however rare occurrences of symmetrical ripples are present within the system.

Ripples are often observed towards the upper surfaces of beds with both laminations and whole preserved features present. Asymmetric, uni-directional ripples dominate the facies (Figure. 8), often preserved as features on exposed bed tops or as ripple-cross lamination within cross-sections of beds. Faint ripple lamination may be present alongside semi-preserved features. Sinuous ripple crests can be observed across bed tops also. Ripple cross-set laminations typically range between 0.01-0.02 m in height with wavelengths of up to 0.15 m. A bi-directional wave ripple was also noted. Ripple features were often observed as solitary features on bed tops due to poor exposure and/or weathering of surfaces, however in cross-section could be observed throughout beds as stacked co-sets or as trains.



Figure 10: Facies Sr. Fully preserved current ripple within a splay deposit.

Interpretation

The bedform stability diagram illustrates ripples form under a range of flow velocities in uni-directional flow and can form in sediments up to 0.7mm (Leeder, 2011). Ripples form under subcritical flow conditions (Froude <1). It should be noted that ripples are defined as not interacting with the water surface and therefore the depth of the channels were large enough to prevent interaction between the basal flow and the channel surface (Bartholdy et al., 2015). On smoothed beds, ripples gradually evolve from chance bed defects that form

through impacting groups of turbulent sweep motions; they may also result from localised flow separation over random bed defects several grains high (Leeder, 2011). At current, there is no clear relationship between ripple size and flow strength or depth, unlike dune bedforms (Leeder, 2011). The observed ripples on upper bed tops that exhibited sinuous crestlines have been proven to be metastable during laboratory channel experiments and will eventually develop into linguoid ripples, given sufficient time (Leeder, 2011). Flow velocities close to the no movement threshold may not occur over extended periods meaning that this may not occur within natural deposits (Leeder, 2011). Ripple cross laminations result from the avalanching of sediment grains down the steep lee slopes of ripples. Climbing ripple laminations result from a similar process, however, the net depositional rate of sediment is high allowing for aggradation, suggesting an influx of sediment into the system with high rates of sediment fall out (Leeder, 2011). The wave ripples observed were likely the result wind action acting upon shallow water deposits or around a bar that exists within the channel to form bi-directional forms, likely as part of floodplain environments or around bars within channels. Erosional bases of beds suggest that at initial bed deposition, flows were powerful enough to erode into underlying deposits before reducing velocity to develop ripples, this process also allows for normal grading to develop. Over time, ripples pass into dune features with increased flow strength, water depth and time (Leeder, 2011). The facies can be observed on the base of fluvial channels, splay deposits and overbank fines as well as superimposed on larger architectural elements such as accretionary deposits and dunes.

2.1.5) Sh Facies

The Sh facies consists of sandstones ranging from fine to coarse grained, averaging as very fine-grained beds. Sediments are well sorted with sub-rounded grains. Beds are pale yellow, some may be grey topped or appear red due to pedogenic alteration.

Horizontal laminations are often well defined and easily observed, however weaker and more vague occurrences may be seen. Laminations are often not laterally continuous but may be observed for several



Figure. 11: Horizontal laminations within a fine sandstone bed. Laminations are laterally discontinuous.

metres before phasing out (Figure. 9). Vertically, laminations may be present for the whole bed height or just a minor constituent.

Interpretation

The Sh Facies is one that must be considered carefully through use of the bedform stability diagram. Previous works have detailed that horizontal laminations may form in both the lower plane and upper plane stage bed regimes (Picard & High, 1973; McBride et al., 1975; Allen, 1982; Best & Bridge, 1992; Yagishita et al., 2004). Best & Bridge (1992) conducted flume tank experiments and determined that laminae are attributed to the effects on sediment movement, such as near bed turbulence or the migration of low relief bedforms, potentially a combination of both (McBride et al., 1975). It was concluded that the existence of these low relief bedwaves formed in the upper plane stage bed regime were out of phase with the water surface (Best & Bridge, 1992). The preservation of horizontal lamination is a function of aggradation rate; smaller bedwaves have greater preservation potential at high aggradation rates (Best & Bridge, 1992). It was suggested by Smith (1971) that shallow water depth is a key requirement for the formation of horizontal laminations. It is inferred that the coarser beds present within the facies are the result of the lower plane stage bed stability field (Harms et al., 1975; Allen, 1982; Southard & Boguchwal, 1990; Fielding, 2006). The well-defined planar laminated beds observed throughout, especially those with thin bed thicknesses, are inferred as the result of shallow, supercritical flow conditions within the upper plane stage bed regime of the bedform stability diagram. Infrequent asymmetrical ripples and cross-beds likely result from fluctuations in flow velocity during deposition. The singular case of inverse grading suggests that sediment supply may have increased during this period or that flow velocity increased. Generally, flow conditions likely remained constant throughout time, resulting in homogenous sand beds.

2.1.6) Mm Facies

The Mm facies consist of mud and siltstones that are devoid of structures. Deposits are comprised of very well sorted, homogenous beds. Beds are grey to pale yellow with vertical burrows also observed.

The Mm facies exhibit no primary sedimentary structures throughout the deposits (Figure. 10). Rootlets and mottling can be observed across all localities in which Mm are observed.



Figure. 12: Mm facies showing developed red mottling and a lack of any other structures.

Interpretation

The structureless nature (Figure. 10) may represent continual, steady-state deposition or potentially the destruction of any initial layering created during deposition (Collinson et al., 2006). It is likely that many of these beds were deposited under continual, steady-state conditions due to the blocky fracturing of beds that is observed. As the system contains a lot of mature sediments, it is likely that the lack of platy grains and minerals within the system may also have prevented the formation of layering within the deposits (Collinson et al., 2006). It is also possible that secondary processes may have destroyed primary structures, as indicated by the presence of roots and mottling.

2.1.7) Mh Facies

The Mh facies consists of silt and mudstone beds, predominantly siltstone. The defining features are horizontal laminations. Inverse grading is observed in a singular bed. Silts are generally mature with a lack of micaceous minerals present. Beds are pale yellow



Figure. 13: Horizontal lamination observed within the Pertusa log section. The lamination can be seen to phase out laterally to the left of the image.

to grey in colour and may show red and purple mottling due to pedogenic alteration.

Horizontal laminations (Figure. 11) may form prominent, bold features or form within fissile beds. Generally, laminations are laterally discontinuous, however can be traced for several metres on rare occasion. Horizontal laminations can sometimes become discontinuous wavy lamination.

Interpretation

The Mh facies forms as a result of suspension settling within fine grained deposits. Flow velocity is minimal to non-existent which allows for horizontal laminations to form within deposits however, repeated influx of sediment and changes in flow velocity may allow for the formation of current ripples that may be observed within the facies. Where flows are shallow, there is also potential for wind-interaction with the water surface to also create uni-directional ripples within the deposits. Due to high concentrations of suspended sediment within flows, aggradation rates were likely higher, allowing for greater preservation potential (Best & Bridge, 1992). Wavy laminations present within beds may suggest disruption of horizontal lamination during dewatering of deposits or through waning of flow velocity. The amalgamation of beds creating the 0.7 m thick deposit was likely the result of multiple pulses of sediment deposition from the same source location, potentially during flood periods that caused erosion of channel banks upstream. This would allow for greater weakening of channel banks which would make channel overspill and breakout more frequent, allowing for multi-pulsed deposition. This is supported by the undulating base of the bed which

suggests that the initial flow infilled pre-existing scours and/or depressions in the floodplain (Martin & Turner, 1998).

2.1.8) Mp Facies

The Mp facies is comprised of developed palaeosols, generally red or grey in colour. Palaeosols are generally silty in nature and lack the presence of any primary structures, however mottling is often very well developed, white to grey in colour. Banding may be well developed as well, indicating oxidative or reductive conditions, however the majority of well-developed palaeosols are red in colour. Palaeosol precursor sediments tend to be silts. The Mp facies shows no primary depositional structures however do exhibit well developed mottling from pedogenesis (Figure. 12). Grading is not observed within the palaeosols. Some bioturbation or preserved rootlets may still be present.

Interpretation

The presence of mottling and rooting within these highly fine-grained beds indicates that these are palaeosol deposits. Palaeosols are important tools for paleoenvironmental reconstruction and solving a diverse array of geological problems (Kraus et al. 1999).

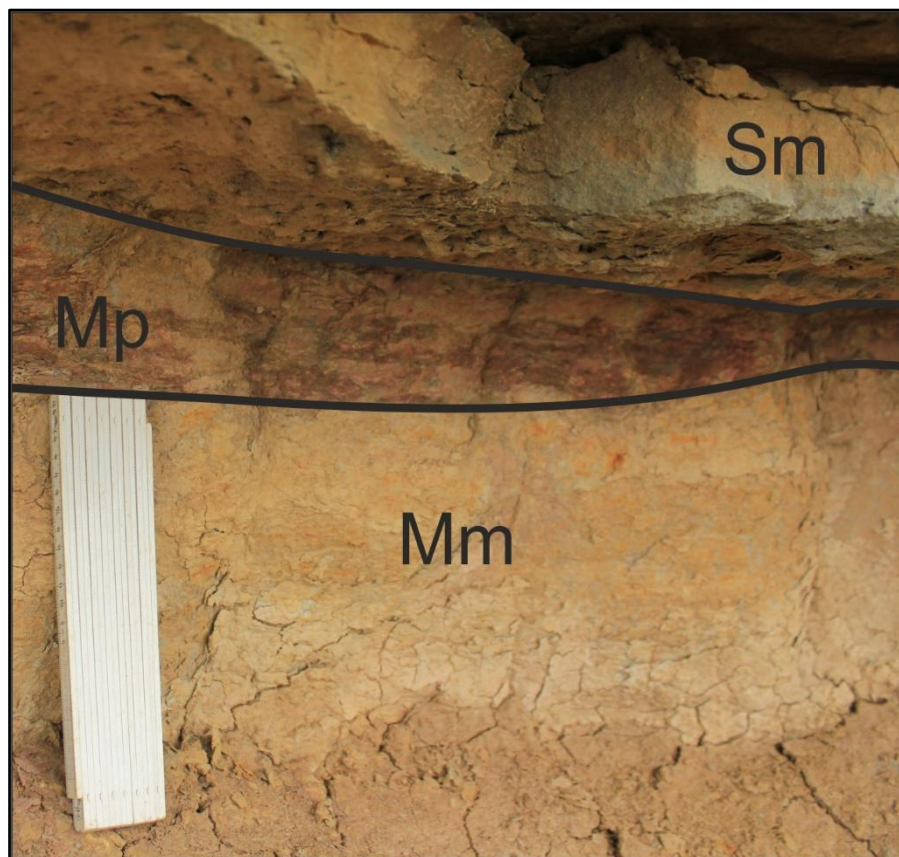


Figure. 14: Deep red, well developed paleosol between massive siltstones and massive, graded sandstone. The paleosol can be seen to pinch out laterally. Ruler: 0.2 m

Palaeosols commonly form due to extended periods of landscape stability under sub-aerial conditions and reflect the complex interplay between sedimentation, erosion and periods of non-deposition (Kraus, 1999). Palaeosols often form vertically stacked deposits when present within net aggradational systems and thick, cumulative deposits during periods where pedogenesis outpaces sedimentation (Kraus, 1999). Within the Huesca DFS, both thick, cumulative palaeosols (1.1 m) and thin, vertically stacked deposits (0.1-0.2 m), are present and both indicate different periods of sedimentation within the basin. Thicker deposits suggest long periods of non-deposition, allowing for pedogenesis to occur whereas thinner deposits may suggest fluctuating conditions within the system that allow for periodic pedogenesis to occur.

Several conditions may influence the development of palaeosols and as a result, the formation of such features is complex. Bridge & Leeder (1979) suggested that autogenic avulsion processes that occur on a century time-scale results in sediment cut off and therefore the encouragement of pedogenesis. The works of Hamer et al. (2007) also note that the parent material, topographic relief and climate are all major influencing factors on soil formation. Colouration of deposits is a common feature noted throughout the Mp facies with the majority of well-developed palaeosols exhibiting a deep red colour, indicative of oxidising conditions, likely the result of increased drainage within splays and levees due to their

Dominant Facies	Other Facies %				Base Erosive	Other Features		Thickness (m)		
	Sg	Sx	Sr	Sh		N. Grading	I. Grading	Min	Max	Avg
Sg	100.0%	0.0%	0.0%	0.0%	100.0%	0.0%	0.0%	0.1	0.3	0.1
Sm	1.7%	2.5%	0.5%	1.1%	5.6%	1.4%	0.6%	0.1	3.60	0.45
Sx	9.0%	100.0%	2.0%	3.0%	10.0%	12.0%	1.0%	0.1	7.80	1.30
Sr	4.0%	0.0%	100.0%	12.5%	4.1%	N/a	N/a	0.1	0.4	0.2
Sh	N/a	5.5%	16.7%	100.0%	8.3%	2.8%	N/a	0.1	2.0	0.45

Table 1: Sandstone facies statistics showing core geometric and facies data compiled across all visited field outcrops.

elevated height in comparison to their surroundings. Grey palaeosols and soils however are more common lower within deposits due to increased proximity to the water table (Duchaufour, 1982).

2.2) Facies Geometries

2.2.1) Sm Bed Geometry

Beds are often observed laterally over 10-100s of metres as part of broad sheet-like geometries that may pinch out laterally or as part of ribbon geometries. Bed thicknesses may vary laterally, thickening and thinning repeatedly in some cases. Upper bounding surfaces are typically planar. Sm may form thick amalgamated successions.

2.2.2) Sx Bed Geometry

Beds extend laterally over 10s – 100s of metres forming broad sheets or thick, ribbon-like geometries. Amalgamation with other beds is common with planar upper surfaces. Sx may transition laterally into other facies.

2.2.3) Sr Bed Geometry

Beds extend laterally over 10s of metres, shifting to other facies laterally. Bed pinch-out is common alongside amalgamation with other sheet-like beds.

2.2.4) Sh Bed Geometry

Beds may extend laterally over 10s of metres, typically as sheets, with discontinuous laminations frequently observed. Upper bed surfaces are planar and lateral amalgamation and pinch-out is common. Sh is most commonly observed within thin, sheet-like beds.

2.2.5) Mm and Mh Bed Geometry

Beds have a sheet-like geometry with both planar upper and lower surfaces. Sheets may thin laterally and extend for 10s to 100s of metres.

2.2.6) Mp Bed Geometry

Palaeosols are commonly thin, sheet-like beds that extend laterally for 10s – 100s of metres. Typically they are vertically stacked deposits with alternating colouration. Upper and lower surfaces are planar.

Dominant Facies	Other Facies %		Other Features			Thickness (Cm)		
	Mh	Mp	Sst Lens	N. Grading	I. Grading	Min	Max	Avg
Mm	0.6%	0.6%	1.2	0.0%	1.2	10	220	38
Mh		0.0%	0	0.0%	0.0%	10	70	30
Mp	0.0%		0	0.0%	0.0%	10	110	42

Table 2: Mudstone facies data compiled from all visited field outcrops.

2.3) Facies Associations

The facies associations described below fall into two categories, fluvial channel and associated floodplain deposits.

2.3.1) Channel Facies Associations

2.3.1A) Lateral Accretion Packages (LA)

Lateral accretion packages consist of Sm, Sx, Sr, Sh and Mm facies with lens-like geometries and characterised by sigmoidal accretion surfaces, dipping ~25°, with accretions shifting vertically into fine-grained sheet-like geometries. Accretion thicknesses range between 0.5 m to 3.8 m. Sm and Sx dominate basal deposits with vertical shifts to Sr, Sh and Mm. Sx paleocurrent readings are typically perpendicular to accretion orientation (Figure. 13) though it should be noted that direct measurement of cross-strata

does not indicate the true bar surface orientation, an issue that should be considered when constructing paleocurrent reconstructions using cross-set measurements (Almeida et al., 2016). There may be a combination of both lateral and downstream accretionary components observed within deposits. Basal contacts are depositional and onlap onto underlying deposits while tops are planar.

Deposition of Sm and Sx facies indicates that deposition was likely occurring in sub-critical flow conditions (Froude <1) whilst the lateral migration of surfaces is interpreted as interplay by secondary flow currents that allow for significant sedimentation on the insides of channel meanders (Miall, 1985; Collinson et al., 2006). Full channel depth may be interpreted where sigmoidal accretions transition into gradational tops, fining-upwards with lateral shifts into Mm and Mh facies (Allen, 1963, 1965; Miall, 1985, 2014). Downstream accretionary components may be observed due to simultaneous accretion resulting from complex interactions between water flow and fluvial barforms (Bluck, 1971; Bridge & Jarvis, 1976; Bridge, 2003).

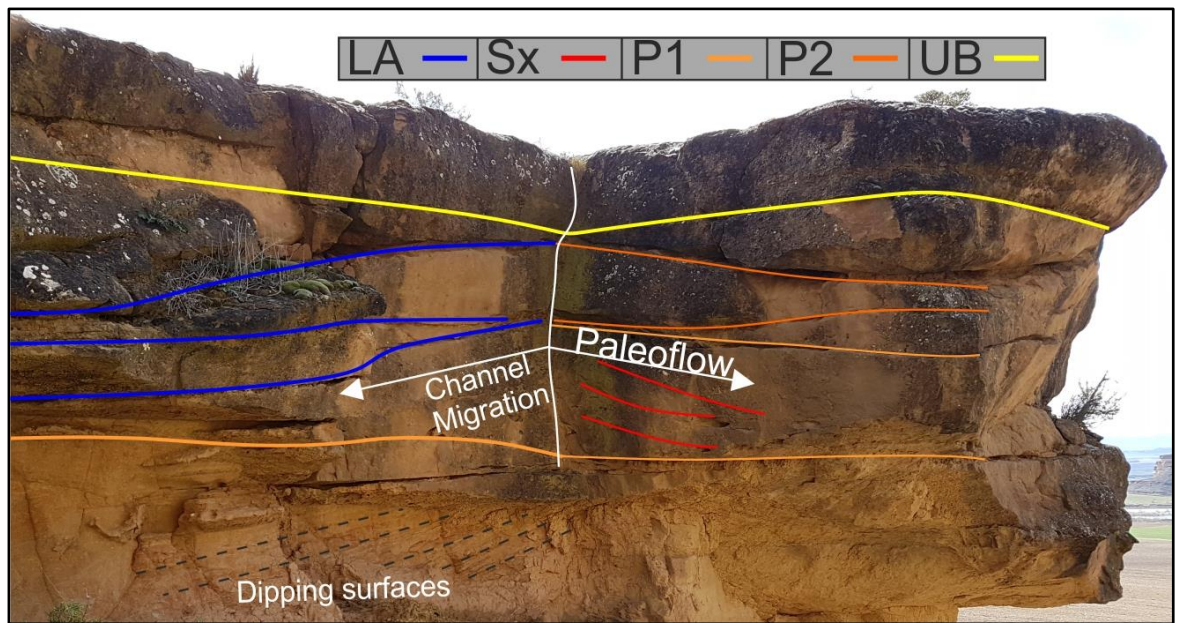


Figure. 15: Lateral accretion packages that exhibit a downstream-migration component also alongside bed pinch out. Packages have been identified pinching and stacking ie; P2 stacks above P1 and begins to pinch out downstream. Dipping surfaces exist beneath the large sandstone body, laterally equivalent to sandstone bodies.

Complex stacking of lateral accretions with vertical and lateral components results in the formation of bank-attached point bar channel elements (CE1) that show 3D propagation downstream. Typically, point bars dominate sinuous river deposits however it should be noted that they are not exclusively observed within such environments. They may also be observed within braided rivers and within meandering-braided transition areas (Miall, 1977; Lunt et al., 2004).

2.3.1B) Downstream Accretion Packages (DA)

The DA facies association is comprised of the same facies as LA however accretionary directions and Sx paleocurrents are parallel with potential to exhibit a small lateral component. Accretions range in high from 0.05 m to 1.8 m and may appear trough shaped in cross-section. Coarse Sm and Sx dominate basal deposits with vertical fining-up and Sh facies. Rooting may be developed along accretion surfaces also. The DA facies association is difficult to accurately determine due to poor exposure however exhibit lens-like geometries. Basal contacts are erosional with planar upper bounding surfaces.

Sm and Sx facies presence indicates sub-critical flow deposition whereby bedforms such as Sx are superimposed onto the downstream migrating bar surface. Accretion heights may not allow us to infer the full channel depth as these features may not reach the upper surface of the channel surface or may extend above it. When bars extend above the channel surface, vegetation may develop, resulting in the rooting observed extending down from accretion surfaces before later being re-submerged. Vegetation also allows for stabilisation of the feature (Tsujiimoto, 1998). The fining-up succession observed suggest waning flow conditions. Lateral migration of deposits typically results from excessive erosion of banks, overwidening the channel and thus creates complex internal architectures (Hooke, 1986; Bridge, 2003).

DA packages often form braid bar elements (CE2) within fluvial deposits, most common in braided environments, however are not exclusively confined to braided systems as shown by the studies of (Knighton, 1972; Hooke, 1986; Luchi et al., 2010; Wintenberger et al., 2015). CE2 often forms in proximal positions within systems and commonly consist of coarser sediment (Lunt & Bridge, 2004; Wintenberger et al., 2015). Determination of whether bars are bank-attached or mid-channel is difficult and as such, this must be considered. Mid-channel bars typically result from complex interactions between subtle

topography on the channel thalweg and areas of low-velocity zones that allow for the deposition of sediment centrally within the channel.

2.3.1C) Unidentifiable Channel Fill (UC)

The UC association is typically comprised of Sm, Sh, with inclusion of Mm and Mh facies. Accretion surfaces are present, ranging from 0.5 m to 3 m. Deposits may extend over 10s of metres with erosional basal contacts and planar upper bounding surfaces. No clear measurements of flow direction can be noted in the form of accretionary packages.

2.3.1D) Abandoned Fill (AF)

The abandoned fill facies association is comprised Sm, Sh, Mm, Mh and Mp. Plugs are often approximately 0.3 m – 1 m thick and can be observed vertically and laterally transitioning from accretionary packages into the CP association. The Sm and Sh facies are common with the development of rooting common. The basal surface often infills the channel depression resulting in a scoop-like geometry whilst the upper bounding surface is planar (Figure. 14).

Channel plugs often form as the result of channel shifting process such as meander cut offs and avulsions. Channel plugs form at bifurcation points of channels where the channel has experienced a cut-off upstream which allows for suspension settling of fine sediments over time to form plugs and Sm/Sh facies (Fisk, 1947; Gagliano & Howard, 1984; Hooke, 1995). These facies may also be formed through the waning of flow velocity as the channel is slowly blocked by the plug. The fining-upwards succession observed within plugs is typically a function of suspension settling, potentially through multiple flood events supplying fine-grained material to the abandoned channel (Toonen et al., 2011). In-channel deposition may be dominated by coarser material if located a short distance from an active channel however,

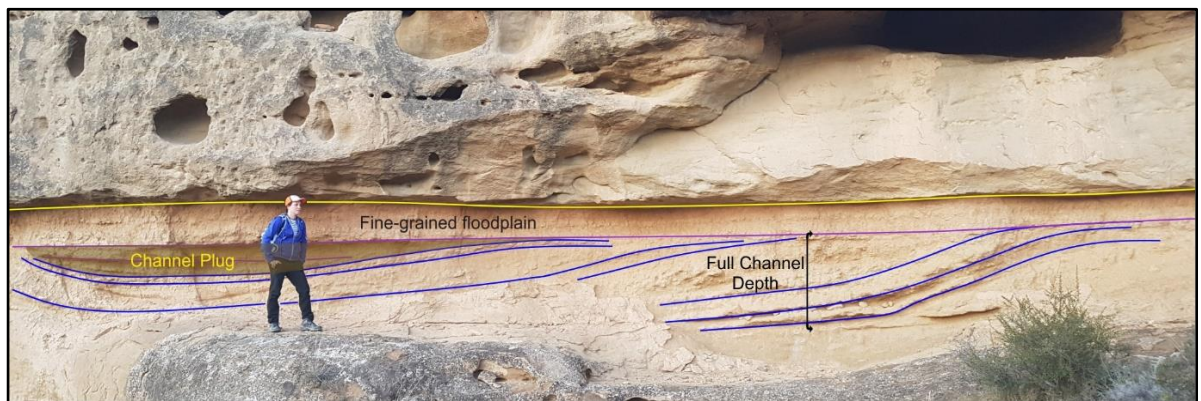


Figure. 16: Lateral accretions providing full channel depth with associated channel plug and overlying floodplain deposits.

mud plugs tend to dominate which suggests greater distance from active channels (Nichols & Fisher, 2007). Whilst channel plugs are not exclusively characteristic of braided or meandering systems, we cannot use the association to determine the fluvial style, however we can use it to determine paleoenvironmental conditions. Typically, plugs may be difficult to observe within overbank successions as there may be little difference between the plug material and surrounding floodplain and therefore may be misrepresented within the rock record (Nichols & Fisher, 2007).

2.3.2) Floodplain Facies Associations

2.3.2A) Splay Sheets

Splay sheets typically consist of fine sands and silts that exhibit a sheet geometry with lateral extent of 10s-100s of metres and thicknesses from 0.1 m beds to <2 m thick splay complexes. Sm, Sr, Mm, and Mh facies are common within the element and rare coarsening-up successions may also be observed.

Beds are typically vertically stacked to form lens-like complexes (meter-scale), however it should be noted that compensational stacking of splay elements is also observed, similar to those noted in submarine lobe deposits (Straub, 2009). Splays, where observed, pinch out laterally, which can be observed well within the compensationally stacked complexes (Figure. 15). Sheet bases are typically planar/undulating with occasional erosional surfaces whilst element tops are planar. Some sheets may undulate with lateral variations in thickness, likely due to local variations in the underlying topography and flow discharge. Splay sheets may be overlain by the Mp facies or eroded into by channel deposits.

Splay sheets form as a result of channel break-outs which supplies sediment to the surrounding floodplain in the form of radially extensive lobate sheets that spread via a point



Figure. 17: Compensationally stacked splay sheets showing clear vertical and lateral offset. Sheets can be seen to pinch out laterally.

source. Undulating bases result from the infilling of subtle topography with sediment, pinching out due to expansion of unconfined flows across a planar/undulating surface. Low velocity flows result in suspension settling of fine sediments.

More tabular sheets of sediment are the result of channel overflow which may occur at multiple points along the channel banks, resulting in a line source supply of sediment. Typically this occurs during periods of flooding and increased discharge that allows the channel to overtop the levee. Sediment sheets that form in this way typically run parallel to the channel and may aid in further development of channel levees over time.

2.3.2B) Splay Channels

Splay channels consist of Sm, Sx, Sr, Mm and Mh facies that exhibit a lens-like geometry with limited lateral extent of several metres and thicknesses up to 1.5 m. Lateral thinning occurs rapidly in both directions relative to the channel and extends into splay sheets. Fining-up successions are common whilst erosive lower-surfaces dominate with planar upper bounding surfaces. Beds may be amalgamated or consist of a singular bed.

Splay channels result from high-velocity flows breaking out of the channel confines and eroding minor channels into the underlying floodplain. Vertical transition into the Mm and Mh facies results in flow cut off and the resultant decrease in velocity allowing for suspended sediment to be deposited and subsequent minor channel fill.

2.4) Sandstone body architecture

Many architectural schemes exist and have been used in conjunction with fluvial facies schemes (Friend et al., 1979; Blakey & Gubitosa, 1984; Hirst, 1991; Cain & Mountney, 2009; Huerta et al., 2011; Gulliford et al., 2014; Owen et al., 2015), however the scheme employed by Owen et al. (2017) allows for quantification on multiple scales and provides a useful and readily transferrable identification scheme. Five sandstone channel body and two floodplain channel geometries are defined within the scheme (Owen et al., 2017). The scheme subdivides traditional “sheet geometries” (e.g. Friend et al., 1979) into separate, identifiable sandstone geometries through external geometry and the internal relationship of storey surfaces (Owen et al., 2017). The scheme will be applied to the Huesca DFS as the described sandstone geometries are able to be put in context with one another alongside allowing us to interpret the formation process of bodies (Owen et al., 2017).

2.4A) Massive Channel Body Geometry

Massive channel body geometries are typically comprised of highly amalgamated, sheet sandstone bodies with large minimum lateral extents which prevent the observation of full lateral extents within singular outcrop sections. Massive channel body geometries often pinch out into floodplain material laterally. Interconnectivity of the channel body is high with none/very little floodplain inclusions (Owen et al., 2017). Pertusa is the only outcrop where the Massive channel body geometry is observed where lateral extents cannot be measured due to discontinuous outcrop. Channel bodies here range between 4.4 m and 19 m dependent on whether the measurement is taken near the centre or the wing of the channel body (Figure. 16). Thicknesses were typically taken from strike sections of channel bodies.

Storey surfaces are often completely missing, sometimes only partially visible within small sections of the channel body; a defining feature for the geometry (Owen et al., 2017). Where storey surfaces are visible, they may occur in frequencies as many as five within a singular outcrop section however these do not cross-cut one another, instead they will pass into sediments laterally. Storey surfaces may be noted over the spacing of ~50 m within this outcrop. This is believed to be related to the coarse grain size often observed within Massive channel body geometries that masks the visibility of full storey surfaces (Owen et al. 2017). The geometry may be composed of facies Sm, Sx, Sh forming LA/DA/UA elements as part of point and mid-channel bars and occasional channel plugs.

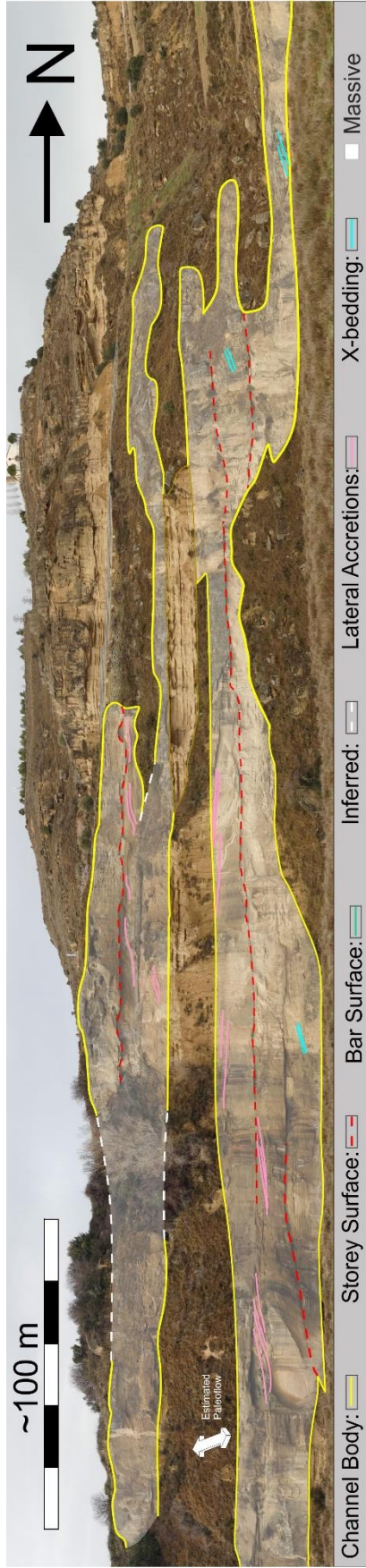


Figure. 18: Two Massive sandstone bodies shown within the centre of the outcrop separated by a small floodplain package. Several storey surfaces are noted within the outcrop, however these often cannot be fully traced throughout the sandstone body. This outcrop is along strike of paleoflow.

2.4B) Semi-Amalgamated Channel Body Geometry

Semi-amalgamated channel body geometries (SA) consist of broad sheet-like bodies with up to 50% of the channel belt base in contact with floodplain deposits, the remainder forms a channel-channel contact (Figure. 17) (Owen et al., 2017). This allows for well interconnected channel bodies amalgamated over large minimum lateral expanses with localised pockets of floodplain separating the bodies (Owen et al., 2017). Owen et al. (2017) found that paleocurrent directions were relatively consistent between amalgamating portions suggesting the amalgamation is not a local feature, rather a complex three-dimensional geometry is present. As noted by Owen et al. (2017) the full lateral extent of SA may not be observed due to its massive form. Exposures may be discontinuous (Monzon) or too large to observe full lateral extents of outcrop (Torrollon/Piraces section) where channel bodies could be followed over kilometres. Channel body thicknesses range from between 1.0 m (at the channel wing) to 13.0 m with the largest minimum lateral extent measured at 1 km at Torrollon.

Storey surfaces are frequent and well developed within geometry SA where spatial isolation or cross-cutting relationships may occur (Owen et al., 2017). A maximum of three storeys were identified at Monzon with an average of 3.7 m thickness. Storey surfaces also transition out across sandstone bodies as seen within the Piraces outcrop panel. Maximum storey thicknesses taken from the Monzon log show storey thicknesses of up to 5.6 m. SA may be composed of facies Sm, Sx, Sh forming LA/DA/UA elements as part of point and mid-channel bars and occasional channel plugs.

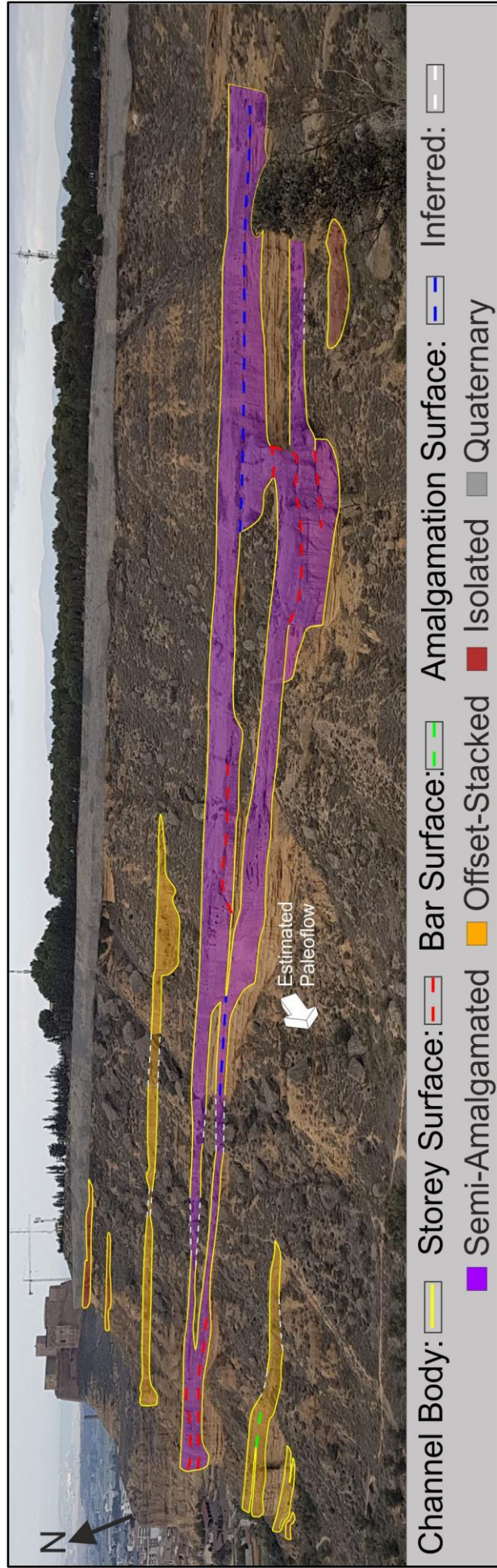


Figure. 19: Semi-amalgamated outcrop shown within the central section. An isolated channel geometry can be observed vertically through the section. Towards the SE, multiple storeys are stacked vertically. This outcrop is along strike from paleoflow.

2.4C) Internally-Amalgamated Channel Body Geometry

Internally-amalgamated channel body geometries (IA) are broad sheet-like forms with simpler geometry to SA with lateral extents up to a kilometer in the Piraces exposure. Exposure may limit this estimate at determining lateral extent and should be used as a minimum. Due to the nature of amalgamation, geometry is simpler and more consistent rather than multiple floodplain pockets being present (Figure. 18). Deposits may pass gradationally into floodplain laterally however exposure of this may not be visible due to scree and boulder cover. This gradational transition typically occurs whereby channels avulse, leaving channels to fill that would eventually overtop the channel banks to form a gradational change from channel sands into unconfined floodplain deposits.

Geometry thicknesses range from 2.0 m to ~11.0 m where multiple storey surfaces stack, many storeys are spatially isolated however may cross cut one another. Many storeys can be described as transitional and are estimated between 1-4 m thick. The geometry is typically composed of Sm, Sx, and Sr as part of LA/DA elements and CE1-2-3. Geometry IA can be recognized in the schemes of Blakey & Gubitosa (1984), Hirst (1991), Pranter & Sommer (2011), Cain & Mountney (2009), Huerta et al. (2011), Owen et al (2015, 2017) described using various terminology such as multi-storey sheets; amalgamated channel fill complexes and intermediate sheet-like bodies.



Figure. 20: The Piraces outcrop shows large lateral extent over several hundred meters. Sand bodies show multiple storey surfaces, many of which are transitional and may cross cut. Isolated bodies are also observed alongside off-set stacked. IA dominates the outcrop with no observable trend in changing geometries upwards through the succession. The outcrop is along strike to paleoflow.

2.4D) Offset-Stacking Channel Body Geometry

The defining feature of the offset-stacked (OS) channel geometry is the internal arrangement of storey surfaces within the channel body (Owen et al. 2017). Storey surfaces juxtapose both vertically and laterally onto one another which causes a stepped geometry of bodies where there may be direct contact with underlying channel deposits and floodplain deposits (Owen et al., 2017). Typically the lateral component of juxtaposition is more prominent than the vertical component with storey surfaces often localised features meaning that the exposure of deposits and the position of measurement determines whether the body is classed as single or multi-storey (Figure. 19). Typically, OA channel bodies have one to three stories present that range in thickness, 1 m to 4 m, which results in a complex external geometry (Figure. 19), often with erosional channel cuts that thin laterally to form large sheet-like geometries. Due to the complex stacking nature of the OA geometry, connectivity of channel bodies is often limited vertically and laterally with highly variable thicknesses, often localised rather than laterally across the whole channel body. The vertical component, though minor in some cases, may result in climbing deposits.

At individual points where only single storeys are present, deposits may only be 1.0 m thick however where stacked, deposits may reach up to 16 m with individual storeys reaching up to 4.6 m at the stacking point (Figure. 19). Exposures typically pinch out laterally however full lateral extents may not always be observed due to lack of exposure. At the Torrollon exposure, channel bodies may be followed for 900 m laterally. The OS geometry is typically comprised of Sm, Sx, Sr and Sh facies as part of LA and CP elements. This geometry has been noted by Owen et al. (2017) in the Bighorn Basin and in the works of Gulliford et al. (2014) as complex type A.

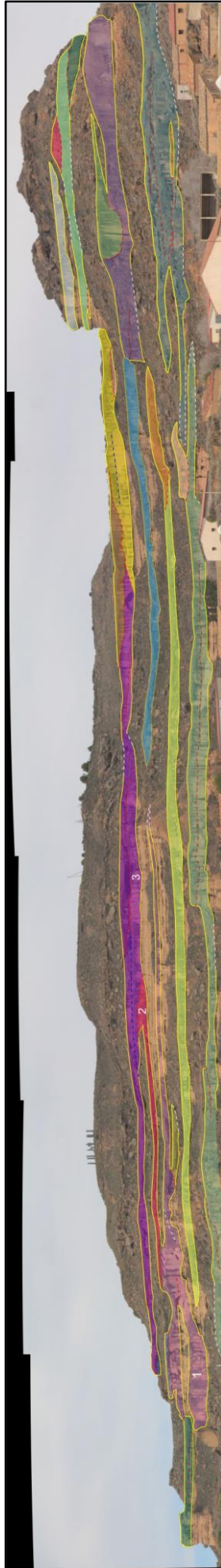


Figure. 21: Truncated outcrop photo panel taken from the roadside. Clear exposures show the complex nature of the OS channel body geometry, exhibited by channel bodies 1, 2 and 3 which highlight both the lateral and vertical interconnectivity of these types of channel bodies. A shift can be seen from IA bodies at the base of the outcrop, to OS and I geometries in the upper extent. The outcrop appears to be along strike from paleoflow.

2.4E) Isolated Channel Geometry (I)

The Isolated Channel Geometry is typified by single storey channel bodies with simple internal and external geometries, much like traditional “ribbon” channel geometries (Figure. 20) (Friend et al., 1979; Blakey & Gubitosa, 1984; Hirst, 1991; Cain & Mountney, 2009; Huerta et al., 2011; Gulliford et al., 2014; Owen et al., 2015). Channel bodies are not linked to each other resulting in no interconnectivity. The body is surrounded by floodplain deposits and channel wings, if present, may graduate into floodplain. Deposits may reach up to 1.5 m thick with minor lateral extent, up to 10s of metres which can be followed out gradationally into floodplain. Storeys, if present, are up to 0.7 m thick. The geometry is composed of Sm, Sr, Sh and Mh facies as part of the CP element. This geometry has been noted throughout multiple works on fluvial systems and is the most recognizable geometry when referring to traditional literature (Friend et al., 1979; Friend, 1983; Miall, 1985; Eberth & Miall, 1991; Nichols & Hirst, 1998; Fisher, 2007; Gonzalez-Bonorino et al., 2010; Owen et al., 2015; Weissman et al., 2015).

Multiple storeys have been observed in the form of re-activation surfaces within some channels which only exhibit a vertically stacked component with no offset. Typically these channels will consist of two storeys, however due to the offset – stacked definition of requiring lateral channel offset, these channels appear to be better suited to the isolated channel geometry category.

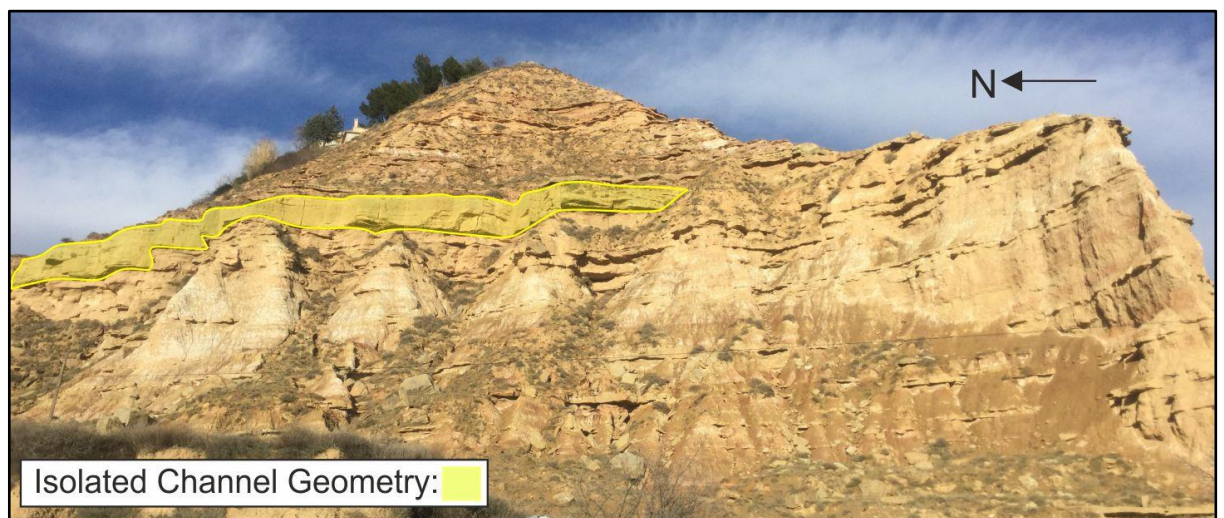


Figure. 22: Isolated channel body seen within the western face of the Bolea outcrop. Crevasse splay sheets are frequently observed within the extensive floodplain deposits.

2.5) Summary

Multiple outcrops visited across the Huesca DFS allowed for vast data collection and the resultant facies analysis using an altered version of Miall's (1985) facies scheme that categorises beds on their dominant facies. Multiple sandstone channel body geometries from the Owen et al. (2017) classification scheme observed within the system and highlighted above indicating that, whilst Owen et al. (2017) took a much larger basin-scale approach, the scheme can also be used on smaller, system-scale studies such as the Huesca DFS. Clear downstream trends could be identified such as a shift from M to I geometries downstream and a reduction in channel body thicknesses downstream.

Core Findings

- Massive channel geometries are noted in the proximal, passing downstream into Semi-Amalgamated, Internally Amalgamated, Offset-stacked and Isolated channel geometries (Owen et al., 2015).
- Channel-body thicknesses and connectivity decrease downstream as shown in architecture panels.
- Storey thicknesses reduce downstream.
- Dominant facies in the proximal and medial system are Sg, Sx and Sr. The dominant facies in the distal system is Mm.
- Facies Associations most commonly noted are LA deposits.

Chapter 3

3.0) Vertical Trend Analyses

Vertical trend analyses are used to determine the presence of trends on various scales and allow us to infer changes in fluvial sedimentation both spatially and temporally. There are multiple methods available to determine vertical trends within outcrops such as Markov Chains, however due to the complexity of this mathematical solution and the changing position of each outcrop across the system, direct comparisons would not be possible between each outcrop dataset (Howard, 1971). Therefore the method of comparing log height against channel body thickness was used to directly compare changes in vertical successions.

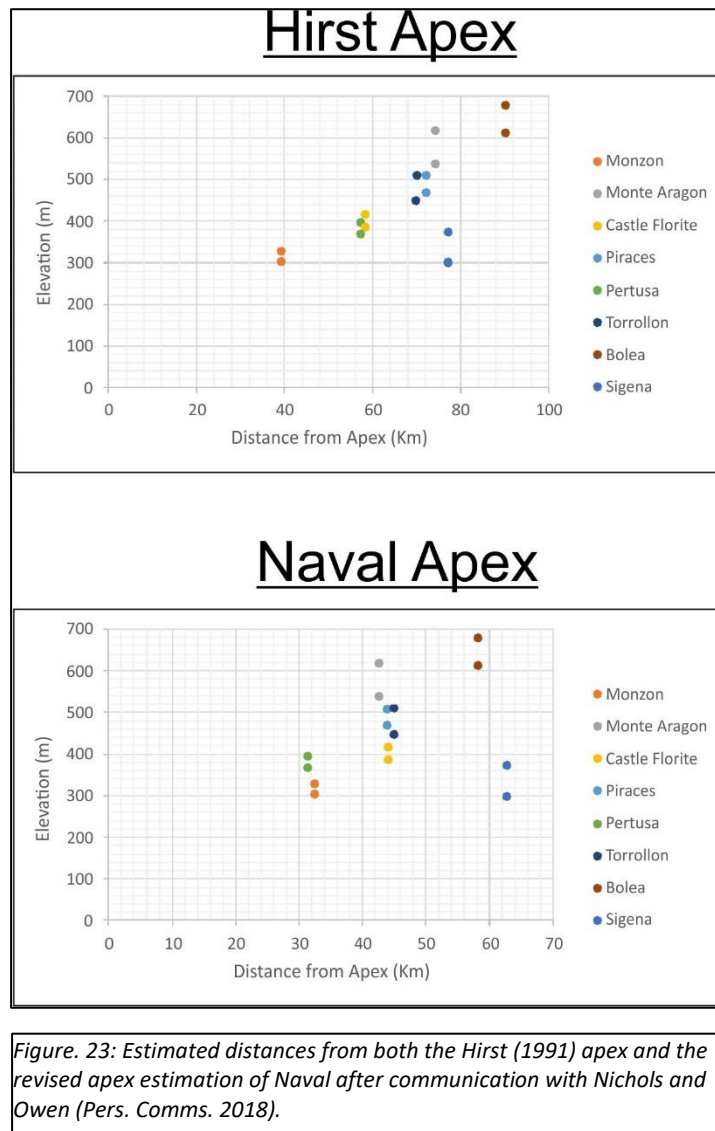


Figure. 23: Estimated distances from both the Hirst (1991) apex and the revised apex estimation of Naval after communication with Nichols and Owen (Pers. Comms. 2018).

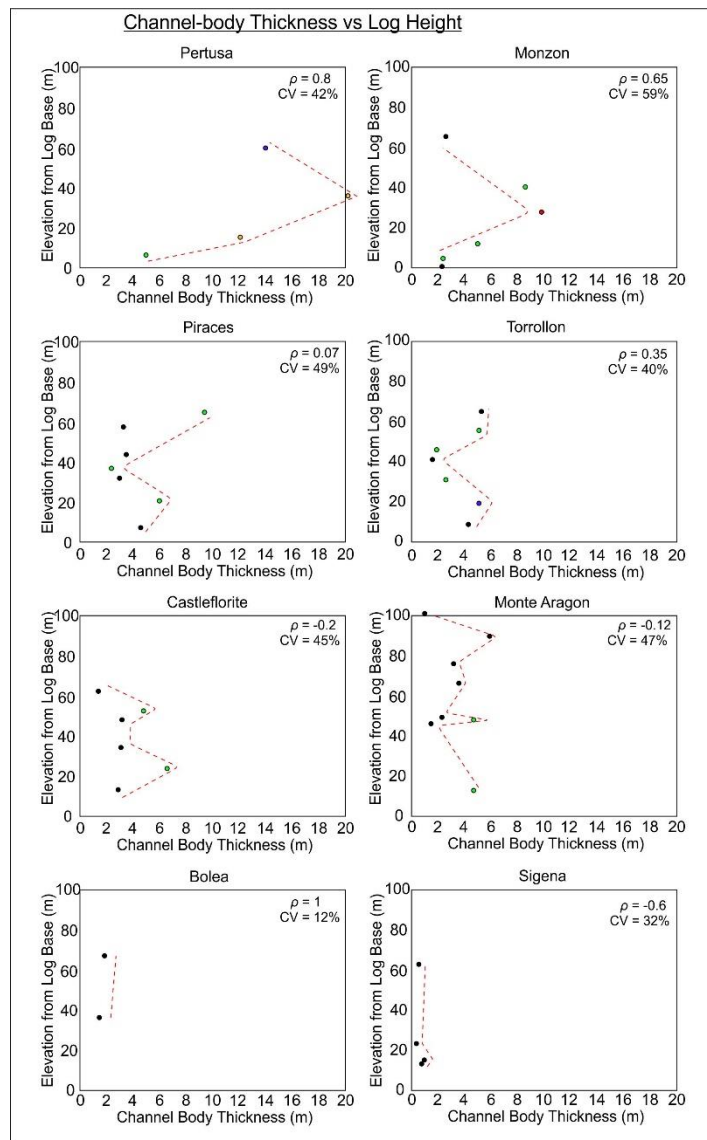
Across the system, successions cannot be correlated fully as deposits are poorly constrained in age; therefore it must be noted that changes in deposits across the system may be due to temporal controls rather than spatial controls. Assessing the interplay between temporal and spatial is difficult due to the lack of age data available for the deposits and will be later discussed in the chapter.

It should be noted that several attempts at calculating the estimated apex point for the Huesca DFS have occurred, the most well-known of these from Hirst (1991). However, using new data collected during this project and further work completed by Owen and Nichols (Pers. Comms. 2018), we believe that this original estimate may need revising (Figure. 21). Through plotting elevation relative to sea level data with log thickness against distance from the estimated apex, it was noted that Pertusa and Castleflorite plotted very closely on the x-axis when using the Hirst (1991) estimate, even though Pertusa is noted to be in a proximal position due to the vertical profile; channel body thicknesses paired with the observed channel geometries; compared with the medial profile of the Castleflorite outcrop. In comparison, using the Naval apex estimation suggested by Owens and Nichols (Pers. Comms. 2018), all outcrop localities plot appropriately in relation to one-another. Therefore, for this thesis the estimated apex used will be the town of Naval, approximately 32 km northwest of the Jupp et al. (1987) estimation.

3.1A) Overview

Changes in average channel body thicknesses are observed proximally-distally but also within outcrops with a range of channel body thicknesses present. Mean values range from 12.8 m to 0.7 m proximally to distally with standard deviation values range from 5.4 m proximally to 0.2 m distally. Coefficient of variation values also show significant ranges, from 60% proximally to 11% distally. Greater coefficient of variation values means that there is a greater variation between the mean and standard deviation values resulting in a more dispersed dataset and in this case, meaning the data is less predictable.

The degree of variability of channel presence within successions is relatively large ranging between 66% at Pertusa and 5% at Bolea. The dominant channel geometry across the system taken from logged successions are offset-stack (OS). The coarser-grained, proximal successions exhibit various channel body geometries (M/SA/IA/OS) whilst lesser amalgamated geometries (OS-I) can be observed within the finer-grained medial and distal deposits.



Key
 • Massive • Semi-amalgamated • Internally amalgamated • Offset-stacked
 • Isolated -- Moving Average ρ = Rho CV = Coefficient of variation

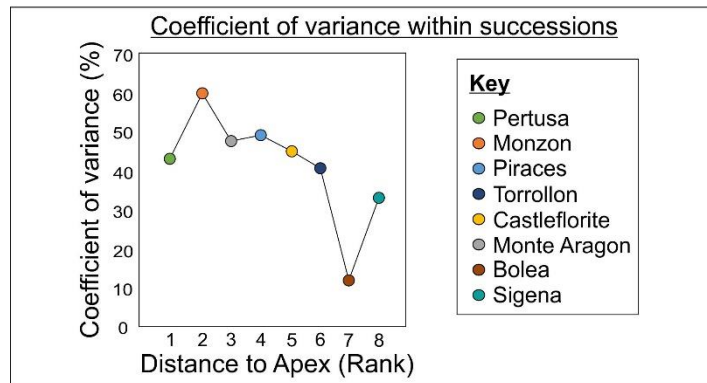


Figure. 24: Moving average plots shown from most proximal to distal. Channel body thicknesses are plotted against log height with channel geometry indicated also showing the shift in geometries with height. Spearman's rank and coefficient of variation (CV) are also calculated and indicated. CV is plotted using rank of distance from apex. Due to the small number of data points (n), the statistical significance is low however this data has been included to allow for direct comparison with the data of Owen et al. (2015).

Small scale trends were determined using Spearman's rank correlation coefficient (ρ) and the coefficient of variation for each log section. Moving averages were plotted showing the shift in channel-body thickness comparatively with succession height (Figure. 22). Successions were grouped using ρ values; the first showing weak or no relationship (less than ± 0.19); the second with a weak relationship ($\pm 0.2-0.39$); group three is a moderate relationship ($\pm 0.4-0.59$); group four a strong relationship ($\pm 0.6-0.79$); group five a very strong relationship ($\pm 0.8-1$).

Figure. 22A however shows spatial groupings with clear, strong trends developed within the proximal and distal deposits whilst medial deposits have the weakest relationships. This indicates that the medial zone of the system likely exhibits the most variability, with both negative and positive relationships in channel body thicknesses vs succession height observed. Figure (B) shows that there is no particular dominance within the successions logged indicating no clear trend of thickening or thinning of channel bodies with increasing succession heights.

The coefficient of variation (ratio of the standard deviation to the mean; CV) was also calculated for all successions. As Figure (B) shows, a range of CV values are observed from 12-59%. Typically, the majority of CV values fall between 40 and 60%, considered to be moderate with a single case of low CV. This suggests that channel body thickness generally varies relatively within each succession. Figure. 22 also indicates that generally, medial deposits show the most variability within deposits however this is a weak spatial trend. The proximal deposits of Monzon and Pertusa show the largest variation of CV values between a spatial grouping (proximal/medial/distal). One must note that the number of channel bodies within successions are reasonably small and therefore the coefficient of variation data should be considered with less weighting when assessing their importance. The data reported here allows for better comparison with the works of Owen et al. (2015).

3.2 Discussion

Whilst the discussed vertical trends above are integral to understanding the temporal and spatial changes that took place during the deposition of the Huesca DFS, it is beyond the scope of this thesis to determine the causes for such changes at each locality. Variations in channel body thicknesses and presence across each locality indicates that the system is heterogeneous. As DFS consist of a radial dispersion of channels with differing rates of avulsion and preservation potential downstream, the heterogeneity of vertical successions

observed goes to further support the notion that the Huesca Fluvial System can be classified as a DFS.

Figure. 22a indicates that channel body thicknesses may increase or decrease systematically up-section, or groups where no to weak relationships can be observed that show no systematic changes. Systematic changes may be the result of a variety of local and regional processes such as changes in sediment supply; subsidence rates; available accommodation space; climactic conditions and palaeosol development. Decreases in channel thickness up-section may be the result of reduced sediment supply due to changing climactic conditions; reduction in accommodation space within the system/basin; increased frequency of channel avulsion or well vegetated floodplain that is more resistant to channel incision alongside system retrogradation over time (Nichols and Fisher, 2007; Hartley et al., 2010; . Increases may be the result of system progradation and expansion; increased stream power allowing for greater channel incision and/or increased basin subsidence and the creation of further accommodation space. Where no/weak relationships exist between channel body thickness and succession height, we can make two inferences. 1) Successions show highly variable deposits where no clear thickening or thinning trend can be observed (low ρ values ($<+/-0.2$) and high CV values ($>45\%$)) such as at Piraces and Monte Aragon. It may be inferred that these deposits are the result of abrupt changes in climactic conditions/sediment supply/accommodation space/base level changes in the central lacustrine deposits of the system that force thickening and thinning of channel body deposits over short periods of time. 2) Channel body thicknesses are relatively consistent up-section, such as Bolea and Sigena, in these cases it can be inferred that fluvial conditions during deposition was consistent over time with relatively little fluctuation in depositional conditions. CV values are typically higher in the proximal and medial regions of the system likely due to the distal deposits being less susceptible to up-stream changes in sediment supply, accommodation space and discharge variations due to relatively consistent conditions in distal regions.

3.2A) Weighted Grain Size Analysis

Weighted grain size analysis was carried out to take into account channel-body thicknesses (Figure. 23). The dominant grain size of beds were used in calculations in order to determine the average grain size of each channel body. This method was employed for each channel-body at each location observed and where silts were noted within channel bodies, a grain size of 0.062mm was used. Sandstone beds typically consisted of medium-sized quartz

grains with a sub-rounded sphericity however more immature sediment was noted within the system. Palaeo-current readings alongside differences in grain sphericity and size suggest that sediment sources may be different for outcrops across the system. Unfortunately, due to the scope of the project, in-depth mineralogical data could not be collected however this would be beneficial for future works.

The coarsest channel-bodies observed within the system are observed within the Monte-Aragon deposits interpreted as an along-strike medial-distal fringe within the system. The lateral position of the deposits relative to the inferred apex point of the system allows for a distal log profile whilst the proximity to the basin margin allows for the coarse-grained nature of the channel bodies present. The lateral deposits of Bolea, also positioned along-strike from Naval, experiences a systematic decrease in grain size over a much smaller distance when compared with that of Monzon and the downstream distal deposits of Sigena. This suggests that along-strike locations experienced rapid deposition of coarse sediment and poor sediment transport potential, likely due to rapidly decreasing stream power along the basin margin.

Monte-Aragon is the only location where an average grain size above 1mm is observed within channel bodies, at all other locations, the general trend of grain-size decreasing downstream can be observed. Monzon and Pertusa, the most proximal downstream deposits to the inferred source of Naval, exhibit the largest average grain sizes (0.94 mm and 0.83 mm respectively) within the system apart from Monte-Aragon. The medial deposits of

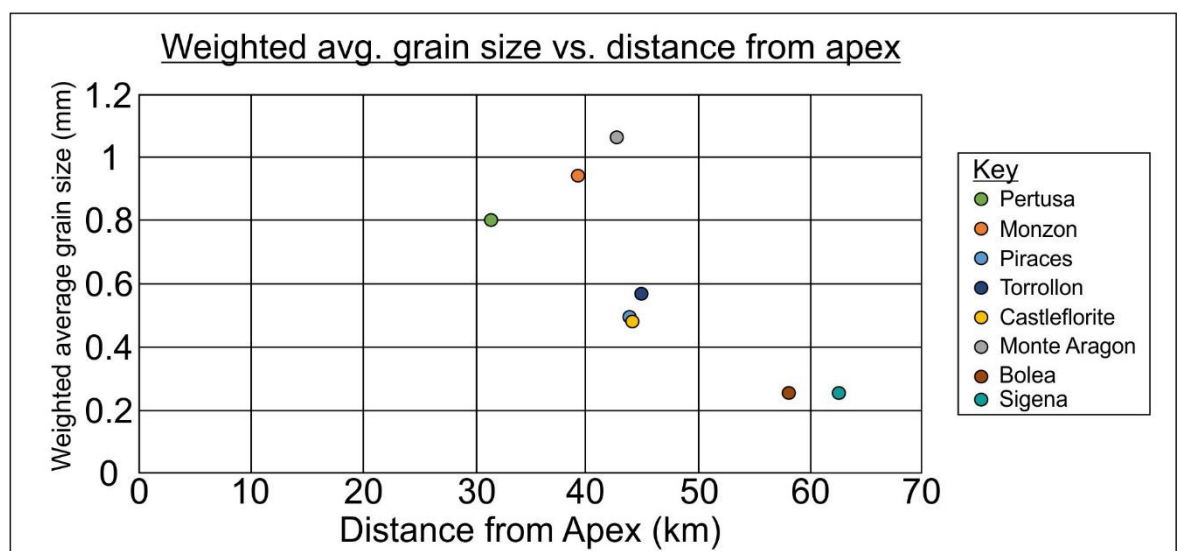
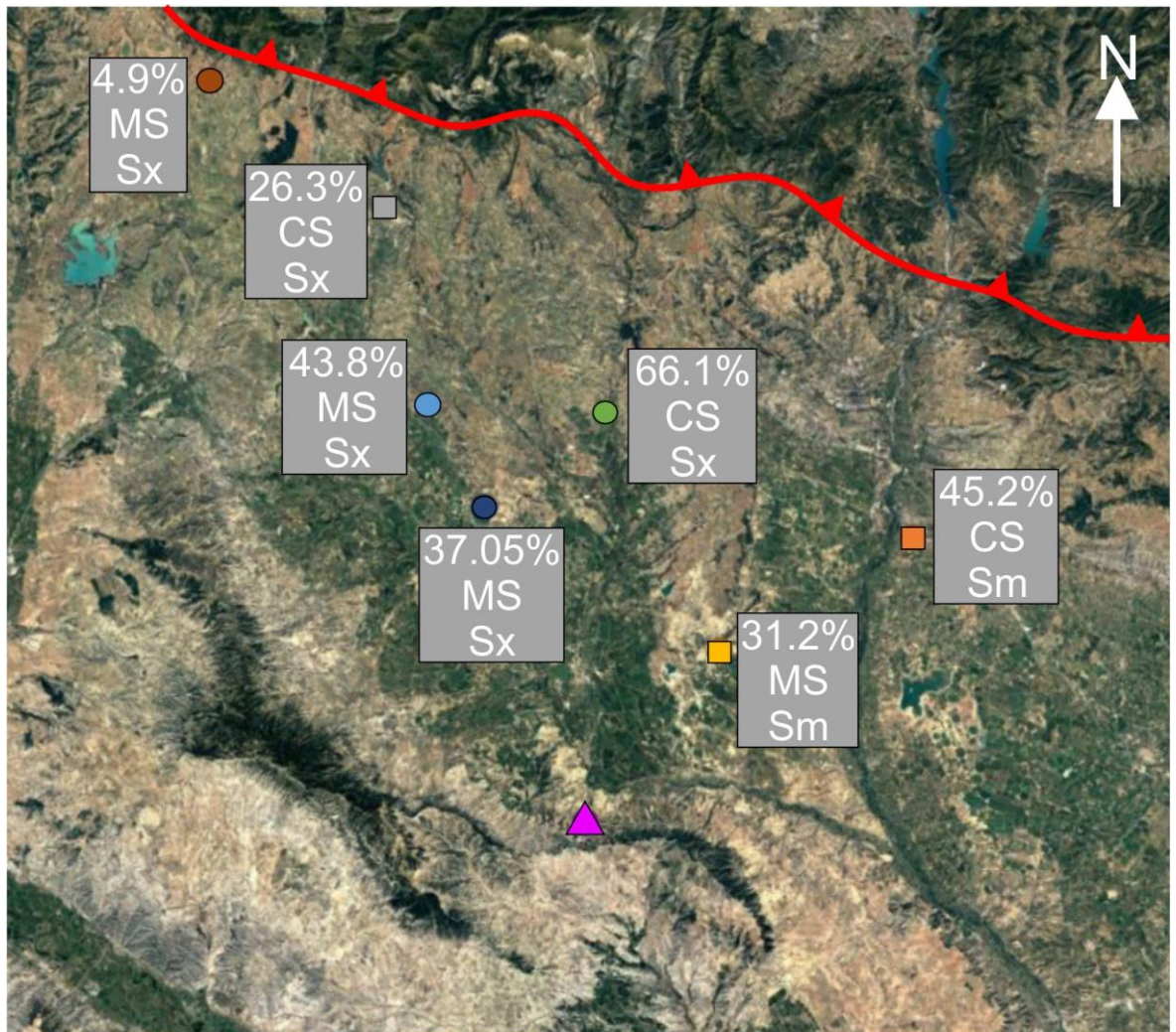


Figure. 25: Graph indicating a shift in grain-size with increasing distance from the apex estimate of Naval. Proximal areas show high degrees of grain-size variation within outcrop with Monte Aragón existing as an outlier due to its proximity to the basin margin.



Key - Locations	
● Pertusa	● Monzon
● Piraces	● Torrollon
● Monte Aragon	● Bolea
● Sigena	—▲— Basin Margin
● Castleflorite	
Key - Data Type	
● Field and Virtual Outcrop Data	■ Field Data Only
▲ Virtual Outcrop Data Only	

Figure 26: Location map showing the position of each outcrop in relation to one another. Data collected from the field is shown next to outcrops in the order of channel-body percentage; average grain size and dominant facies.

Torrollon, Piraces and Castleflorite all exhibit similar average grain sizes (0.567 mm; 0.49 mm and 0.479 mm respectively) decreasing with distance, passing later into fine-grained, distal channel bodies of Sigena. Distal channel bodies observed at Bolea and Sigena both exhibit grain sizes of 0.25 mm, potentially suggesting that there is a finite decrease in grain size that can occur downstream before channel bodies can no longer form in the distal regions of the system due to loss of erosional power.

3.2B) Paleocurrent Analyses

Paleocurrent directions were measured using cross-bedded strata within channel deposits in order to construct a paleocurrent map. Generally, a south-westerly direction is observed (Figure. 24), supporting Hirst's (1991) original findings with paleoflow observed at the westerly deposits of Bolea and Monte Aragon oriented west whilst the axial channel deposits

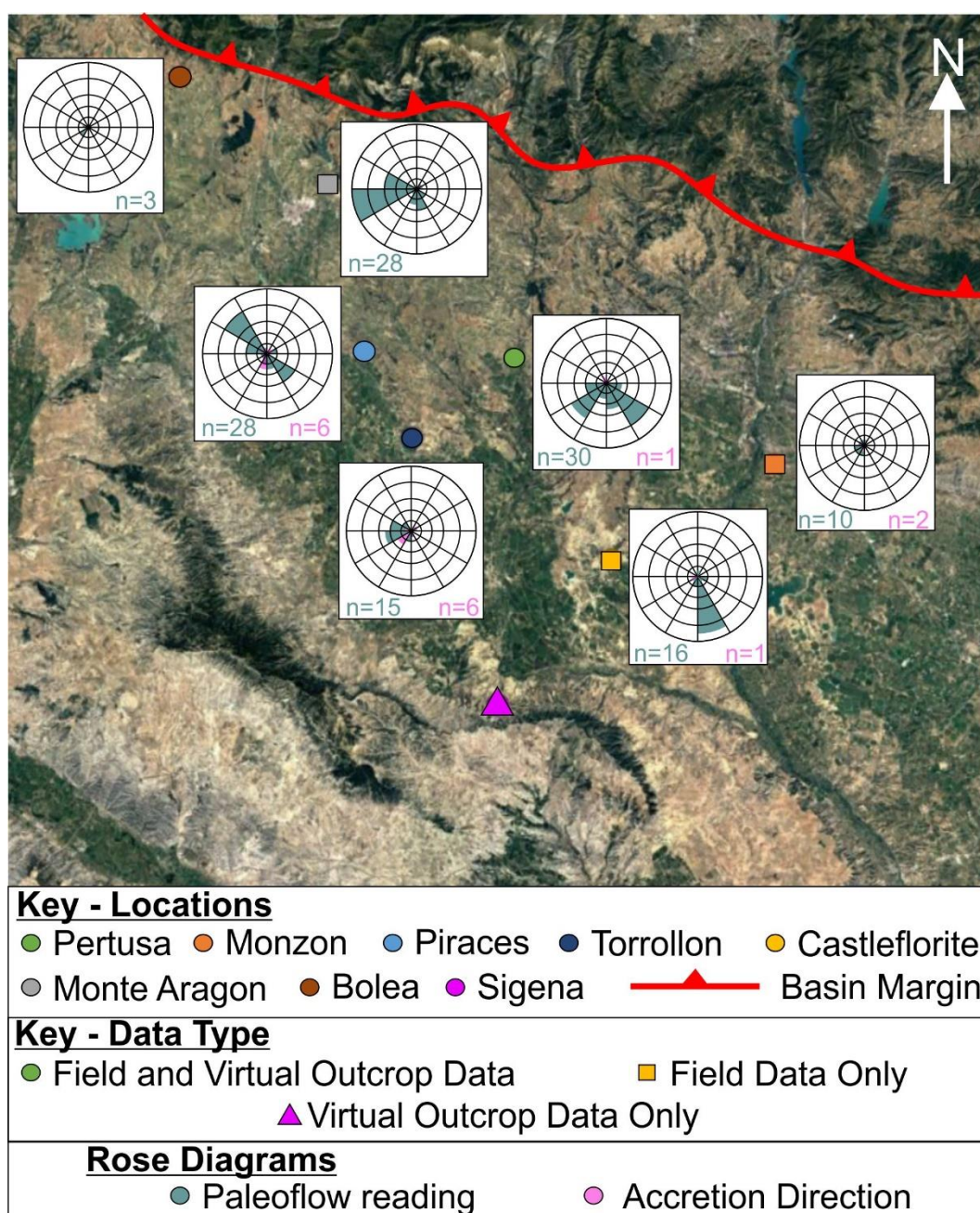


Figure. 27: Location map indicating the basin margin, estimated apex and the studied successions respective locations. Channel paleocurrent data is shown with both regular paleoflow indicators and facies association directions detailed.

of Pertusa and Castleflorite typically flow south. Paleoflow dispersion is focussed between the south and west of the system, likely due to a flow from the source area being diverted when entering the basin. The cause of this diversion is yet to be determined and is outside the scope of this paper however will be a point of interest for future works. At current, no paleocurrent data has been collected east of Monzon due to disruption by the Barbastro anticline.

3.2C) Channel-body Percentages

Channel body percentages were calculated from each log section studied through the basin in order to assess the variability of deposits across the system but also through vertical sections. Covered sections or where exposure was too poor to determine the underlying deposits were either inferred due to exposure of strata laterally or indicated as not observed. In most cases, areas of no/poor exposure were inferred to be siltstones however log locations were chosen to avoid poorly exposed strata as much as possible. Channel body deposits made up a total of 36% of all sediments logged across the system, although channel percentages within individual successions range from 66% to 4% as shown by Figure. 25. The highest channel percentages are observed towards the eastern basin margin in proximal areas with the lowest towards the southerly and most westerly successions. A general downstream trend can be observed with a systematic reduction in channel body percentages.

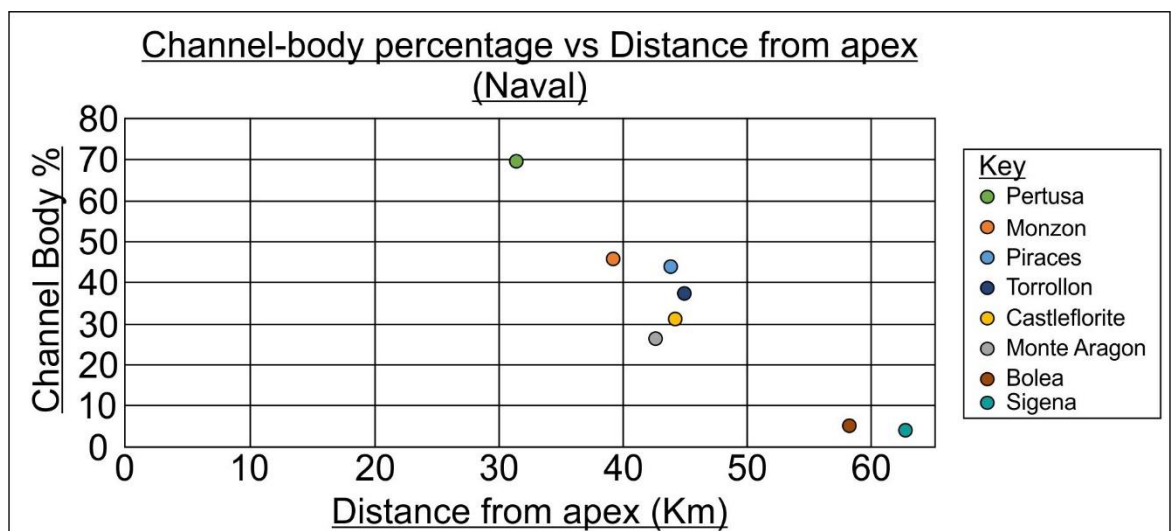


Figure. 28: Channel body percentage plotted against distance from the Naval apex. A downstream trend is observed showing a decrease in channel body percentage.

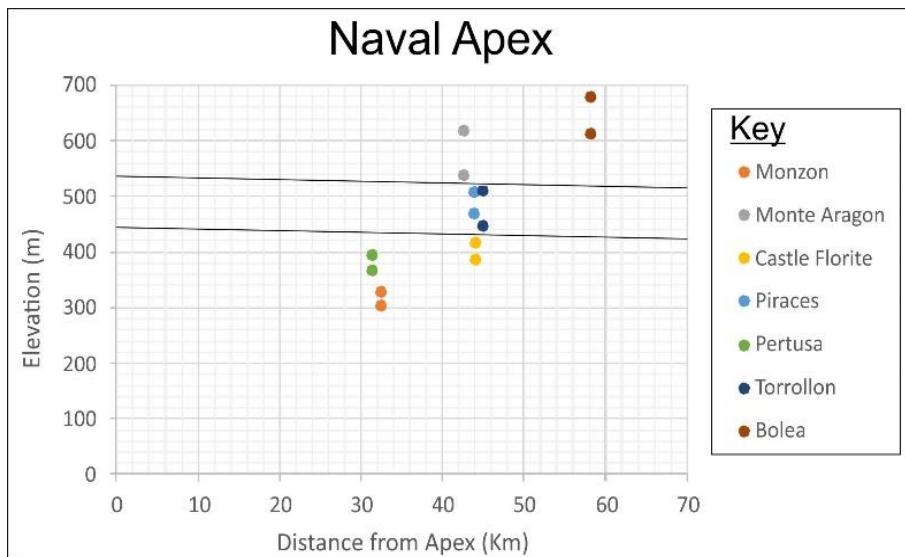


Figure. 29: Estimated temporal groupings of successions determined using elevation vs apex distance data.

Spatial variability is noted within the system, specifically between the medial Castleflorite, Piraces and Torrollon successions. The medial section of the system appears to have a high degree of spatial variability which is yet to be fully characterised. Due to a lack of age data, defining which successions were deposited contemporaneously is difficult, however estimations plotting elevation heights against distance from the apex have provided an estimate into which groups of successions are most closely related (Figure. 26). It should be noted that Torrollon and Monte Aragon show significant differences in elevation height, suggesting these deposits may have been deposited at separate times within the system's history. It is inferred that the deposits at Monte Aragon are older due to this data, however the two show a similar distance from the apex point, Monte Aragon being closer when using the Naval apex. This suggests that the (inferred) older Monte Aragon deposits may have experienced different conditions of deposition when compared with Piraces such as climate; sediment supply; palaeosol development and frequency of channel avulsion may have impacted on this. The grain size analysis (Figure. 23), paleo-current data (Figure. 24) and channel body percentage data (Figure. 25) all support this inference as Monté-Aragon exhibits clear differences from all other locations within the study.

3.2D) Channel-body thickness trends

To analyse the thickness of channel deposits, three quantities were used: average channel-body thickness; maximum channel-body thickness and average storey thickness. These values provide descriptive statistics to determine how channel deposits vary across the system within each succession. The highest average channel-body thickness values could be observed within the most proximal deposits of Pertusa and Monzon with the lowest observed at the distal deposits of Sigena and Bolea (Figure. 27). Average thicknesses range from 8.1 m to 1.7 m with a systematic downstream decrease across the system.

The range in channel-body thicknesses is large (1 m to 20 m) with the largest maximum channel-bodies located at Pertusa and the lowest observed at Sigena (Figure. 28). Downstream decreases in maximum channel-body thickness are observed with high heterogeneity observed within individual vertical successions. Typically, proximal and distal deposits are seen to show strong positive correlations with channel bodies thickening upwards such as at Pertusa, Monzon and Bolea (Figure. 22). Medial deposits however appear to show very weak to no clear correlation within vertical successions. The Torrollon and Piraces successions show a very weak to weak correlation with deposits thinning and thickening again whilst Castleflorite shows a weak negative correlation with channel-bodies generally thinning vertically through the succession (Figure. 22).

When discussing channel bodies, we must also consider storeys and storey surfaces. Storey surfaces are defined as erosional surfaces from the active portion of a channel base that incises into previous channel deposits (Owen et al., 2017). This means that single channel bodies may be comprised of multiple storey surfaces, all representing individual channel-forming events. Storey thicknesses range from 1 m to 5.9 m (Figure. 29) with average thicknesses from 1.6 m to 3.5 m. The logs taken through the Huesca deposits typically didn't pass through multi-storey channel-bodies, often due to the inaccessibility of such deposits. More studies are required to allow fair representation of storey surface frequency and thicknesses. The available data collected however showed that the thickest storeys occurred within the proximal succession of Pertusa with decreasing thicknesses downstream within the medial Castleflorite and Torrollon successions. Storey surface frequency also decreases downstream.

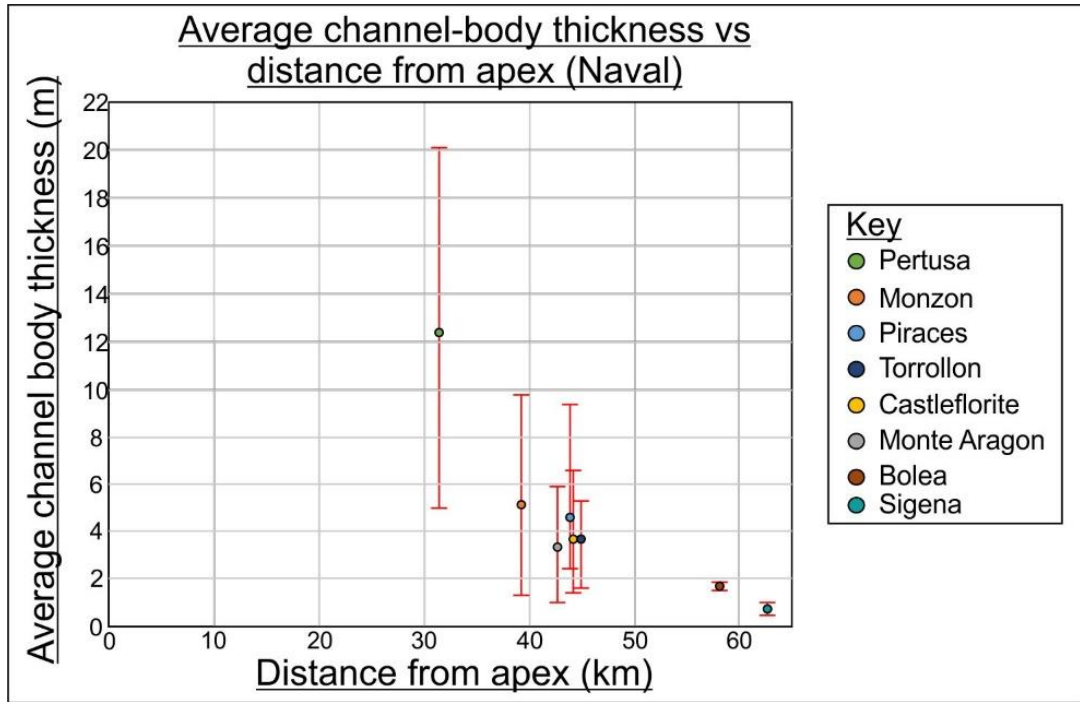


Figure. 30: Average channel-body thicknesses shown decreasing with distance from the estimated apex. Monte Aragon is anomalous however this is thought to be due to the lateral position from the est. apex.

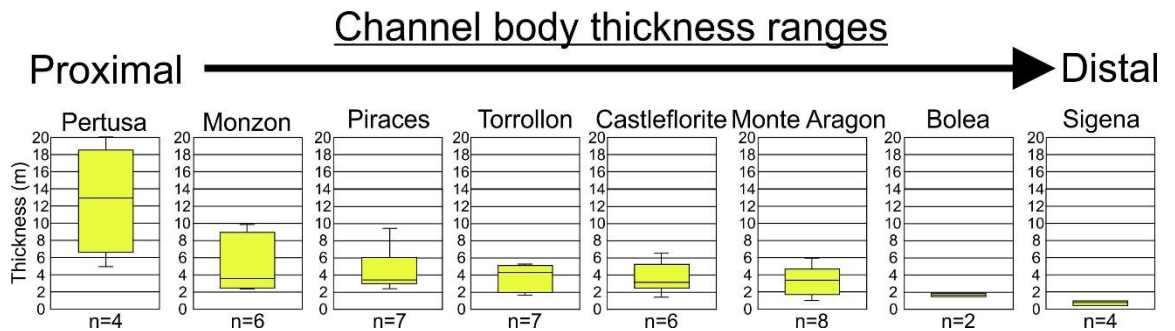


Figure. 31: Range of channel body thicknesses shown generally decreasing downstream. Channel ranges also fluctuate downstream in a less predictable manner.

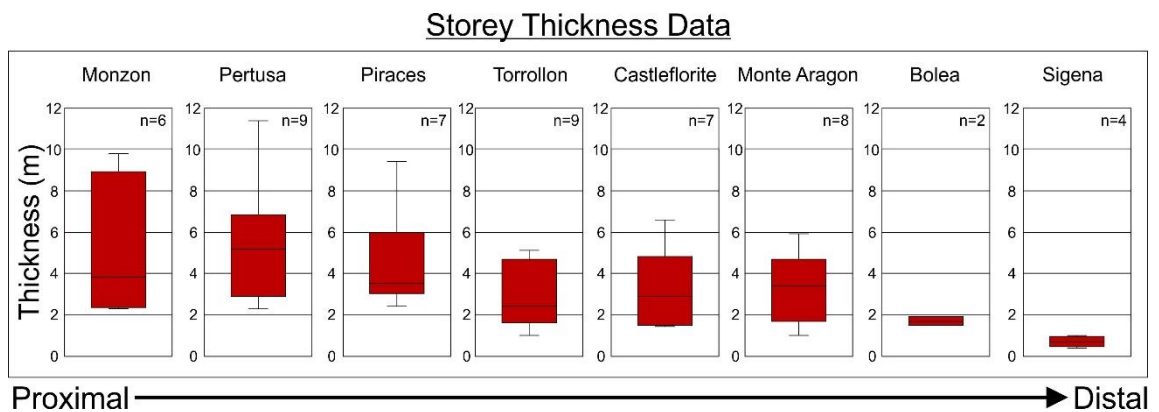


Figure. 31: Storey thickness ranges observed in locations where multiple channel bodies were stacked and underlying deposits eroded into.

3.3 Architecture Panels

Channel body geometries were briefly discussed in the previous chapter however this section aims to consider each outcrop individually and discuss the vertical distribution of channel bodies and associated geometries in relation to one-another. To do this, the channel body geometry scheme of Owen et al. (2017) was applied (Figure. 30).

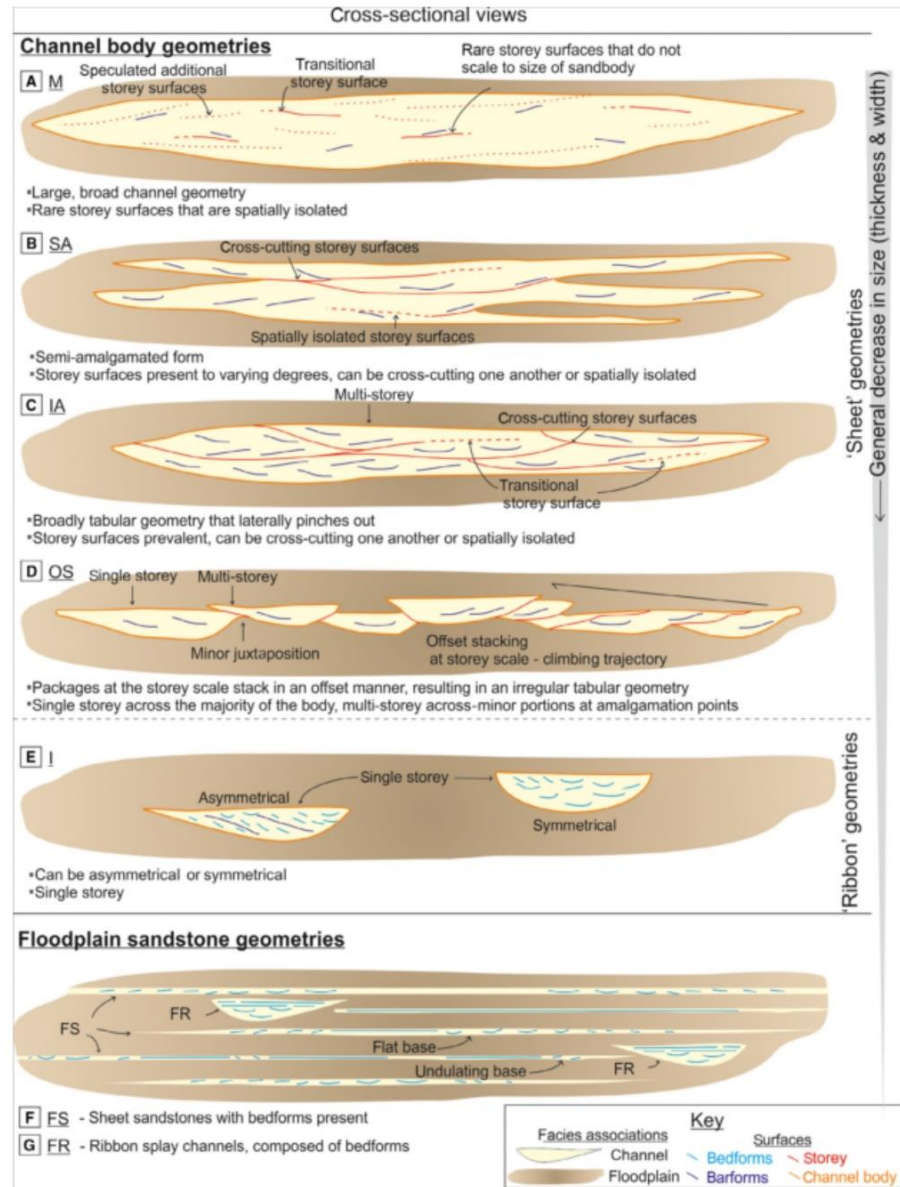


Figure. 33: Channel body geometry scheme of Owen et al. (2015) illustrating Massive, Semi-amalgamated, Internally Amalgamated, Offset Stacked and Isolated geometries.

3.3A) Pertusa

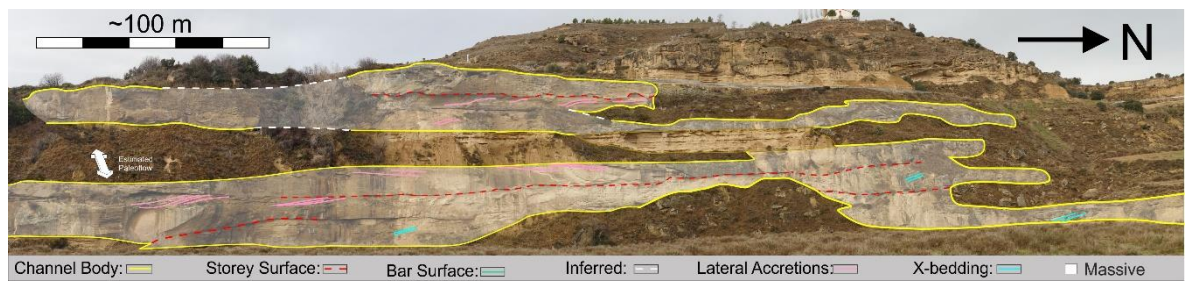


Figure. 34: Pertusa outcrop panel taken from across the river. Multiple channel bodies are observed.

The Pertusa outcrop is located within the most proximal region observed within this study at 31.5km from the estimated apex. The outcrop is observed alongside the river cutting through Pertusa and at a roadcutting higher up. Deposits can be traced along the edge of the river to the South however the outcrop cannot be traced over large distances. The outcrop is roughly 70 m in height with a dip of 0-1°. The channel geometries observed at Pertusa consist of Massive, Internally-Amalgamated and Offset-Stacked (not visible in this panel) with Massive dominating. The Massive channel bodies are present within the lower and medial sections of the image, split by a floodplain package. The Internally-Amalgamated channel body observed in the upper section consists of multiple stories and barforms alongside large cross-sets. The middle channel body is the largest with a maximum thickness of 20 m; multiple storeys; lateral accretion surfaces which may be observed alongside large cross-sets. Massive channel bodies extend over 100s of metres laterally. There is a fairly strong correlation between log height increasing in tandem with increases in channel body thicknesses (Figure. 22), thought to be due to progradation of channel bodies into the system.

3.3B) Monzon

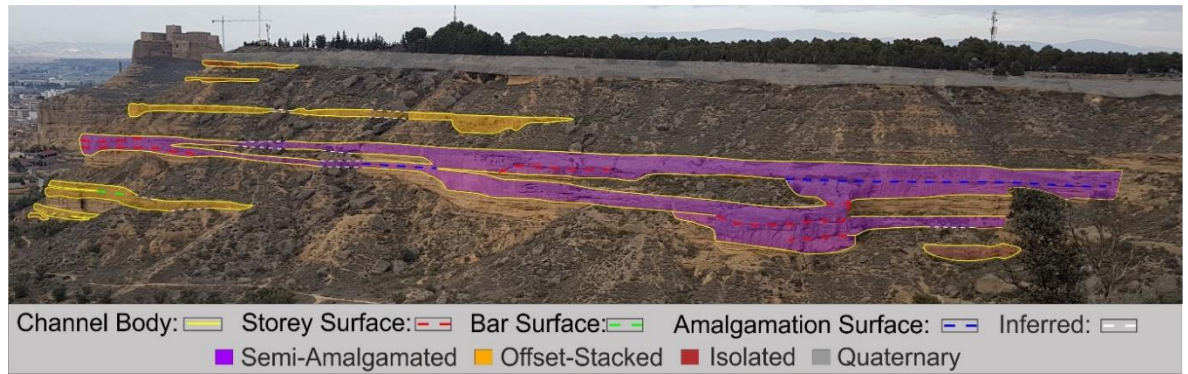


Figure. 35: Monzon outcrop panel taken above the path opposite the outcrop.

The Monzon outcrop is identified as a proximal-medial position within the system, located approximately 37 km from the estimated system apex. The outcrop, shown in Figure. 32, extends over roughly 400 m with an estimated dip of 10° towards the south-southwest with a succession height of up to 90m. The locality exists within a valley meaning that some channel bodies can be observed/inferred across either side. Outcrop is generally easily accessible with scree slopes and vegetation covering some areas. Channel geometries observed are semi-amalgamated, offset-stacked and isolated with maximum channel body thicknesses of 9 m observed with up to 4 storeys present. Offset-stacked geometries dominate the outcrop within the lower and medial succession before giving way to isolated, sheet-like channel towards the upper outcrop sections. Offset-stacked geometries extend laterally across the full outcrop extent within the medial section of outcrop with a maximum of 5 storeys observed and highlighted within Figure. 32. Within the medial section of the outcrop, pockets of floodplain may be observed separating channel deposits creating an SA geometry. The isolated channels observed in the upper section only extend over <10's of metres and exhibit classic “ribbon” geometries that spread to sheets laterally.

3.3C) Piraces

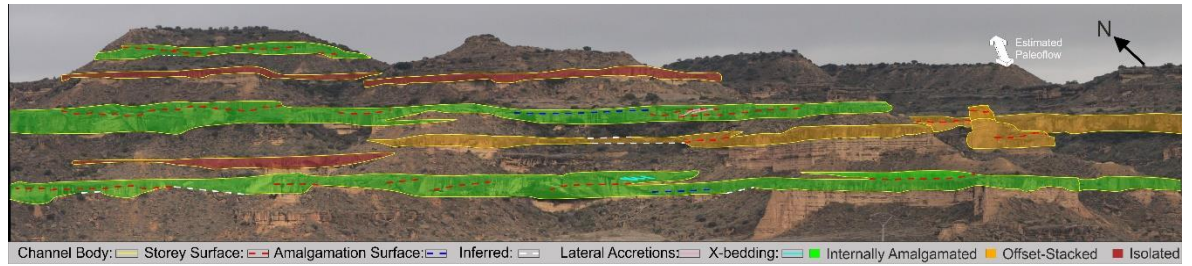


Figure. 36. Piraces outcrop panel taken from the roadside descending towards the village.

The Piraces outcrop is located within the medial zone of the Huesca DFS, approximately 43.5 km from the estimated apex point of the system. The outcrop is part of an outcrop belt that can be followed over several kilometres and contains the Torrollon outcrop. The logged succession is approximately 70 m in height with a dip of 1-2° towards the southwest. The outcrop exists within a valley and therefore channel deposits can be observed on both sides of the valley. Channel geometries observed are Internally-Amalgamated, Offset-Stacked and Isolated. The dominant geometry type is Internally-Amalgamated. The large IA bodies can be observed within the basal and medial parts of the succession, interspersed with OS and I channel geometries. Maximum channel body thicknesses reach 9 m with multiple stories (3-4) noted throughout the succession. Isolated channel body geometries dominate the upper succession with classic “ribbon” channel geometries. There is no correlation between increasing log height and channel body thickness or geometry changes within the Piraces deposits as shown by Figure. 22. As detailed in Figure. 22, channel bodies thicken and thin upwards through the succession, potentially due to progradation and retrogradation of the system during deposition.

3.3D) Torrollon

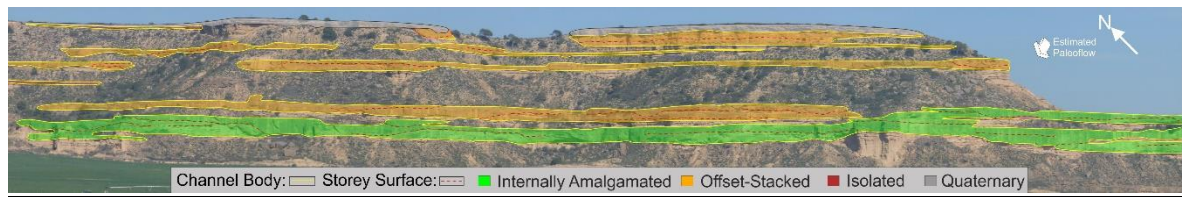


Figure. 37: Torrollon outcrop panel taken by the reservoir.

The Torrollon outcrop is located within the medial zone of the system, approximately 45 km from the estimated apex and is part of the Piraces outcrop belt. The log taken here extends through the IA body at the base and the OS and I channel body geometries observed on the left of Figure. 34. Deposits dip approximately 1-2° to the southwest. OS channel geometries dominate with a large, laterally extensive IA channel geometry observed at the base of the outcrop. Small isolated bodies are also observed towards the upper section of the outcrop. Maximum channel body thicknesses reach 5.3 m with multiple storeys (3-4) present within large channel bodies. Offset stacked geometries extend over 10's to 100's of metres with IA geometries extending laterally over 100's. A weak correlation between channel body thickness and log height is observed within the Torrollon outcrop. Deposits thin upwards towards the medial section before thickening upwards again (Figure. 22); the presence of the thin, isolated channel geometry which gives way to OS channel geometries again towards the upper section of the outcrop may suggest that this location experienced retrogradation of channels before later progradation of the channels back into the system.

3.3E) Castleflorite



Figure. 38: Castleflorite outcrop panel taken from the service road next to the reservoir.

Castleflorite is present within the medial section of the system, approximately 44 km away from the estimated apex. The log taken here extends approximately 70 m vertically and passes through offset-stacked and isolated channel geometries. Deposits are dominated by offset-stacked channel geometries, the thickest reaching a maximum of 6.6 m thick with lateral extents of 10s to 100s of metres. Multiple storeys are noted in the large OS body in the centre of the outcrop with a maximum of 3. Large cross beds can be observed within the medial offset-stacked channel body. Offset-stacked channel geometries show a large vertical component with a small lateral component. A weak, negative correlation is observed through the outcrop (Figure. 22), potentially due to retrogradation of the channels through the system during deposition. This is supported by the lack of channel bodies within the upper outcrop. Due to large amounts of scree and poor exposure in the logged section, as seen in Figure. 35, picking out channel bodies in the image is difficult which is why the upper section of the outcrop image is lacking in channel bodies.

3.3F) Monte Aragon

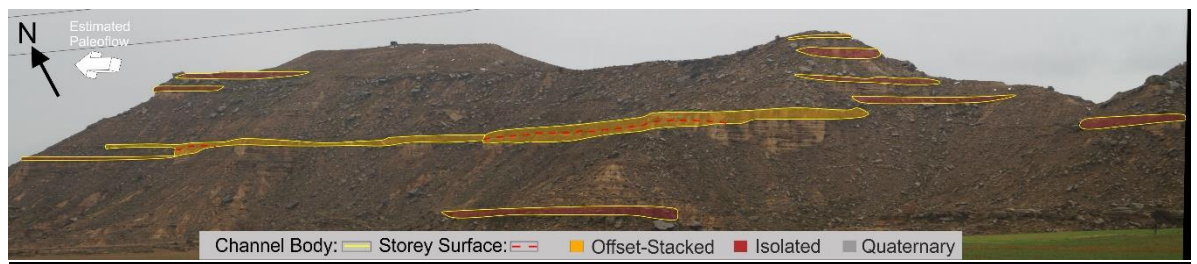


Figure. 39: Monte Aragon outcrop panel taken by the farm road at the edge of the Quicena village.

Monte Aragon is located in the distal, lateral fringe of the Huesca DFS towards the West, approximately 42.7 km from the estimated apex. Whilst Monte Aragon is situated the same distance from the estimated apex as Torrollon, Piraces and Castleflorite, this locality sits proximal to the basin margin. This results in highly immature material (Figure. 23) alongside domination of isolated channel geometries allowing for a distal outcrop profile. The log extends over 100 metres with a singular offset-stacked channel geometry observed within the medial section of the deposit, made up of two storeys. Maximum channel thickness reaches 5.9 m with maximum lateral extents of channel bodies approximately 200m. A very weak negative correlation exists within the Monte Aragon outcrop (Figure. 22), with a general trend in decreasing channel thickness towards the medial outcrop before thickening upwards again, potentially a result of retrogradation and progradation of channels into the system (Figure. 22).

3.3G) Bolea

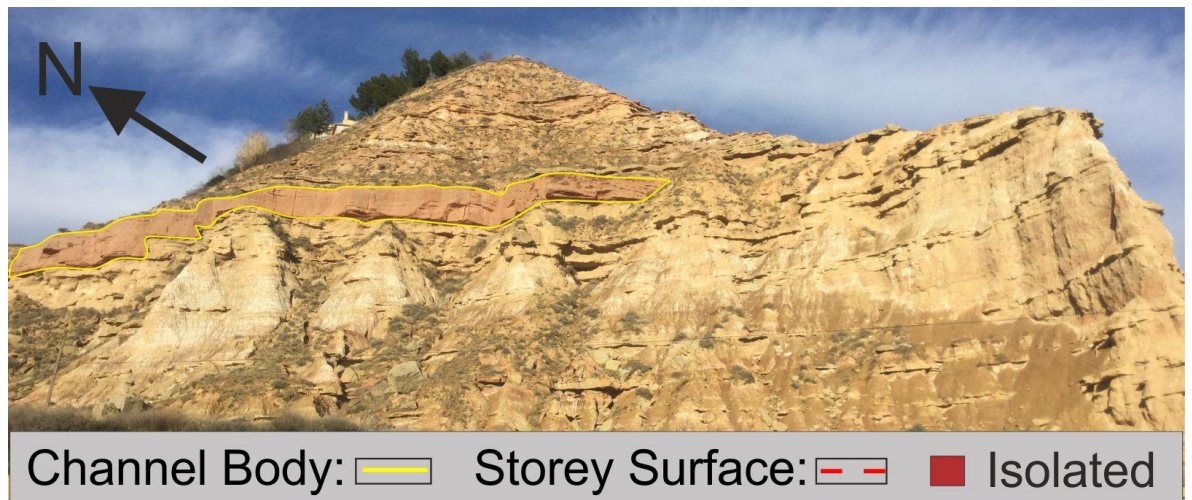


Figure. 40: Bolea outcrop photo taken at the bottom of the turning towards the village.

Bolea is the most distal locality visited situated on the western fringe of the system, approximately 58.2 km away from the estimated apex. Bolea therefore has relatively coarse channel bodies for a distal locality (0.25 m) and a maximum channel body thickness of 1.9 m and a lateral extent of 10's of metres. All channels observed have isolated channel geometries encased by floodplain material and consist of singular storeys. A strong correlation exists with channel bodies thickening upwards (Figure. 22), likely due to progradation of channel bodies out into the lateral fringes of the system.

3.4) Summary

This chapter discusses the prior findings of Hirst (1991) and uses a revised apex estimation in combination with vertical trend analyses and statistics to accurately identify downstream trends observed throughout the outcrops studied. Decreasing channel body thickness, frequency and shifts from massive channel geometries to isolated channel geometries downstream are all observed within outcrop; paleocurrents observed within Figure. 24 also show a radial flow pattern; all characteristics of distributive fluvial systems. Channel bodies in the proximal and medial regions are often comprised of multiple storeys with a decrease in storey frequency downstream also. Analyses using Spearman's Rank has allowed for the identification of correlations between log height and channel body thicknesses, with both positive and negative correlations identified with the medial deposits (Piraces, Torrollon and Castleflorite) all showing very weak/no positive and negative correlations, further emphasising that the medial zone within the DFS is the most poorly understood and difficult to understand.

Chapter 4

4.0) Lateral Variation within Outcrops

In the previous chapter it has been shown that there are considerable downstream trends in the Huesca distributive fluvial system, however this was largely conducted through the analyses of single logs at various locations downstream. This chapter will focus on analysing the lateral variation of channel proportions at selected intervals down the fluvial system. This will be achieved through the use of virtual outcrops to examine how channel bodies change laterally across outcrops. This analysis is integral to further developing our understanding of fluvial reservoirs associated with distributive fluvial systems. By calculating the net:gross for multiple logs, we can begin to understand and quantify variation; how geometry of bodies changes laterally and the degree of channel interconnectivity within outcrops. There are great implications for resource exploration and provides a potential analogue to estimate net:gross and channel inter-connectivity within

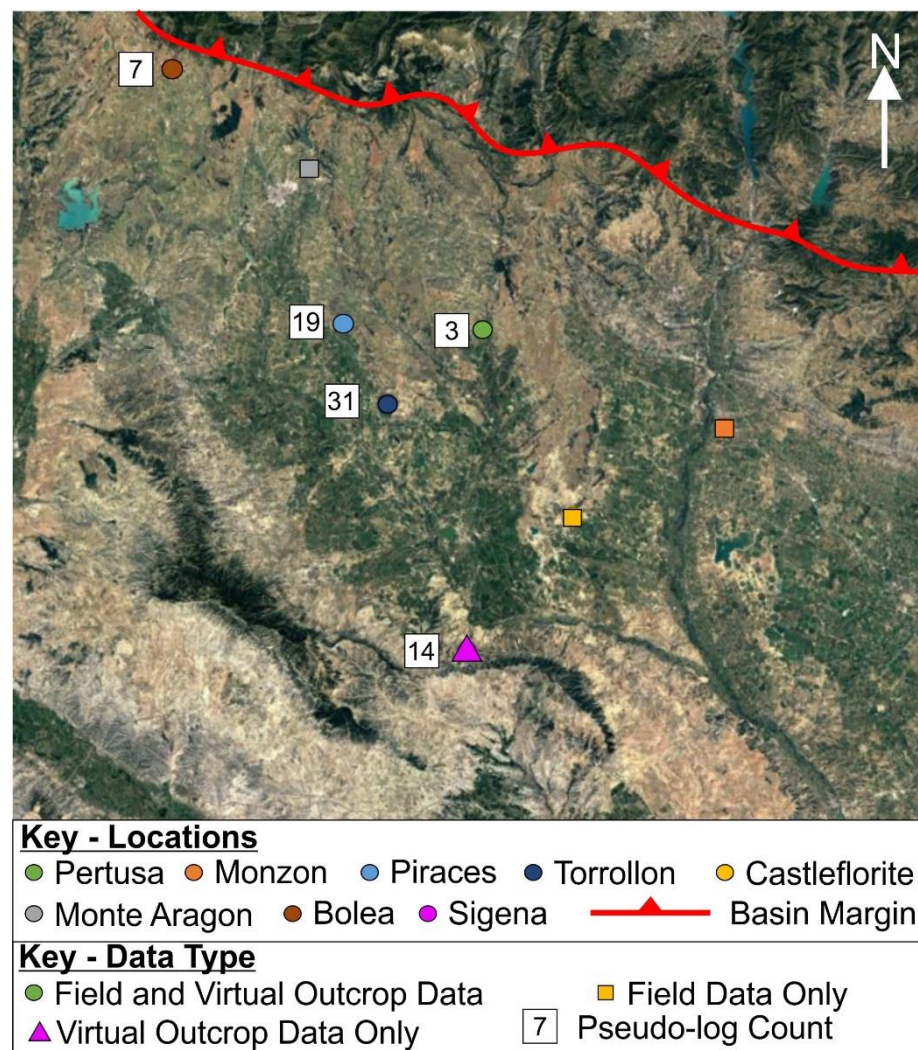


Figure. 41: Location map detailing the number of logs taken for data analyses where virtual outcrop models are available.

exploration targets for resources such as oil and gas plays and aquifers. This analysis was completed at all locations at which virtual outcrop models were available, namely Pertusa (Proximal); Piraces (Medial); Torrollon (Medial); Bolea (Lateral Fringe) and Sigena (Distal Fringe).

Through taking accurate measurements in pseudo-logs, we can quantify an approximate net:gross value for multiple logs rapidly across the outcrop sections observed in the field. Pseudo-logs consist of approximate logs created using the built-in drawing package within the LIME VOG software which allows for accurate vertical measurements on a centimetre-scale to be taken. Logs are comprised of sandstones, floodplain and inferred floodplain where scree or vegetation does not allow for direct observation of the geology. Logs have the potential to jump where poor exposure does not allow determination of the underlying geology; where the underlying geology could be inferred, this is indicated.

A more extensive dataset was collected for both the Piraces and Torrollon outcrops due to their extensive nature and the high degree of variation within outcrops. Fence panels were therefore collected to help visualise the collected data and lateral variability.

4.1A) Pertusa

The Pertusa pseudo-log dataset is relatively limited with only 3 pseudo-logs taken due to the quality of the virtual outcrop model collected alongside poor exposure of outcrop in the section. Some of the measured logs contained channels where the full thickness could not be observed. These channel bodies were not included in the data analysis to prevent bias within the results. Pseudo-logs collected at Pertusa ranged in thickness from 35 m to 42 m.

Generally, across the outcrop over a spacing of 100m, variation of deposits was limited with consistent channel thicknesses observed. Channel bodies were of the Massive and Internally Amalgamated geometry types (Chapter 2.4A/B) with relatively little floodplain observed in pockets.

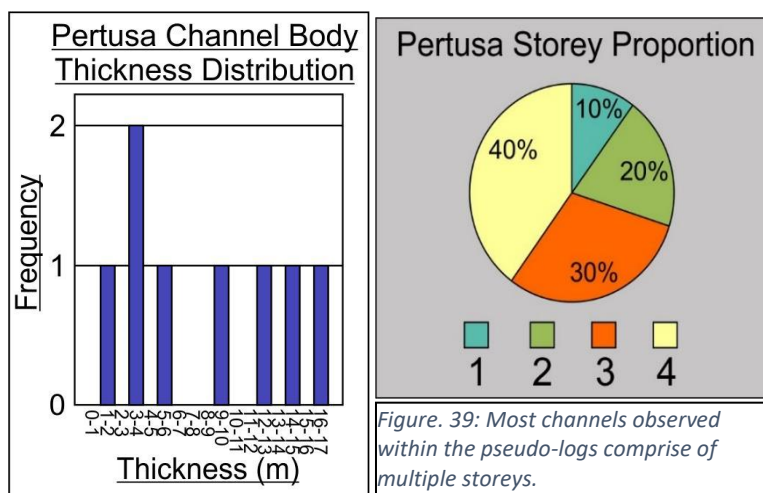


Figure 42: Pertusa channel body thickness and storey proportion.

The Pertusa pseudo-log data exhibits a relatively small range between 77% and 67.5% (9.5%) of channel-body percentage values and an average of 71.3%. The field log presented a channel proportion of 66.1%, the only field log value that falls below the calculated pseudo-log average. Channel body thicknesses ranged between 16.3 m and 1.7 m thick with an average channel body thickness of 8.2 m. Storey data showed thicknesses ranging between 8.4 m and 1.5 m and an average of 4 m, many of which formed channels made of multiple storeys.

4.1B) Piraces

Piraces is situated in the medial portion of the Huesca DFS (Figure. 24), and comprises part of the same outcrop belt as the Torrollon outcrop. Variation in net:gross values are more significant at Piraces in comparison to Pertusa due to its medial position. Nineteen pseudo-logs were collected from the Piraces outcrop model ranged between 45 m and 75 m in thickness and typically pass through 3 channel bodies or more. The pseudo-logs cover a lateral distance of 900 m across the outcrop belt, mainly focussed around the upper outcrop due to poor digital rendering around the base of the model.

A high variance in channel body percentage with a range of 31.9% calculated from 19 pseudo-log sections with a max of 52% and a minimum of 20% is observed. The average channel body percentage calculated is 32.9% in comparison to the field log which exhibits a channel body percentage of 43.8%. The data shows a bi-modal distribution with the majority of logs exhibiting channel-body percentage values between 20-30% and 35-40%.

Channel body thicknesses in the Piraces section range between 14 m and 0.9 m with an average of 5.4 m. Figure. 39 shows the distribution of channel body thicknesses collected from the outcrop. There is a clear multi-modal distribution of channel body thicknesses with a positive skew towards thinner channel bodies (1-4 m thickness). Generally, channels were single storey however where multi-storey channel bodies were observed, these typically consisted of 2 storeys (83%) however instances of 3 (11%) and 4 (6%) stories were noted.

Storey thicknesses exhibit a slightly smaller range of thicknesses from 9.5 m to 0.5 m with an average of 4 m being calculated. The data shows a unimodal distribution with a positive skew towards thinner storey thicknesses with the majority of channel bodies falling between

2-5 m thick. Multi-storey channels appear to have an even distribution across the outcrop with some logs exhibiting several multi-storey channels in succession.

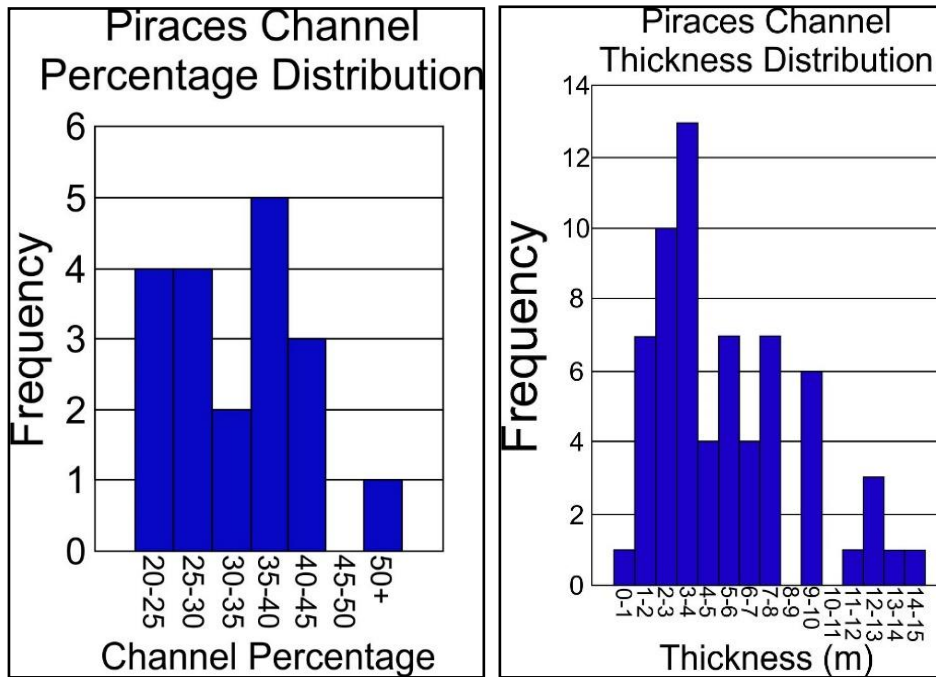


Figure. 43: A split between 20-30% and 35-40% are the most frequent ranges of channel percentage. The distribution of channel thicknesses is multi-modal with positive skew towards thinner channel bodies, typically 1-4 m thick.

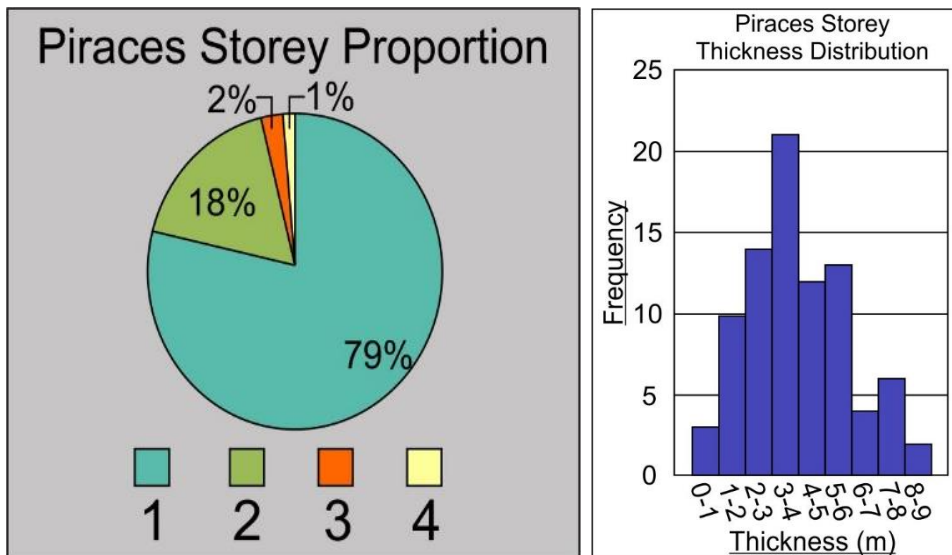


Figure. 44: The Piraces section has a high proportion of single-storey channels. Multi-storey channels are much less frequent in comparison to dual storey channels.

To conduct this stage of research, the models of both Piraces and Torrollon were utilised with a total number of 20 logs taken from each site at an average spacing of 50 m per log (Figure. 42; Figure. 46). The pseudo-log fence panels were created to help visualise outcrop's lateral variability and demonstrate how channel bodies behaved in relation to one another across outcrops.

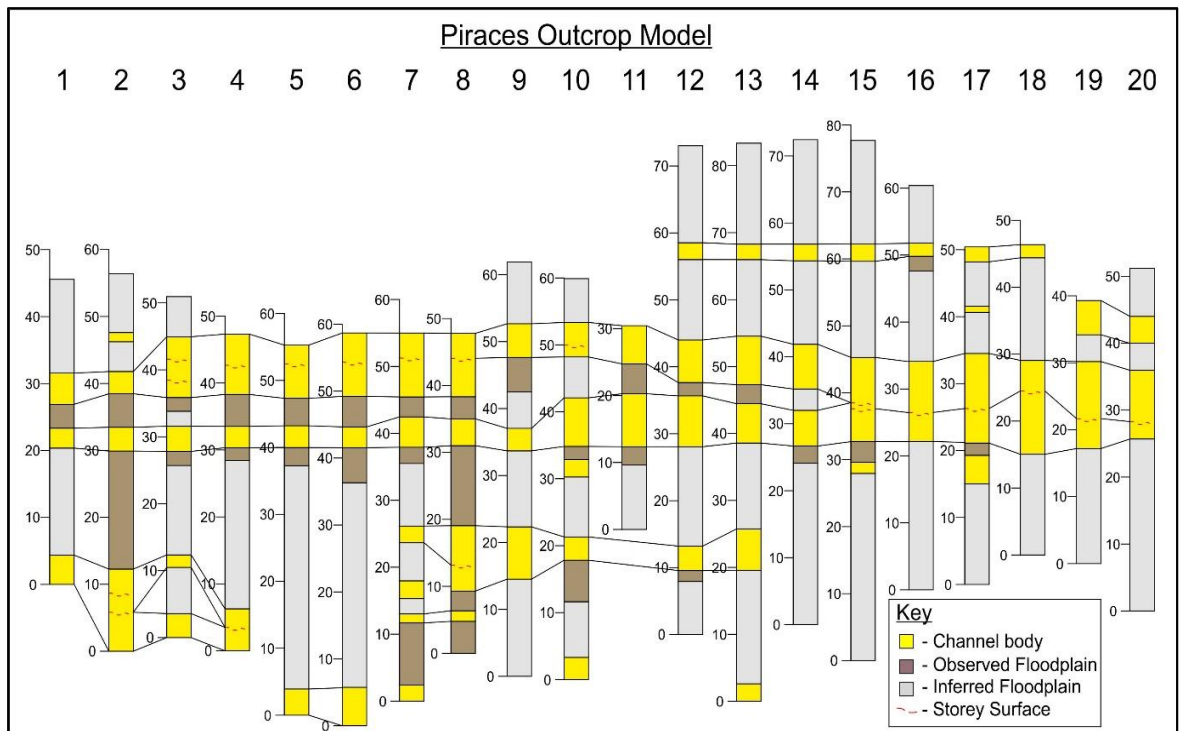


Figure. 45: Pseudo-log fence panel depicting channel bodies and inferred/observed floodplain deposits. Storey surfaces are highlighted in red. The vertical scales has been exaggerated 2 times to ensure minor features in the logs could be recorded.

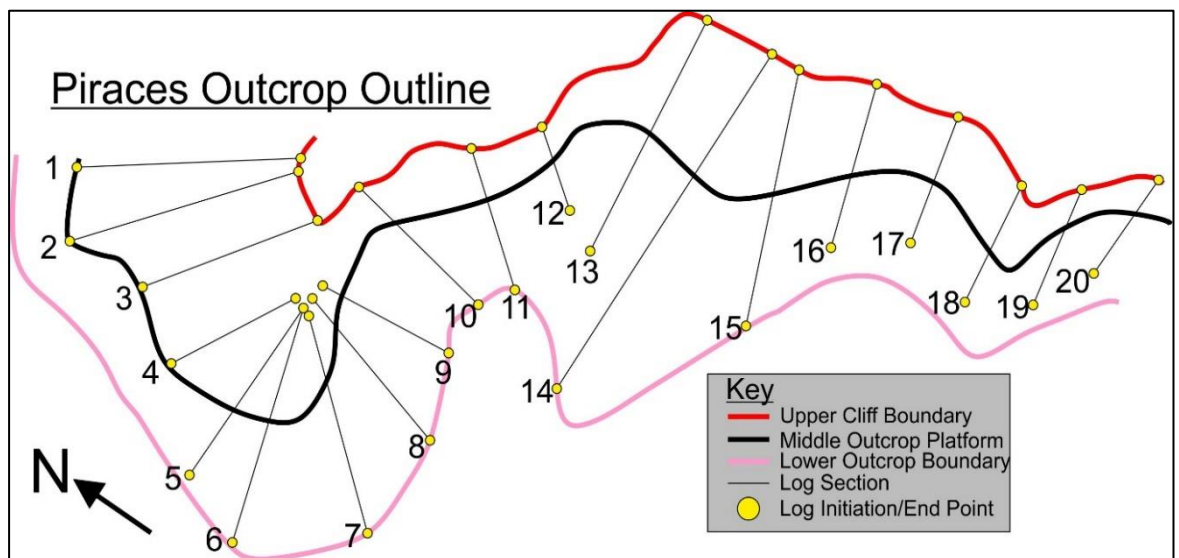


Figure. 46: A bird's eye view of the outcrop showing how log sections relate to one-another.

The Piraces fence panel shows that typically channels are single-storey, or have 2 stories present, with storey surfaces present for large distances across the outcrop. Channels also show large lateral extents, spanning the entire outcrop model as part of a semi-amalgamated channel geometry. Channel bodies remain relatively consistent in thickness across the outcrop. The semi-amalgamated geometry consists of two separate channel bodies that amalgamate, leaving a floodplain pocket sandwiched between the two (See Chapter 2.4B). Channel connectivity within the Piraces outcrop is relatively high due to the high degree of amalgamation in the upper outcrop section.

4.1C) Torrollon

The Torrollon outcrop is also positioned within the medial zone and is part of the same 20 km outcrop belt as Piraces. A large degree of variation is evident both through vertical log sections and laterally across the outcrop belt. Logs range between 39 m and 92 m and span a total lateral distance of 1600 m with full exposure from the base to the top of outcrops common. Thirty log sections were used for data analyses with 20 log sections used in total to create the fence panels to maintain consistency with the lateral variation analyses. All log sections pass through a minimum of 3 channel bodies.

The data collected shows high variance in channel body percentage with a range of 33.6% calculated from 30 log sections with a maximum value of 50.8% and minimum of 17.2%. The average channel body percentage calculated is 34% compared with the field log value of 37.1%. The distribution of channel bodies is unimodal with the majority of channels falling between 30-40% of channel percentage.

The Torrollon pseudo-logs exhibit a variety of channel body thicknesses ranging between 13.4 m and 0.6 m showing an average of 4.6 m. The channel body thicknesses observed show a unimodal distribution and a positive skew towards thinner channel bodies (1 m to 5m thick). Channels typically consist of single storeys however multi-storey (2+) are also observed, comprising 24% of the dataset.

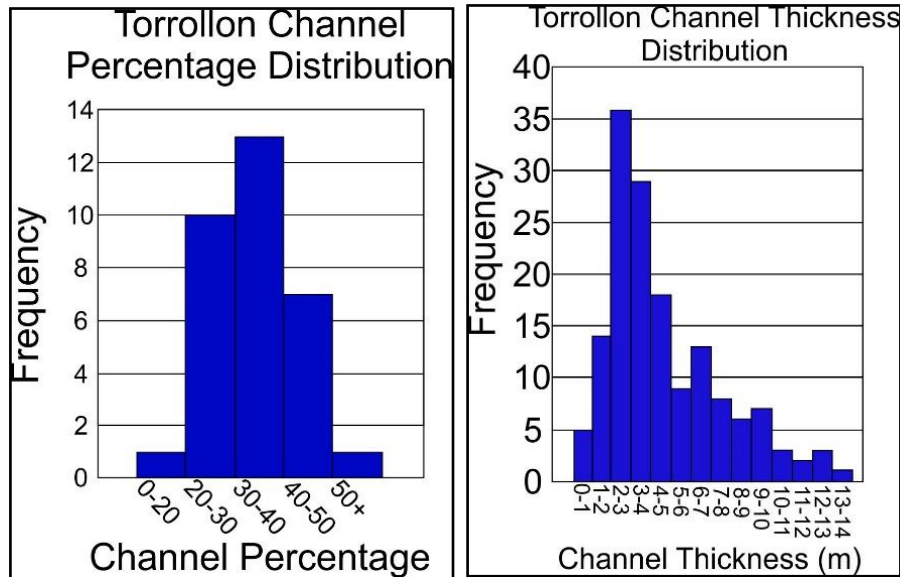


Figure. 47: The Torrollon channel percentage distribution is more unimodal than Piraces with the majority of logs comprised between 30-40% of channel bodies. The channel thickness distribution is similar to Piraces with a more concentrated peak around 2-4 m thick.

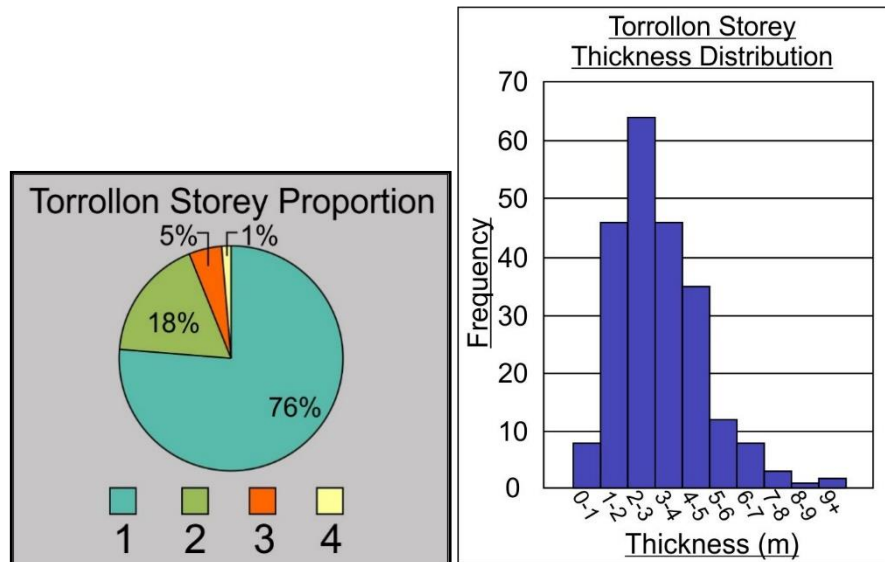


Figure. 48: The Torrollon proportion of dual and multi-storey channel bodies is similar to Piraces with a greater occurrence of triple-storey channels. The histogram presents the unimodal distribution of storey thicknesses.

Storeys exhibit a smaller range of thickness values between 9.2 m and 0.5 m alongside an average of 3.2 m thickness. Storey thickness data exhibits a positive skew and peaks at 2-3 m. Multi-storey and dual storey channels show even distribution across the outcrop belt with a slightly higher density observed in the central section of the observed model.

The Torrollon fence panel exhibits channels with varying degrees of lateral extent (10s to 100s of metres). Typically, the most laterally extensive channel bodies are observed within the lower to mid-sections of the outcrop belt. Many channel bodies consist of multiple storeys and may reach over 10 m's in thickness. These multi-storey channels often shift laterally to become single-storey channels as part of offset-stacked geometries or through the disappearance of storey surfaces. The dominant geometries within Torrollon are comprised of Internally-Amalgamated and Offset-Stacked channel bodies (Chapter 2.4B/D). Moving vertically through the outcrop, there is generally a reduction in channel thicknesses alongside the lateral continuity of channel bodies. Vertical and lateral connectivity also reduces towards the top section of the outcrop.

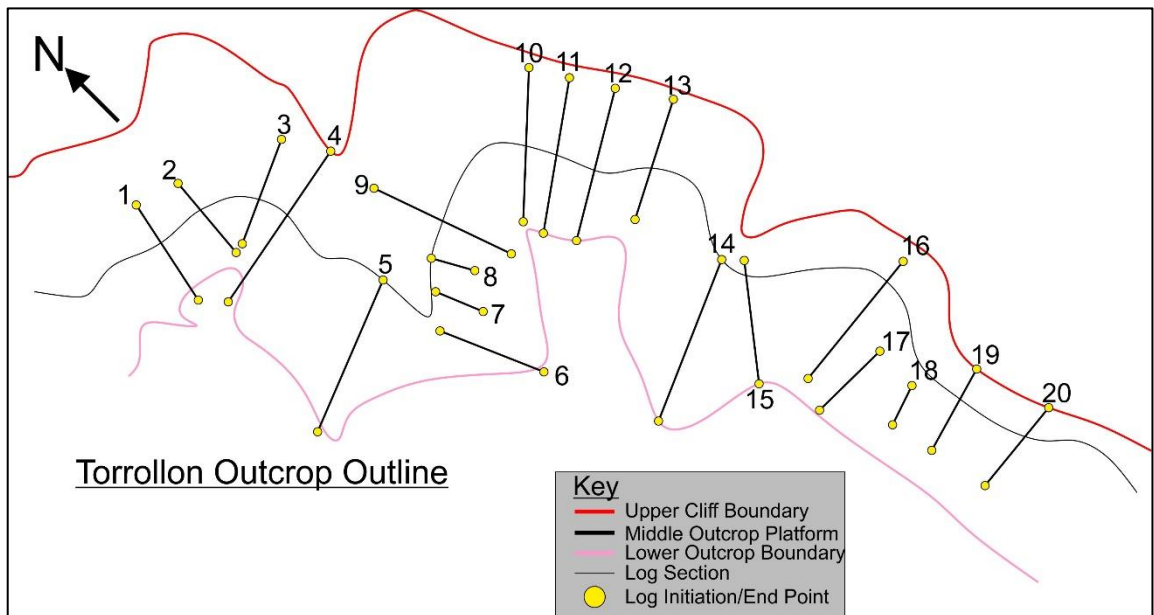
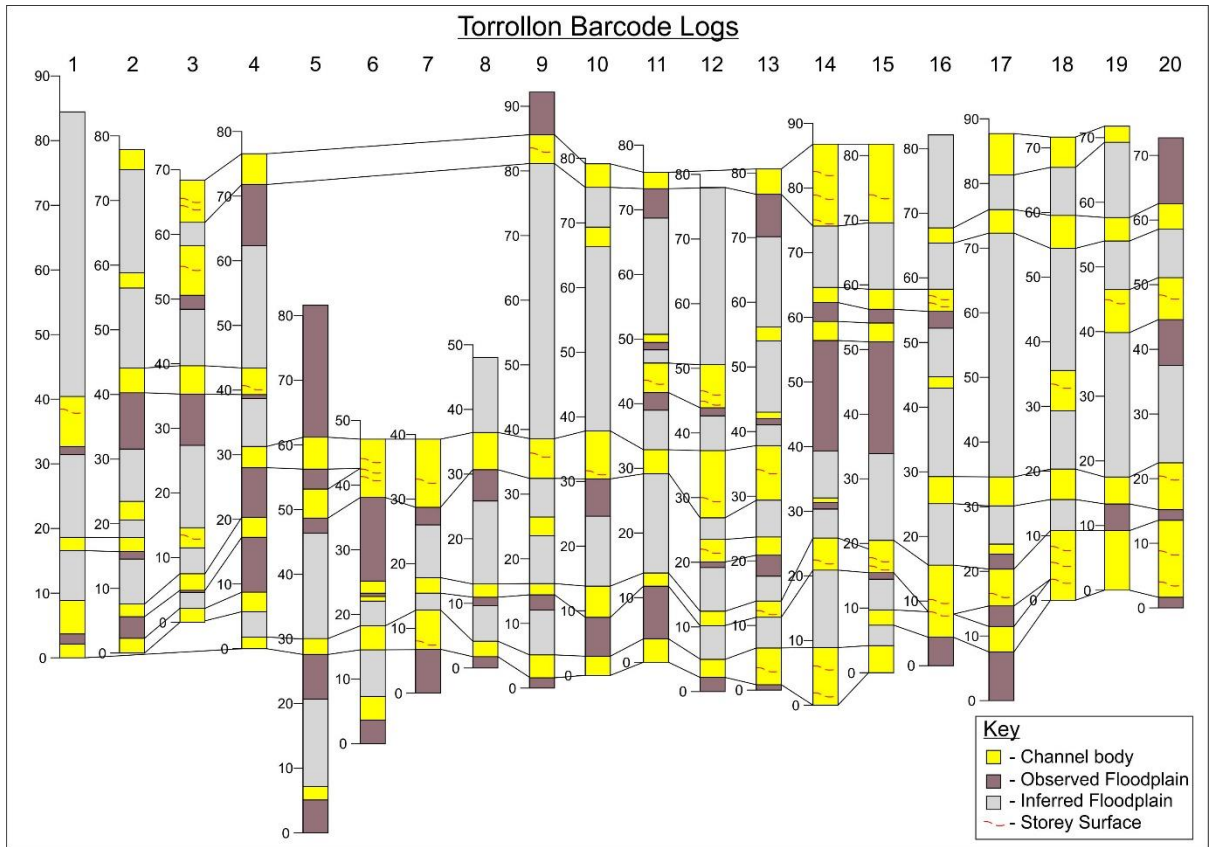


Figure. 49: Barcode log depicting channel bodies and inferred/observed floodplain deposits. Storey surfaces are highlighted in red. The Torrollon Outcrop Outline details how logs are spatially distributed.

4.1D) Bolea – 7 Logs

The Bolea outcrop is observed in a lateral fringe setting of the system along the basin margin and exhibits reduced lateral and vertical variation in comparison with the previously discussed outcrops.

The Bolea virtual outcrop model allows for the observation of a channel body in a three-dimensional section (Figure. 47) and therefore provides a small insight into how the nature of the channel bodies change in space. The 7 Logs range between 51 m and 65 m across a 150m x 100 m outcrop section with full exposure from the base of the section to the top. As the exposure comprises part of a hill section, the base of some logs may be level with the middle of others. Logs generally pass through a single channel body however one log does not exhibit any channel body presence.

The three-dimensional nature of the virtual outcrop model helps to examine how channel bodies change in two planes (A and B). The channel body observed thins along the A plane and continues this thinning into the B plane. The channel body pinches out shortly after following plane B. Overall, the channel body can be followed laterally for approximately 100 m. No palaeoflow indicators can be observed using the virtual outcrop model meaning that channel orientation could not be determined however, literature suggests that the predominant palaeoflow direction is north-westerly (Hirst, 1991).

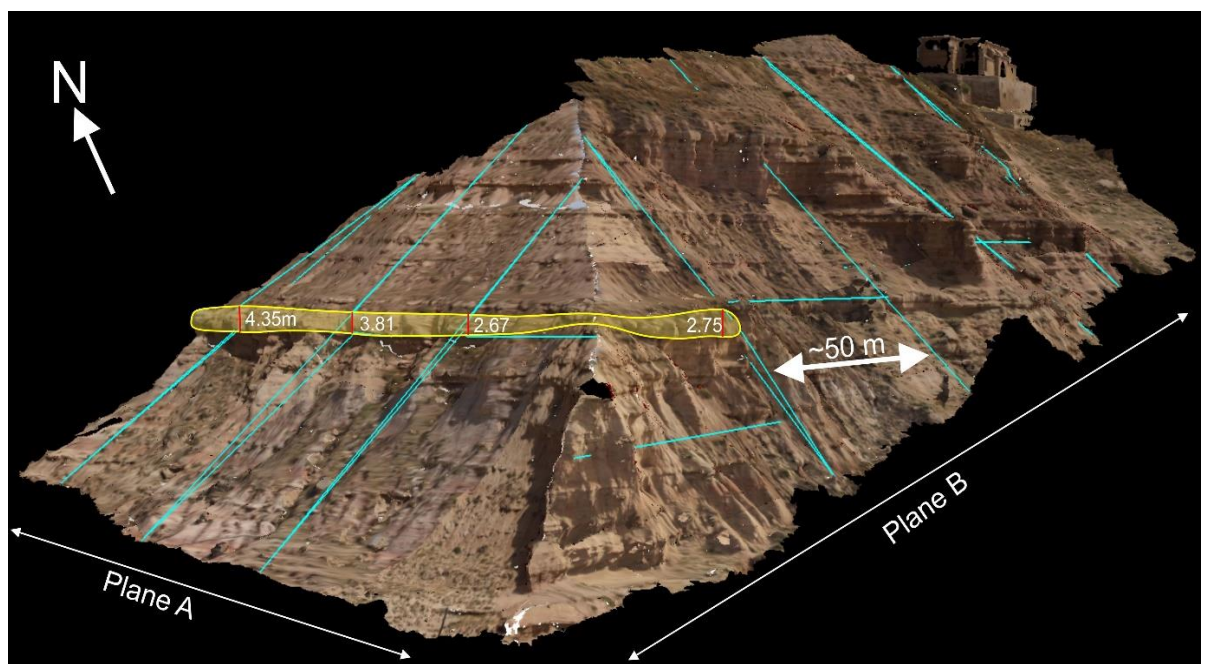


Figure. 50: The Bolea virtual outcrop model annotated to show the 3D exposure of a channel body along Planes A-B.

The Bolea outcrop presents a low-variance data set with a range in channel body percentage of 8.5% with maximum and minimum values of 8.5% and 0% respectively and an average of 4.%. The field log channel percentage exhibits 4.9% in comparison. Typically, channel body percentage ranges between 4-6%. Pseudo-log channel body thicknesses exhibit a relatively small range from a maximum of 4.35 m and a minimum of 1.06 m and an average of 2.31 m. Channel bodies typically fall between 1-3 m thick and consist of single stories. As no multi-storey channels are present, the channel body data also represents storey data.

Bolea Channel Thickness Distribution

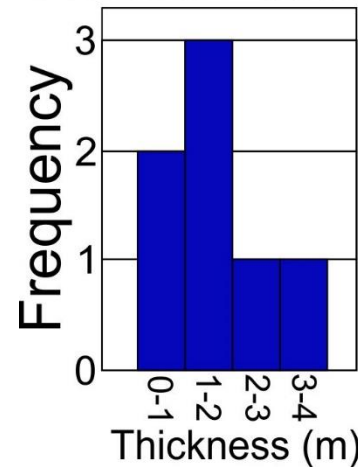
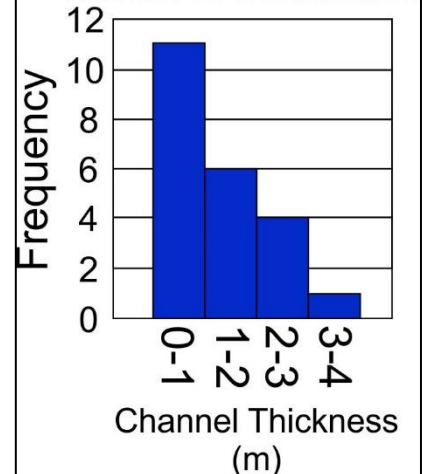


Figure. 51: Channel body thickness data exhibiting unimodal distribution

4.1E) Sigena - 14 Logs

The Sigena outcrop is the most distal locality in the basin and shows a much larger variation in channel proportions compared to Bolea. The Sigena virtual outcrop is extensive and allows for a greater quantity of log data (14) to be collected. Logs range between 17 m and 90 m however typically fall between 30-50 m thick. The data spans approximately 400 m with good exposure from the base of the outcrop to the upper sections of the cliffs. Logs generally pass through more than one channel body however two logs are completely devoid of channels.

Sigena Channel Thickness Distribution



Sigena in comparison with Bolea (the most directly comparable outcrop) exhibits a relatively large range of channel proportion values within the pseudo log sections with a range of 14.5 % alongside an average of 6.9%. The maximum and minimum values are 14.5% and 0% respectively. These values when compared with the field log section (channel proportion average: 3.88%) and Bolea (range: 8.5%; Average: 4%) are much greater.

Sigena Storey Proportion

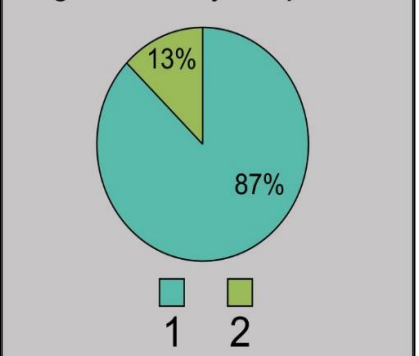


Figure. 52: Channel thickness distribution is unimodal with positive skew towards thinner channel bodies. The pie chart indicates the proportion of single-storey to dual-storey channels.

The pseudo-log data also presents a wider range of channel thickness values when compared with the field log data; 4.2 m to 0.83 m; yet a smaller average value of 1.5 m thick. Channels are often >1 m – 2 m thick and consist of single stories, however three dual-storey channels are present throughout the outcrop (Figure. 49).

4.2) Discussion – Channel Percentage

The overall trend shown by the data is that channel proportion within outcrops decreases downstream with insignificant ranges shown in channel proportions within both the proximal and distal zones. A greater range of channel proportions are observed within the medial zone of the DFS.

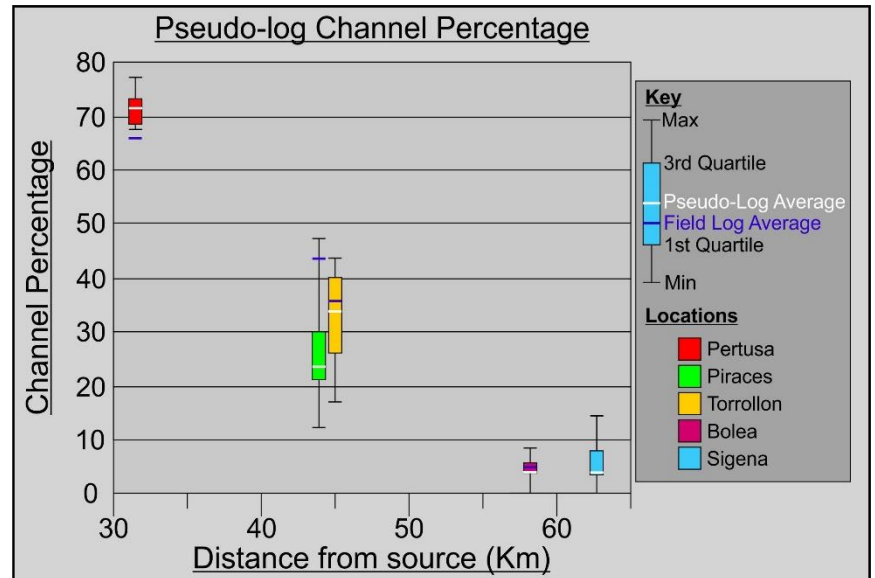


Figure. 53: Channel percentages are shown to decrease with increased distance from the source. The medial zone exhibits the highest range in values.

Typically, the channel percentage values determined from the field logs fall within a 6% variance of the pseudo-log averages calculated from the above datasets. As Table. 3 exhibits, logs show both positive and negative variances when compared with field data. The minor variance values observed indicate that pseudo-logs could be used as representative examples where field data is unavailable.

The outlier of Piraces shows a variance of -20.9% on channel percentage when compared with the field log. This is likely due to where the field log was taken through the section and how many channels the log passes through in comparison with where the pseudo-logs are taken. The Piraces virtual outcrop panel was also shot using LIDAR rather than drone imagery and therefore a large section at the base of the outcrop is missing. Due to shifts in vertical trends (Chapter 3) over time, the missing basal section of the outcrop is likely to have severely impacted the quality of the collected data from the Piraces Virtual Outcrop Panel. Therefore, the Piraces data comparison is significant as this highlights that pseudo-logging may result in significant variances from the actual data dependent on how much of

the outcrops are captured within virtual outcrop sections. The point at which field logs are taken through outcrops should also be a core consideration to ensure that the most representative log section of the outcrop may be collected.

Locality	System Position	Average Pseudo-log Channel %	Average Field Log Channel %	Variance %
Pertusa	Proximal	71.3	66.1	+5.2
Piraces	Medial	23.8	43.8	-20.9
Torrollon	Medial	34	37.1	-3.1
Bolea	Lateral Fringe	4	4.9	-0.9
Sigena	Distal	6.9	3.8	+3.1

Table 3: Pseudo-log average channel percentage data compared with Field Log average channel percentage data.

4.2A) Channel Thickness

Channel thicknesses observed across the system show a downstream reduction across outcrops. The proximal zone shows a high degree of variation in channel thicknesses across the outcrop with higher pseudo log averages calculated field log averages. It should be noted that with increasing distance, the difference between the calculated averages from the field and pseudo-logs also increases (Table 4).

In the medial zone, a large range in channel thicknesses is still observed while the distal region exhibits a reduced range in channel body thicknesses. This is often because channels are single storey and widely distributed across outcrops meaning that pseudo-logs may not pass through channels.

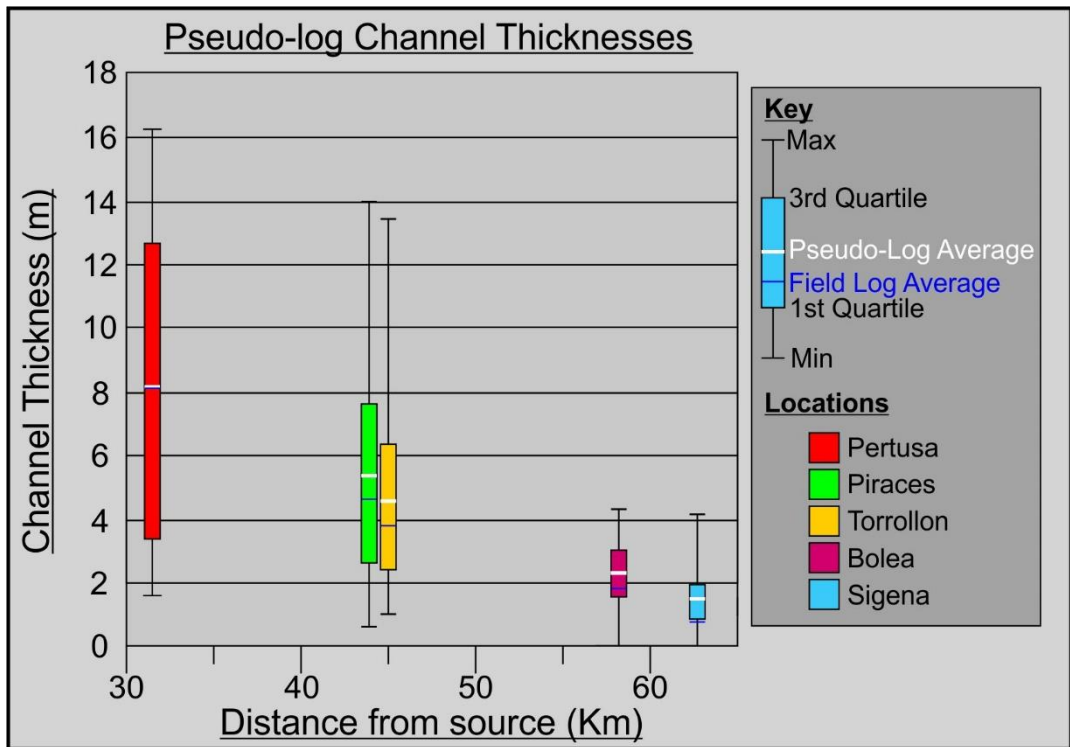


Figure. 54: Channel body thicknesses generally decrease downstream with increasing difference between the field log channel thickness values and the pseudo-log channel thickness values. The range of values also decreases with downstream distance.

Locality	System Position	Average Pseudo-log Channel Thickness	Average Field Log Channel Thickness	Variance %
Pertusa	Proximal	8.9	8.1	+0.8
Piraces	Medial	5.6	4.6	+17.3
Torrollon	Medial	4.6	3.7	+19.4
Bolea	Lateral Fringe	2.3	1.7	+26.5
Sigena	Distal	1.3	0.7	+45.7

Table 4: Pseudo-log average channel thickness data compared with Field Log average channel thickness data.

4.2B) Storey Thickness

Pseudo-log storey thickness data exhibits a similar trend to the channel thickness data with the medial zone occupying the largest range of thicknesses and the proximal zone exhibiting a slightly reduced range. Typically, average values in storey thickness reduce downstream, as do the 3rd and 1st quartile values.

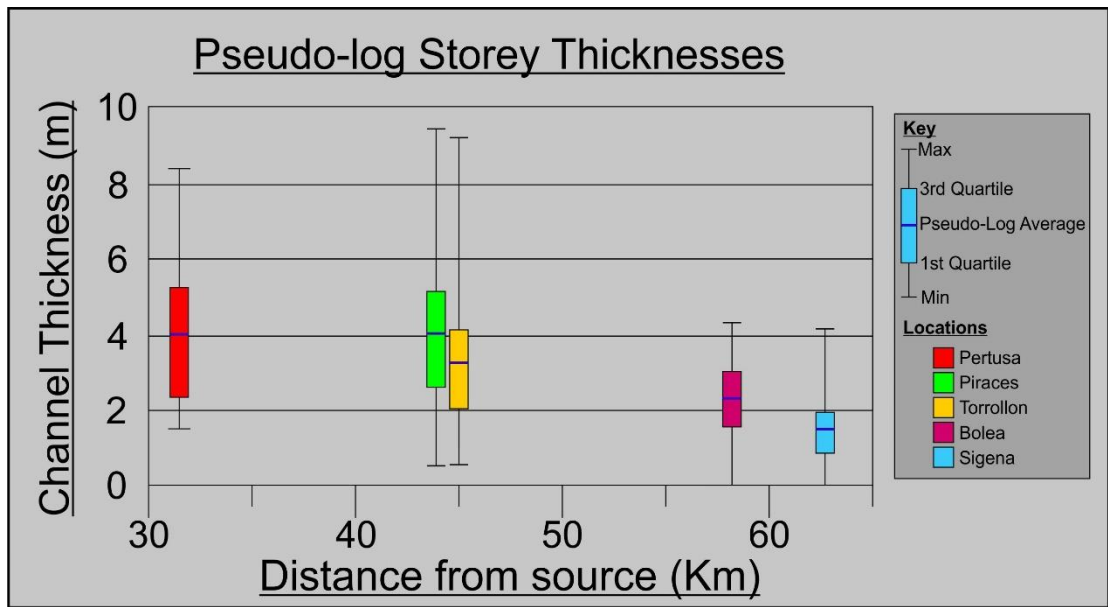


Figure. 55: Pseudo-log storey thickness ranges shown. Increases in range within the medial zone due to some vertical sections experiencing greater amalgamation and more frequent storey surfaces. The general trend shows a decrease in thickness with increasing distance.

Locality	System Position	Average Pseudo-log Storey Thickness	Average Field Log Storey Thickness	Variance %
Pertusa	Proximal	4.06	5.4	-24.8
Piraces	Medial	4.07	4.6	-11.5
Torrollon	Medial	3.19	2.87	+10
Sigena	Distal	1.45	0.7	+51.7
Bolea	Lateral Fringe	2.313	1.7	+26.5

Table. 5: Variations in Pseudo-log storey thickness data. Proximal areas exhibit decreased variance on actual field data whereas medial and distal locations exhibit increased variance on field data.

4.3) Summary

In summary, the proximal region shows a low variance in channel body percentage, but a wide range in channel body thicknesses. The Medial zones have a wide range in both channel body thickness and presence while the distal zone shows a lower degree in channel percentage variance and thickness. It should be noted that with increasing distance, the difference between the calculated averages from the field and pseudo-log channel thicknesses also increases (Table 5). As we shift further from the apex position of the system, greater system variability is experienced meaning that the consistency of channel presence across outcrops weakens and therefore, dependent on the position of the logs taken, results may vary significantly between virtual outcrop and field logs. The above data suggests that the field logs taken may not be entirely representative of the expected channel thicknesses in the area however the skew for the data-set is relatively small and does not impact the interpretations made within this study.

The variability experienced across the localities is controlled by a multitude of factors: climate, stream power, sediment load, floodplain competency and avulsion frequency (Hartley et al., 2010; Weissman et al. 2010; Fisher & Nichols, 2013; Nichols, 2017). The overall decrease in channel percentage downstream is the result of reduced stream power and sediment load with increasing distance from the source area, combined with increased bifurcation and evapotranspiration throughout the system (Hirst, 1991, Nichols & Fisher, 2007, Weissman et. al. 2013, Owen et. al. 2015, Weissmann et. al. 2015). In the proximal zone there is a fairly consistent amount of channel bodies present, which is interpreted to be due to the most proximal zone of the fluvial system undergoing more frequent avulsions, and therefore a high degree of channel reworking, over a smaller area when compared to the medial and distal areas which results in a consistent high channel percentage through channel amalgamation. However, a wide range in channel body thicknesses is present in the proximal zone. It is possible that the most proximal region will be more susceptible to changes in discharge and sediment load, and as a result will have a high amount of variation in incision and reworking rates as the river responds to these fluctuations which may be related to climatic and sediment supply changes in the catchment area. Internal factors will also have major impacts on the system with frequency of channel avulsion and bar migration also determining the presence of a wide range of channel body thicknesses. It is most likely that the internal controls of channel avulsion are the dominant control of channel body thicknesses within the proximal zone. As this area is the least susceptible to high degrees of

channel avulsion and compensational stacking, greater channel amalgamation and thicker channel deposits occurs as the system has less space to avulse into. This also leads to the development of a greater amount of storey surfaces present within the proximal channel developments with a high proportion of truncated channels.

The largest variation in channel percentage and thickness is observed within the medial outcrops of Piraces and Torrollon. As previously noted in the Vertical Trends chapter (Chapter 3.2A), the medial zone shows the most variation in channel proportion, geometry types and channel thicknesses. This data further supports that the medial zone of the DFS is the area that exhibits the most variation of channel data and therefore is more complex. In the medial zone the river has a wider area to avulse over, and with reduced sediment supply rates in comparison to the proximal zone there is a higher chance of depositing and preserving floodplain material (Nichols, 1987; Nichols & Fisher, 2007; Weissman et al., 2015; Owen et al., 2017). However, data presented in this chapter indicates that the fluvial system is still susceptible to variations in incision and reworking, resulting in a high range in both channel and storey thickness data. A greater range in channel percentage is observed in the medial zone when compared to the proximal zone (37.8% and 9.5% respectively). This is interpreted to be due to the fact that the channel body deposits start to become vertically separated by floodplain packages, however as can be seen in Figure. 42 and 46, the channel bodies are not consistently or fully separated by floodplain packages due to a variation in the degree of channel body amalgamation. As a result, the multitude of pseudo-logs captures the variation in amalgamation across outcrops showing that although an increase in accommodation is observed, it is not yet enough to consistently separate out the channel body deposits through fully developed floodplains.

The distal zone again exhibits a range in both channel body thicknesss and percentage. In the distal region, thinner channel bodies (1.9 m to 0.4 m) are observed, which is interpreted to be the result of small channels due to downstream bifurcation and low avulsion frequencies over a wide area allowing for the preservation of floodplain in greater proportions (Nichols, 1987; Nichols & Fisher, 2007; Weissman et al., 2010; Weissman et al., 2015; Owen et al., 2017). It is interpreted that the range in thickness is larger a function of where the pseudo-logs are taken from, as the channel percentage may vary dependent on whether the logs pass through singular channels or stacked intervals. If the log also passes through the wings of a channel, this can also alter the results of the measured channel percentage.

Overall, the data analysed above reinforces the early interpretations made through the paper in regard to downstream trends that occur ie: decreases in channel and storey thicknesses alongside storey surface frequencies. The data has also highlighted the complexity of the medial zone further. The medial zone shows the largest range in channel and storey thicknesses and channel percentages, therefore indicating the most variability observed. The collected field data's relevance is bolstered by the pseudo-log data, which shows the extent of channel bodies across outcrops and how they vary laterally rather than a singular log section to represent the entire outcrop. The implications show that depending on where in the system or outcrop that a log is taken there may be a large, or small, degree of variability laterally and vertically.

Chapter 5

5.0 Discussion

The Huesca fluvial system has shown downstream trends indicative of a distributive fluvial system. Radial paleocurrents are observed alongside downstream decreases in channel body percentage (66.1% proximally to 3.9% distally; a loss of 62.2%), channel body thickness (20.2-0.4 m; 98% loss), storey thickness (5.4m-1.7m; 68% loss), channel grain size (1.06mm– 0.25mm; 76.4% loss) and a shift in channel body geometries from M-IA dominated in the proximal system to OS-I dominated in the distal regions. The quantified data collected (Chapter 3.2) is consistent with the previous works of Hirst (1991), who first determined the Huesca system as a fluvial fan system, and fits within the characteristics of a distributive fluvial system suggested by recent works (Hartley et al., 2010; Weissman et al., 2010; 2015). These trends are likely attributed to a downstream decrease in stream power as a function of channel avulsion/bifurcation alongside infiltration and evaporation processes. The decrease in energy away from the apex of the system severely impacts the development of thick, amalgamated channel bodies and leads to the formation of thinner, isolated channel bodies. As the basin was endorheic, eustatic sea-level changes are considered to have no impact on the development of the DFS however ephemeral lakes on the distal fringe of the system may have altered development of the system over large time scales determined by climate within the basin. The impact that these terminal lakes may have had could not be fully assessed due to the scope of this project and would require further research in the future. From the data collected within this study, we have determined that the Huesca fluvial system is primarily influenced by upstream changes in sediment supply and stream power (Kukulski et al. 2013).

Two main facies associations, channel and floodplain, are identified on the Huesca DFS and can be split into 6 sub-associations: 4 channel sub-associations and 2 floodplain. 8 core facies were identified; 5 sandstone facies and 3 mudstone facies (see Chapter 2.1 for summary). At a larger scale five key sandstone body channel geometries were also defined using the scheme of Owen et al. (2017), namely Massive; Semi-Amalgamated; Internally-Amalgamated; Offset-Stacked and Isolated channel bodies; the presence and characteristics of which were also quantified (see Chapter 2.4). Facies schemes have traditionally allowed for interpretation of where a system sits on the continuum of braided and meandering fluvial styles and to an extent, they provide insight into what styles may be more prevalent. As

previously noted (Chapter 2), downstream and lateral accretion packages can be present within both meandering and braided fluvial systems and therefore we must consider a systems position along a continuum between the two styles rather than definitively one fluvial style or the other.

The channel body geometry scheme provides insight into where the outcrops fall within the proximal-distal zones alongside channel body stacking patterns, avulsion frequency and estimation of stream power. This study found the dominant sandstone facies to be Sx (Cross-bedded sandstone) throughout the system with LA (lateral accretion surfaces) to be the predominant facies sub-association. The M/SA/IA channel body geometries dominate the proximal region (Pertusa & Monzon) before giving way to OS/I geometries at the rest of the system outcrops. Through the examination of facies and their associated sub-associations alongside channel geometries, this provides insight into the different types of fluvial styles exhibited within the system. As the Sx facies; LA facies sub-association and OS channel geometries dominate the majority of the system, it is inferred that the fluvial style for almost all outcrops was meandering. The outcrop of Pertusa is highly important within this study as whilst the outcrop exhibits the only massive channel body geometry, it also exhibits a mixture of LA and DA packages within log sections which is suggestive of both a braided and meandering fluvial style. No other outcrops share these characteristics which is significant as the Pertusa outcrop may represent a transitional zone between a predominately braided fluvial style and a predominately meandering fluvial style. However, consideration must be given to how fluvial planforms are recognised in the rock record. For example, Swann et al. (2018) showed that whilst the Salt Wash fluvial system is largely sand-dominated, meandering features (i.e. scroll bars) can be identified, which traditional facies models do not account for. Swan et al., (2018) demonstrated through detailed work of an exhumed sand-rich point bar that downstream accretionary packages were dominant in the upstream and downstream portions of the point bar. This work therefore highlights that care does need to be taken when interpreting fluvial planform from vertical successions alone. However, in the case of Pertusa, the lack of paleocurrent variability that is indicative of meandering systems is not observed, and therefore it is considered that this area of the system had a mixed meandering-braided style. The style of meandering across the majority of the system was likely wandering as there is a distinct lack of well-developed paleosols exhibiting the presence of extensive rooting and a lack of preserved organic material within floodplain deposits. This interpretation is supported by the paleocurrents observed across the system.

5.1A) Apex location

The previous works of Jupp et al. (1987) and Hirst (1991) suggest that the Huesca fluvial system was supplied by a “broad apical area” due to the elongate apex estimations calculated. This study agrees with this hypothesis however, new statistical estimations alongside field work show that the apical area likely exists 32 km northwest of the Jupp et al. (1987) estimation surrounding the town of Naval (see Figure. 53). The channel percentage data alongside channel body geometry data collected within this study also suggest that the initial apex estimation may be incorrect. Comparing the channel body percentage data against the distances from the initial apex estimation of Jupp et al. (1987), the outcrop pattern makes little geological sense, positioning Pertusa and Castleflorite together in a medial position whilst the Monzon outcrop is the most proximal. Using the revised estimation of the area surrounding Naval as the source area for the system, all outcrops and their associated characteristics fit a distributive fluvial system model better. It is therefore concluded using paleocurrent analysis using data from this paper and later works by Owen and Nichols (pers. Comms, 2018), it is more likely that the area surrounding the town of Naval was the source area for the development of the fluvial system.

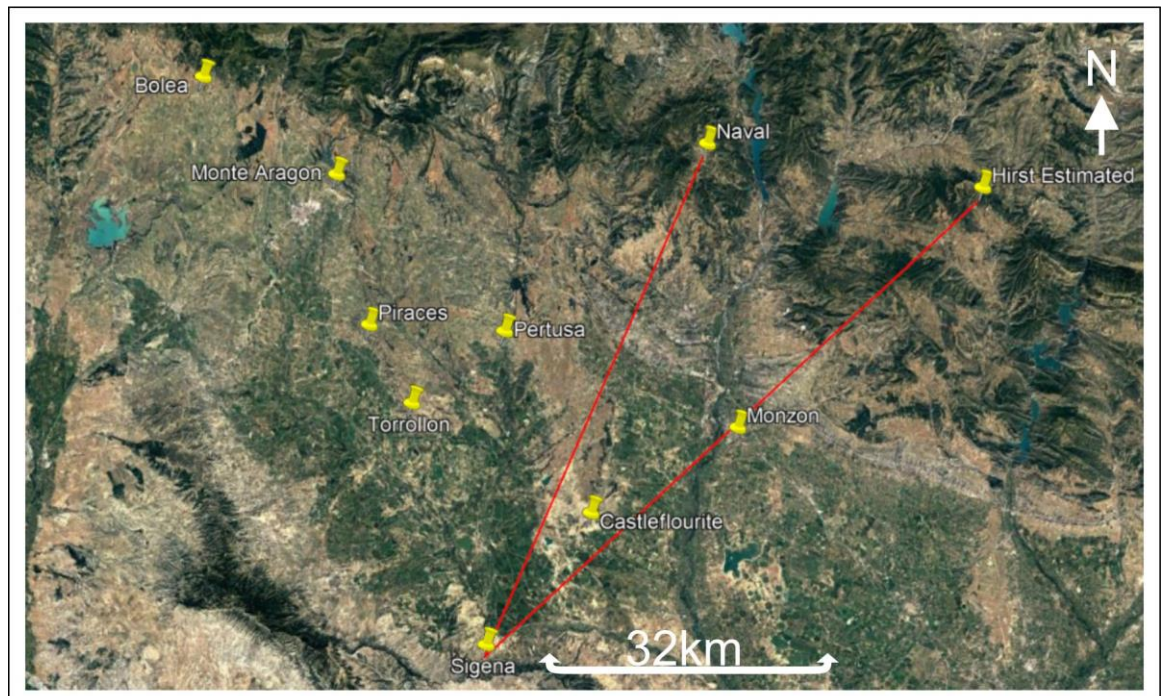


Figure 56. Location map showing the difference between estimated apex positions (Hirst, 1991).

5.1B) Spatial Trend Analyses

Large variations in net:gross values were observed between the 7 studied field localities. Channel body percentage reached 66% of the logged outcrop at Pertusa down to a low of 3.9% at the distal locality of Sigena. This downstream decrease in channel body percentage is similar to that observed in Hirst (1991), however the only quantified outcrop that is comparable between the two studies is Pertusa. Hirst's data shows an in-channel component of 55% in comparison with this study's 66% channel body presence within the field log. Whilst only one outcrop is directly comparable, the trends shown between the two datasets is similar: downstream decreases in channel body proportion and channel body thicknesses and an increase in the presence of classic ribbon sandstones, identified as I channel body geometries within this study. In comparison with the more recent studies on other systems, the observed trends are similar within this study and that of Hirst's (1991) are also present (Hartley et al. 2010; Weissman et al. 2010; Owen et al. 2015; Nichols, 2017).

Whilst the field log data was collected in the field (Appendix A) to represent the outcrop, the use of virtual outcrop models was also implemented in order to understand how channel body presence varies laterally and vertically across large scale outcrops for five localities. This combined usage of field and outcrop data allowed for the comparison of field log and digitally created data to provide a broader understanding of net:gross variation across outcrops alongside calculated averages of net:gross values. The resulting data showed that whilst the proximal and distal zones show reasonably consistent data between field and digital logs, this section of the research highlighted the large variations that can be present in net:gross within outcrops in the medial zone. The medial zone is the most poorly understood region within distributive fluvial systems and the data within this study highlights the importance of understanding lateral variation within medial zones. Without this, the exploitation of resources within the region carries high risk depending on where a log or well is placed, and in some cases may lead to a misinterpretation of position within a DFS. The presented data builds on the previous works of Hirst's (1991) drawn outcrop diagrams using more modern techniques to examine outcrops in higher resolution which allows for quantification of vast swathes of outcrop. The pseudo logs constructed also allows for the analysis of channel connectivity within between log sections adding another aspect of quantification that has been omitted in previous works.

Much like net: gross values, channel body thicknesses also decrease downstream as described in previous works (Hirst, 1991; Hartley et al. 2010; Weissman et al. 2010; Owen et al. 2015; Owen et al. 2017; Nichols, 2017) with decreases in stream power, increased avulsion rates and channel bifurcation alongside evapotranspiration and floodplain infiltration. This results in reduced ability to erode floodplain and reduced channel depth and width, similar to trends observed today within modern systems such as the Okavango delta. This will also heavily impact on how resource exploitation takes place with increasing distance from the apex as reservoirs will decrease in size and the degree of connectivity.

Grain size data was also included within this study which was previously not included within the works of Hirst (1991). The inclusion of this data highlights the decreasing grain size downstream, decreasing from coarse in the proximal to fine in the distal regions. The data also highlights that lateral fringe outcrops such as Monte Aragon receive coarse, immature material due to their proximity with the basin margin. Whilst basin margin localities typically exhibit low net: gross values, their channel bodies are typically coarse with potential for high degrees of porosity, dependent on grain sphericity. Whilst porosity may be high in these regions, net: gross values and channel connectivity is typically poor making resource exploitation in these areas high risk.

5.1C) Basin margin localities

Peripheral localities examined in this paper are those of Monte Aragon and Bolea, both of which lie adjacent to the thrust front. Monte Aragon specifically is significant as this outcrop steps away from some of the trends experienced throughout the rest of the system. The outcrop is situated within the same elevation grouping as Bolea, suggesting that the outcrops likely formed at around the same time (see Chapter 3.0). The Monte Aragon outcrop also falls within the “medial” grouping of outcrops in terms of distance from the apex. What must be considered is that whilst the distance from the estimated apex is similar to the other medial localities, Monte Aragon is part of a lateral fringe rather than a traditional “downstream” locality. This is likely the reason that Monte Aragon exhibits the highest average weighted grain size for every locality studied alongside similar channel body and storey thickness data as those observed within the medial deposits of Piraces, Torrollon and Castleflorite. This is likely due to the proximity of the outcrop to the basin margin with channels located at Monte Aragon receiving much greater quantities of immature sediments leading to anomalously high grain size averages. Whilst the channel body thicknesses are similar to those in the

medial zone, there is an anomalously low channel percentage (20%) observed within the outcrop which is likely the result of the outcrop being influenced by a paleochannel that avulsed before significant channel migration could take place and more amalgamated channel bodies could form (Hirst, 1991). This suggests that whilst the lateral fringe is close to the basin margin, these deposits exhibit the characteristics of outcrops and deposits within the distal zone. This must be taken into consideration when undertaking exploration close to basin margins as deposits here are likely to have poor resource yield with poor channel connectivity.

5.2) Case Study Comparison: Salt Wash DFS

To date there are few fully quantified complete DFS datasets. The Salt Wash DFS of the Jurassic Morrison Formation (Owen et al., 2015) provides the only rock record example for which this study can draw direct comparisons with. The Salt Wash was deposited during early stages of foreland basin development (Decelles, 2004; Turner and Peterson, 2004) and had relatively dry climate that has been likened to modern day African Savannah (Turner and Peterson, 2004). The climatic and tectonic settings are therefore relatively similar between the systems, with key differences being their size (Salt Wash estimated to be ~550 Km in length and the Huesca ~70 Km) and basin drainage configuration (Salt Wash is not considered to be an endorheic basin).

It should be noted that one of the issues with comparing the Huesca and Salt Wash Systems is that whilst the Salt Wash is relatively unaffected by tectonic activity, the most proximal regions of the Huesca have experienced significant deformation which makes Pertusa the most proximal locality within the system. Due to this, the full Huesca system is not captured. This study however believes that this makes little difference to the findings discussed below as the rest of the Huesca system is untouched by tectonic deformation and can still be directly correlated with the Salt Wash.

Owen et al., (2015b) found that the proximal region was typically composed of laterally extensive, highly amalgamated sheet sandstones which are also identified within the Huesca system at the Pertusa outcrop and both systems exhibit high sandstone connectivity, between 80-90% in the proximal zones. Within the medial region, the Salt Wash exhibits organized channel-belt packages that may span laterally over >1km with up to 20% channel connectivity observed (Owen et al., 2017). The medial region of the Huesca system shows similar trends: laterally expansive channel bodies with reasonable connectivity best observed

within the Torrollon and Piraces outcrop panels in Chapter 3.7e and 3.7f. Finally, within the distal region of the Huesca DFS the distribution and fluvial style of channels is comparable with that of the Salt Wash: isolated channel bodies with connectivity rarely observed and floodplain dominating outcrops (Owen et al., 2015b). Both systems show a systematic decrease in channel body connectivity and thicknesses; amalgamation; percentage and grain size with increasing distance from the inferred system apices. These similarities are to be expected as down-system fining and changes in geometry architecture are both functions of hydraulic sorting which leads to “self-similarity” within systems (Fedele & Paola, 2007; Allen et al., 2015

As noted above, the systems are distinctly different in size: the Huesca extends ~70 km in comparison with an expanse of over ~550 km in the Salt Wash DFS (Owen et al., 2015a). As a result, general trends are directly comparable between the system, however the point at which many of these trends begin to shift happen at different points within the system. Statistical comparison is best completed using percentage downstream rather than arbitrary distances in order for direct comparisons to be made.

One of the most notable differences between the Salt Wash and the Huesca DFS is the grain size distribution (Figure. 54). The Huesca system typically is a much coarser system when compared with the Salt Wash. The results show that typically, the grain size in the 40-50% downstream bracket are of a similar size between both systems with gradual decrease with increasing distance. The decrease noted in the Salt Wash is much less gradual between 40-50% and 50-70% downstream in comparison to the Huesca. The trendlines displayed within the data appear to show that the Huesca system has a faster rate of grain-size degradation within the system in comparison to the Salt Wash which is likely a function of the scale of the basin: smaller basins experience faster degradation of grain-size. Within the Salt Wash dataset two distinct groups in grain size can be observed, 30-50% downstream is much higher than the grouping found at 60-80% downstream (~0.25 mm). Although the Huesca shows a more gradual transition in grain size, two distinct groups can also be observed with Pertusa, Monzon and Monte Aragon being distinctly coarser than the rest. The two distinct grain size groupings within both systems possibly suggest the passing over a hydrodynamic threshold where the stream power of the river decreases to the point at which it can no longer carry coarse grain sizes (>10mm). The difference in grain size seen in the Huesca reflects the difference in source area sediment supply, flow competency alongside discharge rate and

gradient, all of which impact on grain size decrease and distribution of sediment within the system (Shukla et al. 2001).

Channel percentages are reasonably similar when comparing the Huesca and Salt Wash systems as shown within Figure. 55. However, the trendline gradients are notably different. A more rapid decrease in channel percentage downstream is present in the Huesca dataset which potentially suggests that discharge rate/flow competency within the Huesca decreased much faster than in the Salt Wash. This is likely the result of a difference in the size and source areas of the systems with a greater source area in the Salt Wash providing much greater quantities of water into the system, therefore maintaining flow rate within the system for much greater distances.

Channel body thickness data (Figure. 56) exhibits the most variation of all quantified data observed between the two systems. Typically, the Huesca deposits show similar average channel body thicknesses when compared with the amalgamated channel body values for the Salt Wash, specifically in the medial zone. The distal localities of Bolea and Sigena however pair up with the isolated channel body data of the Salt Wash dataset as typically, distal localities exhibit classic, thin isolated ribbon geometries rather than thick amalgamated bodies such as those in the proximal and medial zones. The channel body thickness data shows that the medial sections of both systems could be used as analogues for one-another as many values match up closely however, caution should be taken as these values are within the lower range of values for their respective distances. Once again, the rate of decrease in values from the Huesca occurs at a steeper gradient than the Salt Wash. However a note here needs to be made that the datasets are not directly comparable as the data from the Huesca included both amalgamated and isolated channel bodies while the published Salt Wash data splits the thicknesses up into amalgamated and isolated channel forms.

The above data highlights that whilst the Salt Wash and the Huesca systems are intrinsically different in terms of their size, the trends displayed within the data and the percentage downstream at which the systems appear to show similar values are integral to our understanding of the DFS model. The collated quantified data allows for the application of quantified data from this study to other analogues to provide a better understanding of how DFS may respond over two different system scales.

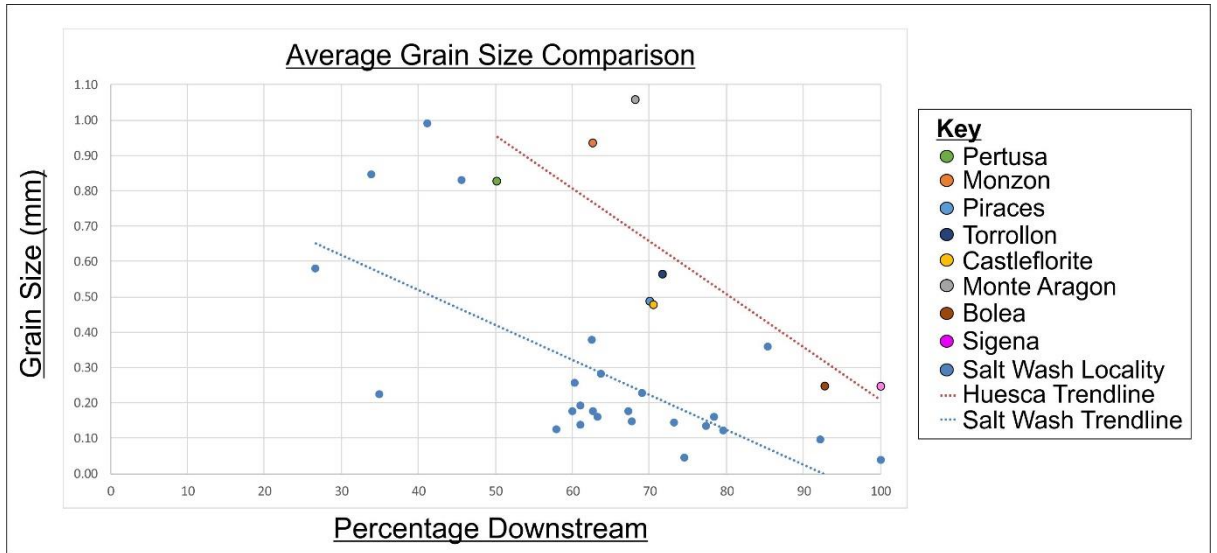


Figure 57. Grain size data comparison between the Salt Wash and Huesca DFS localities (Owen et al. 2015).

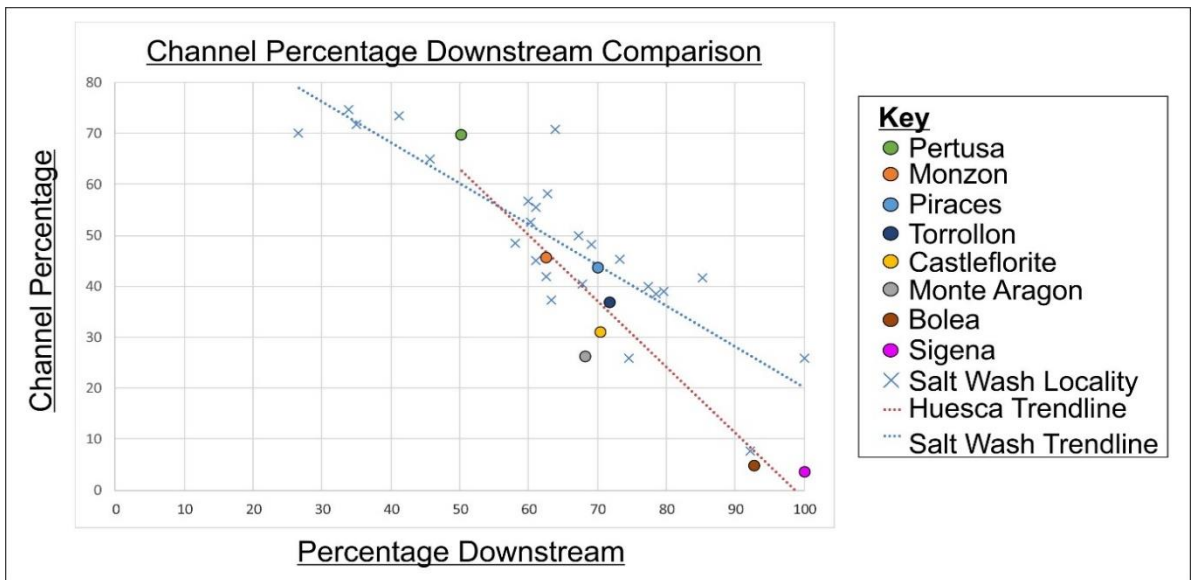


Figure 58. Channel percentage data comparison between the Huesca and Salt Wash DFS (Owen et al. 2015)

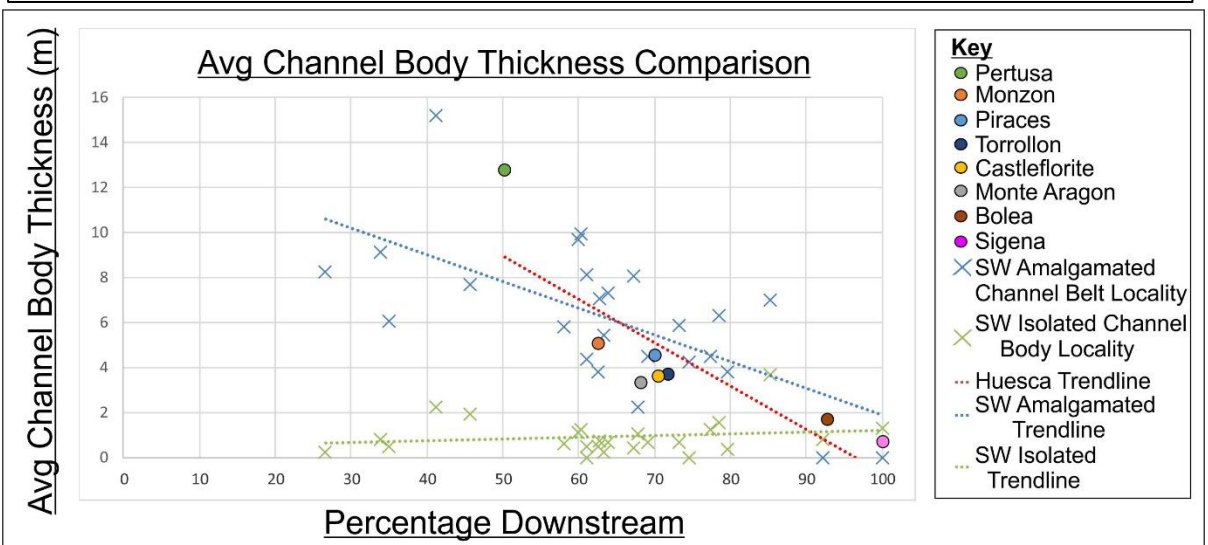


Figure 59: Average channel body thickness comparison between the Huesca localities and the Salt Wash DFS. The Salt Wash data is split into amalgamated and isolated channel belt data however the Huesca data is combined (Owen et al. 2015).

Similarities are also noted between the Organ Rock Formation (Cain and Mountney, 2009) and the Huesca DFS. The Organ Rock Fm, Utah exhibits amalgamated channel-fill complexes in the proximal regions which may extend up to 5 km laterally with poor overbank element representation, similar to the fluvial style observed at the Pertusa outcrop. The system experiences a decrease in grain size downstream as the result of increased infiltration and channel bifurcation. The medial zone is dominated by ribbon channel bodies up to 7-8 m thick that also extend laterally over large distances. Both channelized and sheet-flood processes are noted in the medial zone, similarities shared with the Huesca DFS. Finally, the distal region is dominated by floodplain elements, poor channel development and connectivity and typically thin, isolated channel bodies with the finest grain size observed within channels. Whilst the Organ Rock DFS displays similar observable trends as the Huesca DFS, the lack of quantifiable data makes direct comparison difficult however the general DFS trends are identified.

The data from all three studies supports the DFS model and suggests that these analogues can be used over various scales to accurately determine the typical characteristics at various percentages downstream. Further work could be carried out on previously studied DFS, such as the Organ Rock Fm. (Cain and Mountney, 2009), to better constrain where, and why, similarities and differences occur.

5.3 Depositional Model

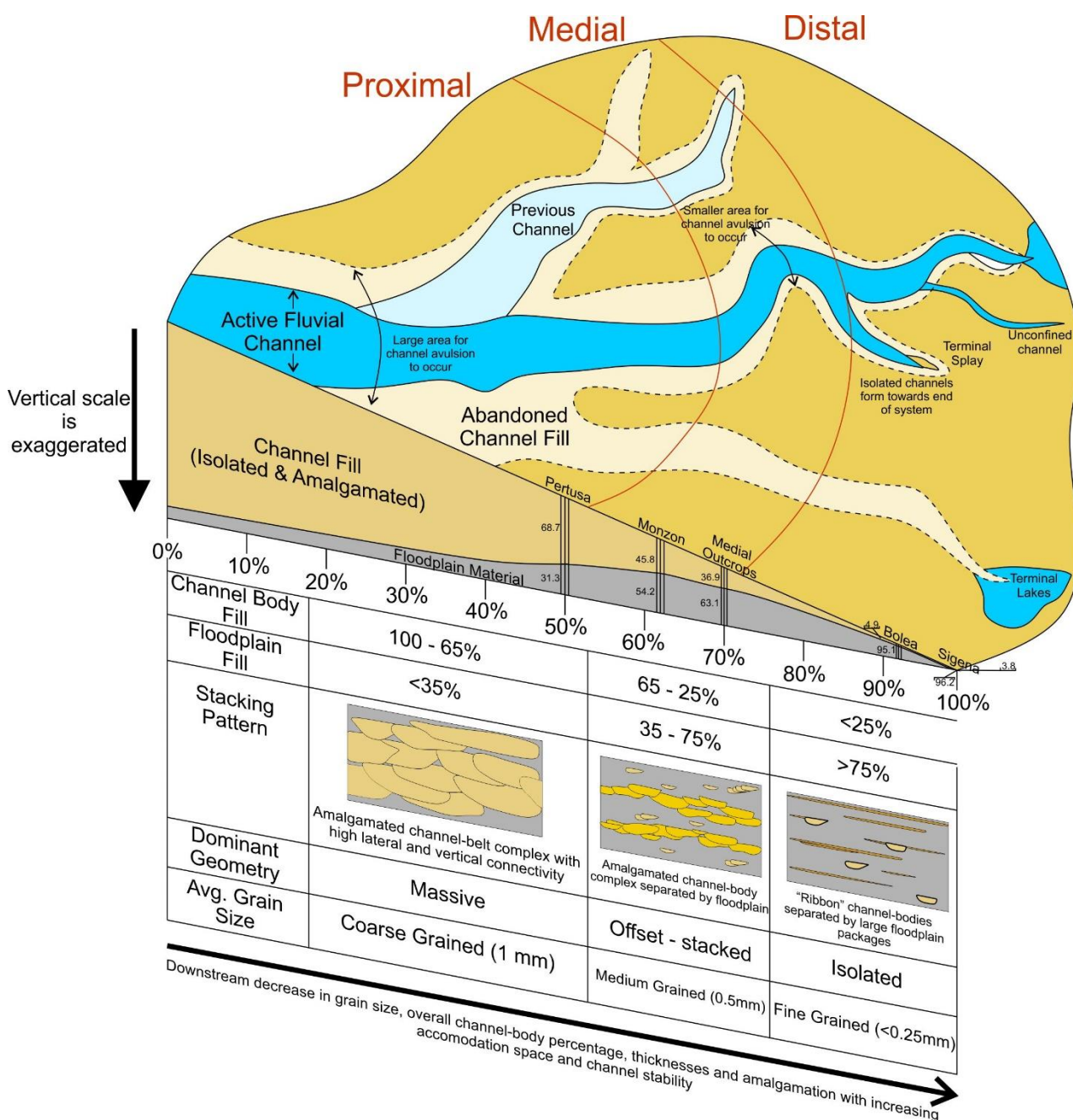


Figure 60: A visualised, schematic depositional model of the Huesca Fluvial System.

5.4) Implications

These results show that the DFS model is to some extent scalable implying that it can be widely applied, however, as noted above more quantified examples are needed. Direct comparisons with modern river systems will also help better constrain the DFS model, however data that is comparable to the rock record (such as bar heights and grain size distribution) are at present limited within the current modern literature for DFS and is another area for potential further work. Despite a lack of quantified examples, observations made on modern DFS (e.g. Weissmann et al., 2010; 2015) are observed in rock record examples (e.g. decrease in channel presence, radial flow pattern, decrease in the area of which the channel migrates over (ultimately forming the channel body)).

The presented data helps better refine the DFS model, specifically where areas of net: gross can vary laterally, as well as allowing the model to be tested in respect to its scalability. Specifically, the data presented will aid resource exploration in the oil and gas sector, but also with respect to better understanding the distribution of aquifer prone sands. This may allow for better understanding in stressed environments, such as those documented in India, where water resource availability and management is a pressing issue, particularly with the respect to understanding pollutant pathways (e.g. Mukherjee et al., 2015; MacDonald et al., 2017; Bhanja et al., 2017).

6.0 Conclusions

This study of the Huesca fluvial system builds on the works of Hirst (1991) and has collected quantified data, using this to test proximal-to-distal trends within the DFS and directly compare the results of which with other examples within the literature (Cain and Mountney, 2007; Owen et al., 2015; Owen et al., 2017b). The downstream trends show that channel thicknesses decrease from 20.2 m to 0.4m; grain size decreases from coarse to fine with decreases in the channel percentage from 66% to 4%. Storey thicknesses also decrease downstream from 11.4 m to 0.4 m and a decrease in storey frequency from a max of 4 to single storey bodies. The proximal regions of the DFS are dominated by highly amalgamated, laterally extensive, coarse-medium grained sandstone bodies with high interchannel connectivity. Distal regions however exhibit single storey, thin ribbon channel sandstones with poor to no connectivity between channel bodies and typically dominated by mud-rich floodplain packages. Whilst some trends may not be quantified (architectural changes downstream), this information is included to provide insight into how the system changes and responds to various controls. With increased distance from the system apex, fluvial discharge rates decrease due to flow expansion upon entering the basin, channels bifurcate alongside infiltration of water which are interpreted to be key controls that contribute towards the proximal-to-distal trends observed.

When compared with data from other systems, there appears to be clear parallels between datasets that would allow for a scalable DFS model to be constructed through further works on similar systems of varying size. The data will also allow for direct comparison with other systems that are deposited under different tectonic and climatic conditions which will build towards better predictions and understanding of how DFS respond to such changes. This will further go on to aid resource exploration and reservoir characterization for both large scale economic industries and water resource exploitation within stressed environments.

References

- Allen, J. R. L. 1963. The classification of cross-stratified units, with notes on their origin. *Sedimentology* 2, p. 93-114.
- Allen, J.R.L. 1965. A review of the origin and characteristics of recent alluvial sediments. *Sedimentology* 5, 89–191.
- Allen, J. R. L. 1982. Sedimentary structures: Their character and physical basis. *Developments in Sedimentology* 30A-30B. Amsterdam: Elsevier Scientific Publishing Company.
- Allen, P.A., Michael, N. A., D'arcy, M., Roda-Boluda, D. C., Whittaker, A.C., Duller, R. A. & Armitage, J. J. 2015. Fractionation of grain size in terrestrial sediment routing systems. *Basin Research*, 29(2). Doi: <https://doi.org/10.1111/bre.12172>
- Almeida, R. P., Freitas, B. T., Turra, B. B., Figueiredo, F. T., Marconato, A., & Janikian, L. 2016. Reconstructing fluvial bar surfaces from compound cross-strata and the interpretation of bar accretion direction in large river deposits. *Sedimentology*, 63(3), 609–628. Doi:<https://doi.org/10.1111/sed.12230>
- Alonso-Zarza, A.M. and Calvo, J.P. 2000. Palustrine sedimentation in an episodically subsiding basin: the Miocene of the northern Teruel Graben (Spain). *Palaeogeography, Palaeoclimatology, Palaeoecology* 160, 1–21.
- Álvarez Sierra, M.A., Daams, R., Lacombe, J.I., López Martínez, N., Van der Meulen, A.J., Sesé, C., De Visser, J. 1990. Paleontology and biostratigraphy (micromammals) of the continental Oligocene – Miocene deposits of the north-central Ebro Basin (Huesca, Spain). *Scripta Geologica* 94, 1–77.
- Arenas, C. and Pardo, G. 2000. Neogene lacustrine deposits of the north- central Ebro Basin, north-eastern Spain. In: Gierlowski-Kordesch, E.H., Kelts, K.R. (Eds.), *Lake Basins Through Space and Time*. AAPG Studies in Geology 46, 395–406.
- Arnott, R.W.C. and Hand, B.M. 1989. Bedforms, primary structures and grain fabric in the presence of suspended sediment rain. *J. Sediment. Petrol.* 59, 1062–1069.

Assine, M.L. 2005. River avulsions on the Taquari megafan, Pantanal wetland, Brazil. *Geomorphology* 70, 357–371.

Barberà, X., Cabrera, L., Marzo, M., Parés, J.M., and Agustí, J. 2001. A complete terrestrial Oligocene magnetobiostratigraphy from the Ebro Basin, Spain. *Earth and Planetary Science Letters* 187, 1–16.

Bartholdy, J., Ernstsén, V. B., Flemming, B. W., Winter, C., Bartholomä, A., and Kroon, A. 2015. On the formation of current ripples. *Scientific Reports* 5, 1–9.
<https://doi.org/10.1038/srep11390>

Best, J.L., and Bridge, J.S. 1992. The morphology and dynamics of low amplitude bedwaves upon upper stage plane beds and the preservation of planar laminae. *Sedimentology* 39, 737–752.

Bhanja, S. N., Mukherjee, A., Rodell, M., Wada, Yoshihide, W., Chattopadhyay, S., Velicogna, I., Pangaluru, K. and Famiglietti, J. S. 2017. Groundwater rejuvenation in parts of India influenced by water-policy change implementation. *Scientific Reports*, 7(1), 7453. Doi:<https://doi.org/10.1038/s41598-017-07058-2>

Blakey, R.C. and Gubitosa, R. 1984. Controls of sandstone body geometry and architecture in the Chinle Formation (Upper Triassic), Colorado Plateau. *Sediment. Geol.* 38, 51-86.

Bluck, B.J. 1971. Sedimentation in the meandering River Endrick. *Scott. J. Geol.* 7, 93-138.

Bridge, J.S. 2003. *Rivers and Floodplains*. Blackwell Science, Oxford, UK.

Bridge, J.S. and Leeder, M.R. 1979 A simulation model of alluvial stratigraphy. *Sedimentology* 26, 617–644.

Bridge, J.S. and Jarvis, J. 1976. Flow and sedimentary processes in the meandering River South Esk, Glen Clova, Scotland. *Earth Surface Processes* 1, 303-336.

- Brierley, G. J. 1989. River planform facies models: the sedimentology of braided, wandering and meandering reaches of the Squamish River, British Columbia. *Sedimentary Geology*, 61(1–2), 17–35. Doi:[https://doi.org/10.1016/0037-0738\(89\)90039-0](https://doi.org/10.1016/0037-0738(89)90039-0)
- Bristow, C.S., Skelly, R.L., and Ethridge, F.G. 1999. Crevasse splays from the rapidly aggrading, sand-bed, braided Niobrara River, Nebraska: effect of base-level rise. *Sedimentology* 46, 1029-1048.
- Buehler, H.A., Weissmann, G.S., Scuderi, L.A., and Hartley, A.J. 2011, Spatial and temporal evolution of an avulsion on the Taquari River distributive fluvial system from satellite image analysis. *Journal of Sedimentary Research* 81, 630–640.
- Calvo, R., and Ramos, E. 2015. Unlocking the correlation in fluvial outcrops by using a DOM-derived virtual datum: Method description and field tests in the Huesca fluvial fan, Ebro Basin (Spain). *Geosphere* 11(5), 1507–1529.
doi:<https://doi.org/10.1130/GES01058.1>
- Cain, S.A. and Mountney, N.P. 2009. Spatial and temporal evolution of a terminal fluvial fan system: the Permian Organ Rock Formation, south east Utah, USA. *Sedimentology* 56, 1774–1800.
- Carling, P. A. 1990. Particle over-passing on depth-limited gravel bars. *Sedimentology* 37, 345-355. doi: <https://doi.org/10.1111/j.1365-3091.1990.tb00963.x>
- Carling, P.A. and Glaister, M.S. 1987. Rapid deposition of sand and gravel mixtures downstream of a negative step: the role of matrix-infilling and particle-overpassing in the process of bar-front accretion. *Journal of the Geological Society*, 144, 543-551.
Doi:<https://doi.org/10.1144/gsjgs.144.4.0543>
- Cavagnetto, C. and Anadón, P. 1996. Preliminary palynological data on floristic and climatic changes during the middle Eocene–early Oligocene of the eastern Ebro Basin, northeast Spain. *Reviews in Palaeobotany and Palynology* 92, 281–305.
- Coleman, S.E. 1991. *The mechanics of alluvial stream bed forms*. Ph.D. thesis, The University of Auckland.

- Coleman, S. E., and Fenton, J. D. 2000. Potential-flow instability theory and alluvial stream bed forms. *J. Fluid Mechanics* 418, 101-117.
- Coleman, S. E., and Melville, B. W. 1994. Bed-form development. *Journal of Hydraulic Engineering*, ASCE 120, 544–560.
- Coleman, S. E., and Nikora, V. I. 2011. Fluvial dunes: Initiation, characterization, flow structure. *Earth Surface Processes and Landforms* 36(1), 39–57.
Doi:<https://doi.org/10.1002/esp.2096>
- Collinson, J.D., Mountney, N. P. and Thompson, D. B. (2006) *Sedimentary Structures*. 3rd edn, Terra Publishing, Harpenden, 292 pp
- Colombera, L., Mountney, N. P., and McCaffrey, W. D. 2012. A relational database for the digitization of fluvial architecture: concepts and example applications. *Petroleum Geoscience* 18(1), 129–140. Doi:<https://doi.org/10.1144/1354-079311-021>
- Coney, P.J., Muñoz, J.A., McClay, K.R., and Evenchick, C.A. 1996. Syntectonic burial and post-tectonic exhumation of the southern Pyrenees foreland fold-thrust belt. *J. Geol. Soc.* 153, 9–16.
- Craig, L.C., Holmes, C.N., Cadigan, R.A., Freeman, V.L., Mullens, T.E., and Weir, G.W. 1955. Stratigraphy of the Morrison and related formations Colorado Plateau Region, a preliminary report. *U.S. Geological Survey Bulletin* 1009-E, 125–168.
- Decelles, P.G. 2004. Late Jurassic to Eocene evolution of the Cordilleran thrust belt and foreland basin system, western U.S.A. *Am. J. Sci.* 304, 105–168.
- Ditchfield, R., and Best, J. 1992 Development of bed features. *Journal of Management in Engineering* 118(4), 647-650.
- Duchaufour, P., 1982. *Pedology*. Allen and Unwin, London, 448.
- Eberth, D.A., and Miall, A.D. 1991. Stratigraphy, sedimentology and evolution of a vertebrate-bearing, braided to anastomosed fluvial system, Cutler Formation (Permian-Pennsylvanian), north- central New Mexico. *Sediment Geol* 72, 225–252.

- Fedele, J. J., and Paola, C. 2007. Similarity solutions for fluvial sediment fining by selective deposition. *Journal of Geophysical Research: Earth Surface*. 112, F2. Doi:<https://doi.org/10.1029/2005JF000409>
- Fielding, C. R. 2006. Upper flow regime sheets, lenses and scour fills: Extending the range of architectural elements for fluvial sediment bodies. *Sedimentary Geology* 190(1–4), 227–240. Doi:<https://doi.org/10.1016/j.sedgeo.2006.05.009>
- Fielding, C.R., Allen, J.P., Alexander, J., and Gibling, M.R. 2009. A facies model for fluvial systems in the seasonal tropics and subtropics. *Geology* 37, 623–626.
- Fisher, J.A., 2007. *Depositional Processes and Products in Distal Dryland Fluvial Systems*. Ph.D. thesis, University of London.
- Fisher, J.A., and Nichols, G.J. 2013. Interpreting the stratigraphic architecture of fluvial systems in internally drained basins. *Journal of the Geological Society, London* 170, 57–65. Doi:<https://doi.org/10.1144/jgs.2011-134>
- Fisk, H.N. 1947. Fine-grained alluvial deposits and their effects on Mississippi River activity. *U.S. Army Corps of Engineers, Waterways Experiment Stations*, 82.
- Friend, P.F., Slater, M.J., and Williams, R.C. 1979. Vertical and lateral building of river sandstone bodies, Ebro Basin, Spain. *Geological Society of London* 136, 39–46.
- Gagliano, S.M., and Howard, P.C. 1984. The neck cut-off oxbow lake cycle along the lower Mississippi River. *Am. Soc. Civ. Eng.*, 147-158
- Gallik, J., & Bolešová, L. 2016. SUAS and their application in observing geomorphological processes. *Solid Earth* 7(4), 1033–1042. Doi:<https://doi.org/10.5194/se-7-1033-2016>
- Garcia-Castellanos, D., Vergés, J., Gaspar-Escribano, J., and Cloetingh, S. 2003. Interplay between tectonics, climate, and fluvial transport during the Cenozoic evolution of the Ebro Basin (NE Iberia): *Journal of Geophysical Research* 108, 2347. doi: <https://doi.org/10.1029/2002jb002073>.

- González-Bonorino, G., Colombo, F., and Abascal, L. 2010. Architecture of an Oligocene fluvial ribbon sandstone in the Ebro Basin, North-eastern Spain. *Sedimentology* 57(3), 845–856. Doi:<https://doi.org/10.1111/j.1365-3091.2009.01122.x>
- Gulliford, A.R., Flint, S.S., and Hodgson, D.M. 2014. Testing applicability of models of distributive fluvial systems or trunk rivers in ephemeral systems: reconstructing 3-D fluvial architecture in the Beaufort group, South Africa. *J. Sediment. Res.* 84, 1147–1169.
- Hamer, J. M. M., Sheldon, N. D., Nichols, G. J., and Collinson, M. E. 2007. Late Oligocene–Early Miocene palaeosols of distal fluvial systems, Ebro Basin, Spain. *Palaeogeography, Palaeoclimatology, Palaeoecology* 247(3–4), 220–235. Doi:<https://doi.org/10.1016/j.palaeo.2006.10.016>
- Harms, J.C., Southard, J.B., Spearing, D.R., and Walker, R.G. 1975. Depositional environments as interpreted from primary sedimentary and stratification sequences. *Society of Economic Paleontologists and Mineralogists, Short Course 2*, 161.
- Harms, J. C., Southard, J. B., and Walker, R. G., 1982, Structures and sequences in clastic rocks. *SEPM Short Course 9*, 253.
- Hartley, A.J., Weissmann, G.S., Nichols, G.J., and Warwick, G.L. 2010. Large distributive fluvial systems: characteristics, distribution and controls on development. *Journal of Sedimentary Research* 80, 167–183.
- Hein, F.J., and Walker, R.G. 1977. Bar evolution and development of stratification in the gravelly, braided, Kicking Horse River, British Columbia. *Can. J. Earth Sci.* 14, 562-570.
- Hino, M. 1968. Equilibrium–range spectra of sand waves formed by flowing water, *J. Fluid Mech.* 34(3), 565–573.
- Hirst, J.P.P. 1991. Variations in alluvial architecture across the Oligo-Miocene Huesca fluvial system, Ebro Basin, Spain. In: Miall, A.D., Tyler, N. (Eds.), *The Three-dimensional Facies Architecture of Terrigenous Clastic Sediments and Its Implications*

for Hydrocarbon Discovery and Recovery. SEPM Concepts in Sedimentology and Paleontology, 3, 111–121.

Hirst, J.P.P., and Nichols, G.J. 1986. Thrust tectonic controls on alluvial sedimentation patterns, southern Pyrenees. In Allen, P.A., and Homewood, P., (Eds), *Foreland Basins: International Association of Sedimentologists*, Special Publication 8, 247–258.

Hjellbakk, A. 1997. Facies and fluvial architecture of a high-energy braided river: The Upper Proterozoic Seglommen Member, Varanger Peninsula, northern Norway. *Sedimentary Geology* 114(1–4), 131–161. Doi:[https://doi.org/10.1016/S0037-0738\(97\)00075-4](https://doi.org/10.1016/S0037-0738(97)00075-4)

Hooke, J.M. 1986. The significance of mid-channel bars in an active meandering river. *Sedimentology* 33(6), 839–850.

Hooke, J. M. 1995. Processes of channel planform change on meandering channels in the UK. In: Gurnell, A., and Petts, G. E., (Eds.), *Changing River Channels*, Chichester: John Wiley and Sons, 87-116.

Horn, J.D., Joeckel, R.M., and Fielding, C.R. 2012. Progressive abandonment and planform changes of the central Platte River in Nebraska, central USA, over historical timeframes. *Geomorphology* 139-140, 372-383. doi: <https://doi.org/10.1016/j.geomorph.2011.11.003>

Howard, R. A. 1971. *Dynamic Probabilistic Systems*. John Wiley and Sons, 1.

Huerta, P., Armenteros, I., and Silva, P.G. 2011 Large-scale architecture in non-marine basins: the response to the interplay between accommodation space and sediment supply. *Sedimentology* 58, 1716–1736.

Jain, S. C., and Kennedy, J. F. 1974. The spectral evolution of sedimentary bed forms. *Journal of Fluid Mechanics* 63, 301–314.

Jupp, P.E., Spurr, B., Nichols, G.J., and Hirst, J.P.P. 1987, Statistical estimation of the apex of a sediment distribution system from palaeocurrent data. *Mathematical Geology* 19, 319–333.

- Kelly, S.B., and Olsen, H. 1993. Terminal fans—a review with reference to Devonian examples. *Sedimentary Geology* 85, 339–374.
- Knighton, A.D. 1972. Changes in a braided reach. *Bulletin of the Geological Society of America* 83(12), 3813–3822.
- Kraus, M.J., 1999, Palaeosols in clastic sedimentary rocks: their geologic applications. *Earth Science Reviews* 47, 41-70.
- Kreylos, O., Oskin, M., Cowgill, E., Gold, P., Elliott, A., and Kellogg, L.H. 2013. Point-based computing on scanned terrain with LidarViewer. *Geosphere* 9(3), 546–556. Doi:<https://doi.org/10.1130/GES00705.1>.
- Kukulski, R.B., Hubbard, S.M., Moslow, T.F., and Keegan Raines, M. 2013. Basin-scale stratigraphic architecture of upstream fluvial deposits: Jurassic–Cretaceous Foredeep, Alberta Basin, Canada: *Journal of Sedimentary Research* 83, 704–722.
- Leeder, M. 2011. (Eds) *Sedimentology and Sedimentary Basins. From Turbulence to Tectonics*. 16, 592. Oxford, Blackwell Science.
- Lowe, D.R. 1982. Sediment gravity flows: II. Depositional models with special reference to deposits of high-density turbidity currents. *J. Sediment. Petrol.* 52, 279–297.
- Luchi, R., Hooke, J. M., Zolezzi, G., and Bertoldi, W. 2010. Width variations and mid-channel bar inception in meanders: River Bollin (UK). *Geomorphology* 119(1–2), 1–8. Doi:<https://doi.org/10.1016/j.geomorph.2010.01.010>
- Lunt, I. A., Bridge, J.S., and Tye, R.S. 2004. A quantitative, three-dimensional depositional model of gravelly braided rivers. *Sedimentology* 51, 377–414
- MacDonald, A. M., Bonsor, H.C., Ahmed, K.M., Burgess, W.G., Basharat, M., Calow, R. C., Foster, S. S. D., Gopal, K., Lapworth, D. J., Lark, R. M., Moench, M., Mukherjee, A., Rao, M. S., Shamsudduha, M., Smith, L., Taylor, R. G., Tucker, J., van Steenbergen, F., and Yadav, S. K. 2016. Groundwater quality and depletion in the

- Indo-Gangetic Basin mapped from in situ observations. *Nature Geoscience*, 9, 762. Nature Publishing Group. Doi:<https://doi.org/10.1038/ngeo2791>.
- Mackay, S. D., and Bridge, J. S. 1995. Three-dimensional model of alluvial stratigraphy: theory and application. *Journal of Sedimentary Research* B65, 7–31.
- Madjid, M. Y. A., Vandeginste, Hampson, G., and Booth, A.D. 2018. Drones in carbonate geology: Opportunities and challenges, and application in diagenetic dolomite geobody mapping. *Marine and Petroleum Geology* 91, 723–734. Doi:<https://doi.org/10.1016/j.marpetgeo.2018.02.002>.
- Martin, C.A.L. 1995. *The Origins of Massive Sandstones in Braided River Systems*. Unpublished PhD Thesis, University of Durham, UK.
- Martin, C. A. L., and Turner, B. R. 1998. Origins of massive-type sandstones in braided river systems. *Earth Science Reviews*, 44(1–2), 15–38. Doi:[https://doi.org/10.1016/S0012-8252\(98\)00019-1](https://doi.org/10.1016/S0012-8252(98)00019-1).
- McBride, E.F., Shepherd, R.G., and Grawley, R.A., 1975. Origin of parallel, near-horizontal laminae by migration of bedforms in a small flume. *J. Sed. Petrol.* 45, 132–139.
- McLean S.R. 1990. The stability of ripples and dunes. *Earth-Science Review* 29, 131–144.
- Miall, A.D. 1985. Architectural-element analysis: a new method of facies analysis applied to fluvial deposits. *Earth Science Reviews* 22, 261–308.
- Miall, A.D. 1996. *The Geology of Fluvial Deposits*. Springer-Verlag, New York.
- Miall, A. D. 2013. *The Geology of Stratigraphic Sequences*. Springer Berlin Heidelberg.
- Miall, A. D. 2014. *The Facies and Architecture of Fluvial Systems*. Doi:https://doi.org/10.1007/978-3-319-00666-6_2.

Middleton, G. V, Southard, J. B. and Section, S. of E. P. and M. E. 1978. *Mechanics of Sediment Movement*. Society of Economic Paleontologists and Mineralogists (SEPM short course).

Moscariello, A. 2005. Exploration potential of the mature Southern North Sea basin margins: some unconventional plays based on alluvial and fluvial fan sedimentation models. In: Doré, A.G., and Vinnin, B.A., (Eds.) *Petroleum Geology, North-West Europe and Global Perspectives*, Geological Society of London, 6th Petroleum Geology Conference, Proceedings, 595–605.

Mukherjee, A., Saha, D., Harvey, C. F., Taylor, R. G., Ahmed, K. M., and Bhanja, S. N. 2015. Journal of Hydrology : Regional Studies Groundwater systems of the Indian. *Journal of Hydrology: Regional Studies*. Elsevier B 4, 1–14.

Doi:<https://doi.org/10.1016/j.ejrh.2015.03.005>.

Mullens, T.E., and Freeman, V.L. 1957. Lithofacies of the Salt Wash Member of the Morrison Formation, Colorado Plateau. *Geological Society of America, Bulletin* 68, 505–526.

Nakagawa, H., and Tsujimoto, T. 1984. Spectral analysis of sand bed instability. *Journal of Hydraulic Engineering ASCE* 110, 467–483.

Nichols, G.J. 1987. Structural controls on fluvial distributary systems—the Luna System, Northern Spain. In: Ethridge, F.G., Flores, R.M., and Harvey, M.D. (Eds.) *Recent Developments in Fluvial Sedimentology*, SEPM, Special Publication 39, 269–277.

Nichols, G.J. 2004. Sedimentation and base level in an endorheic basin: the early Miocene of the Ebro Basin, Spain. *Bol. Geol. Min.* 115, 427–438.

Nichols, G.J. 2005. Tertiary alluvial fans at the northern margin of the Ebro Basin. In: Harvey, A.M., Mather, A.E., and Stokes, M. (Eds) *Alluvial Fans: Geomorphology, Sedimentology, Dynamics*, Geological Society, London, Special Publications, 251, 187–206. Doi:<https://doi.org/10.1144/GSL.SP.2005.251.01.13>

Nichols, G. 2017. High-resolution estimates of rates of depositional processes from an alluvial fan succession in the Miocene of the Ebro Basin, northern Spain. *Geological Society of London, Special Publications* 440, 15. Doi:<https://doi.org/10.1144/SP440.12>.

Nichols, G.J., and Fisher, J.A. 2007. Processes, facies and architecture of fluvial distributary system deposits. *Sedimentary Geology* 195, 75–90.

Nichols, G.J., and Hirst, J.P. 1998. Alluvial fans and fluvial distributary systems, Oligo-Miocene, northern Spain: contrasting processes and products. *J. Sed. Res.* 68, 879– 889.

Nikora, V.I., Sukhodolov, A.N., and Rowinski, P.M. 1997. Statistical sand wave dynamics in one-directional waterflows. *J. Fluid Mech* 351, 17–39.

Owen and Nichols (2018) Email to Amanda Owen, 17 October.

Owen, A., Nichols, G.J., Hartley, A.J., Weissmann, G.S., and Scuderi, L.A. 2015. Quantification of a distributive fluvial system: The Salt Wash DFS of the Morrison Formation, SW USA. *Journal of Sedimentary Research* 85, 544–561.

Owen, A., Ebinghaus, A., Hartley, A.J., Santos, M.G.M., and Weissmann, G.S. 2017a. Multi-scale classification of fluvial architecture: An example from the Palaeocene–Eocene Bighorn Basin, Wyoming. *Sedimentology* 64(6), 1572–1596. Doi:<https://doi.org/10.1111/sed.12364>.

Owen, A., Nichols, G.J., Hartley, A.J., and Weissmann, G.S. 2017b. Vertical trends within the prograding Salt Wash distributive fluvial system, SW United States. *Basin Research* 29(1), 64–80. Doi:<https://doi.org/10.1111/bre.12165>.

Peterson, F. 1977. Uranium deposits related to depositional environments in the Morrison Formation (Upper Jurassic), Henry Mountains mineral belt of southern Utah. *U.S. Geological Survey, Uranium-Thorium Symposium, Short Papers, Circular 753*, 45–47.

Picard, M.D., and High, L.R. 1973. *Sedimentary Structures of Ephemeral Streams. Developments in Sedimentology* 17, 223. Elsevier, Amsterdam.

- Pranter, M.J., and Sommer, N.K. 2011. Static connectivity of fluvial sandstones in a lower coastal-plain setting: an example from the Upper Cretaceous lower Williams Fork Formation, Piceance Basin, Colorado. *AAPG Bull.* 95, 899–923.
- Pudefàbregas, C., Muñoz, J.A., and Vergès, J. 1992. Thrusting and foreland basin evolution in the Southern Pyrenees. In: McClay, K.R. (Eds), *Thrust Tectonics*. Chapman and Hall, London, 247–254.
- Raudkivi, A.J., and Witte, H. H. 1990. Development of bed features. *J. Hydraul. Eng.* 116, 1063–1079.
- Retallack, G.J. 2001 *Soils of the Past. An Introduction to Paleopedology*. 520. Blackwell Science, Oxford, UK.
- Reynolds, A.D. 1989. The emergence of a thrust front across a major fluvial system: the Collegats Formation of the South Pyrenean foreland basin. In: *Programme and Abstracts, 4th International Conference on Fluvial Sedimentology*, Barcelona, October 2 – 4th, 1989, Servei Geologic de Catalunya, 207.
- Riba, O., Reguant, S., and Villena, J., 1983. Ensayo de síntesis estratigráfica y evolutiva de la cuenca terciaria del Ebro. In: Comba, J.A. (Eds.), *Geología de España*, Libro Jubilar J.M. Ríos. Instituto Geológico y Minero de España, Madrid, 131–159.
- Shukla, U.K., Singh, I.B., Sharma, M., and Sharma, S. 2001. A model of alluvial megafan sedimentation: Ganga Megafan. *Sedimentary Geology* 144, 243–262.
- Smith, N.D. 1971. Transverse bars and braiding in the lower Platte River, Nebraska. *Geol. Soc. Am. Bull.* 82, 3407– 3420.
- Southard, J. B., and Boguchwal, L. A. 1990. Bed configurations in steady unidirectional water flows. Part 2. Synthesis of flume data. *Journal of Sedimentary Petrology* 60(5), 658–679.
- Stanistreet, I.G., and McCarthy, T.S., 1993. The Okavango Fan and the classification of subaerial fan systems. *Sedimentary Geology* 85, 115–133.

- Straub, K.M., Paola, C., Mohrid, D., Wolinsky, M.A. and George, T. 2009. Compensational stacking of channelized sedimentary deposits. *J. Sed. Res.* 79, 673–688.
- Swan, A., Hartley, A.J., Owen, A., and Howell, J. 2018. Reconstruction of a sandy point-bar deposit: implications for fluvial facies analysis. *Int. Assoc. Sedimentol. Spec. Publ.* 48, 445-474.
- Toonen, W. H. J., Kleinhans, M. G. and Cohen, K. M. 2012. Sedimentary architecture of abandoned channel fills. *Earth Surface Processes and Landforms* 37(4), 459–472. Doi:<https://doi.org/10.1002/esp.3189>.
- Tsujimoto, T. 1998. Development of sand island with vegetation in fluvial fan river under degradation. In: Abt, S.R., Young-Pezeshk, J., Watson, C.C. (Eds.), *Proc. Water Resource Engineering* 98, 574-579.
- Turner-Peterson, C.E. 1986. Fluvial sedimentology of a major Uranium-bearing sandstone: a study of the Westwater Canyon Member of the Morrison Formation, San Juan Basin, New Mexico. In: Turner-Peterson, C.E., Santos, E.S., and Fishman, N.S., (Eds), *A Basin Analysis Case Study: The Morrison Formation, Grants Uranium Region, New Mexico*. American Association of Petroleum Geologists, Studies in Geology, 22, 47–76.
- Turner, C.E., and Peterson, F. 2004. Reconstruction of the Upper Jurassic Morrison Formation extinct ecosystem: a synthesis. *Sedimentary Geology* 167, 309–355.
- Van der Voo, R. 1993. *Paleomagnetism of the Atlantic, Tethys and Iapetus Oceans*. Cambridge University Press, 411.
- Walker, R.G. (Eds). 1984. *Facies Models*. Geoscience Canada Reprint Ser. 1.
- Wang, J, Plink-Björklund, P. 2019. Stratigraphic complexity in fluvial fans: Lower Eocene Green River Formation, Uinta Basin, USA. *Basin Res.* 00, 1– 28. <https://doi.org/10.1111/bre.12350>

Watts, A.C., Ambrosia, V.G. and Hinkley, E.A. 2012. Unmanned aircraft systems in remote sensing and scientific research: classification and considerations of use. *Rem. Sens.* 4, 1671–1692.

Weissmann, G. and Fogg, G. 1999. Multiscale alluvial fan heterogeneity modelled with transition probability geostatistics in sequence stratigraphic framework. *Journal of Hydrology* 226, 48-65. doi: [https://doi.org/10.1016/S0022-1694\(99\)00160-2](https://doi.org/10.1016/S0022-1694(99)00160-2).

Weissmann, G.S., Mount, J.F. and Fogg, G.E. 2002. Glacially driven cycles in accumulation space and sequence stratigraphy of a stream-dominated alluvial fan, San Joaquin Valley, California, USA. *Journal of Sedimentary Research* 72, 240–251.

Weissmann, G., Zhang, Y., Fogg, G., and Mount, J.F. 2004. Influence of incised valley fill deposits on hydrogeology of a glacially-influenced, stream-dominated alluvial fan. In: Bridge, J.S., and Hyndman, D.W. (Eds), *Aquifer Characterization*, SEPM Society for Sedimentary Geology. doi: <https://doi.org/10.2110/pec.04.80.0015>.

Weissmann, G.S., Hartley, A.J., Nichols, G.J., Scuderi, L.A., Olson, M., Buehler, H., and Banteah, R. 2010. Fluvial form in modern continental sedimentary basins: Distributive fluvial systems. *Geology* 38, 39–42.

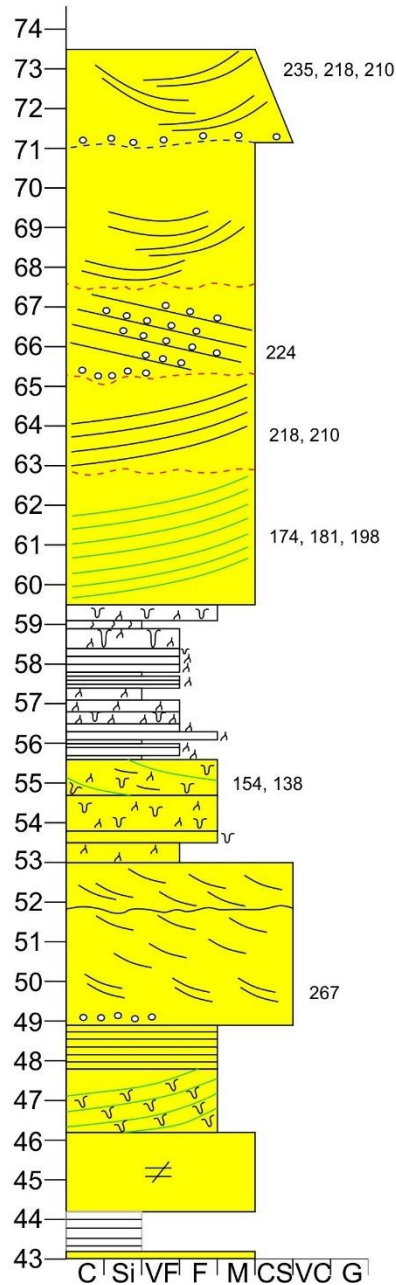
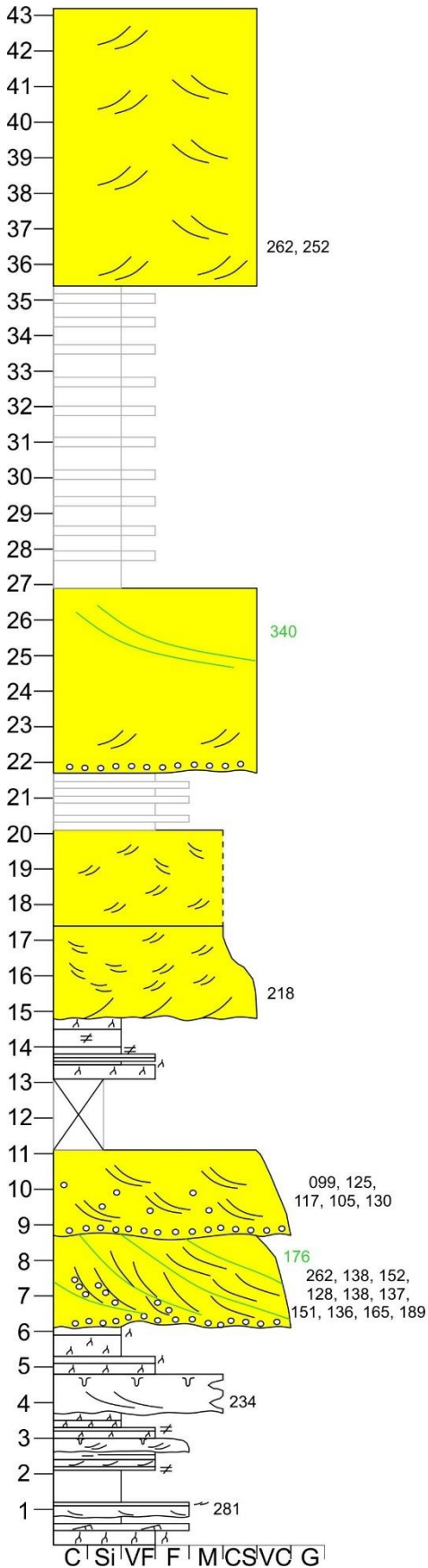
Weissman, G.S., Hartley, A.J., Nichols, G.J., Scuderi, L.A., Olson, M.E., Buehler, H.A., and Massengill, L.C. 2011 Alluvial facies distributions in continental sedimentary basins—distributive fluvial systems. In: Davidson, S.K., Leleu, S., and North, C.P. (Eds) *From river to rock record* 97. Society for Sedimentary Geology (SEPM), Special Publication, 327–355.

Weissmann, G. S. *et al.* 2013. Prograding distributive fluvial systems - geomorphic models and ancient examples. In: Dreise, S. G., Nordt, L. C., and McCarthy, P. L. (Eds) *New Frontiers in Paleopedology and Terrestrial paleoclimatology*. SEPM Special Number 104, 131–147. doi: <https://doi.org/10.2110/sepmsp.104.16>.

Wintenberger, C. L., Rodrigues, S., Claude, N., Jugé, P., Bréhéret. And Villar, M. 2015. Dynamics of nonmigrating mid-channel bar and superimposed dunes in a sandy-gravelly river (Loire River, France). *Geomorphology* 248, 185–204. Elsevier B.V., doi:<https://doi.org/10.1016/j.geomorph.2015.07.032>.

Yagishita, K., Ashi, J., Ninomiya, S., Taira, A. 2004. Two types of plane beds under upper-flow-regime in flume experiments: Evidence from grain fabric. *Sedimentary Geology* 163. 229-236. Doi: [https://doi.org/10.1016/S0037-0738\(03\)00196-9](https://doi.org/10.1016/S0037-0738(03)00196-9).

Accompanying Material

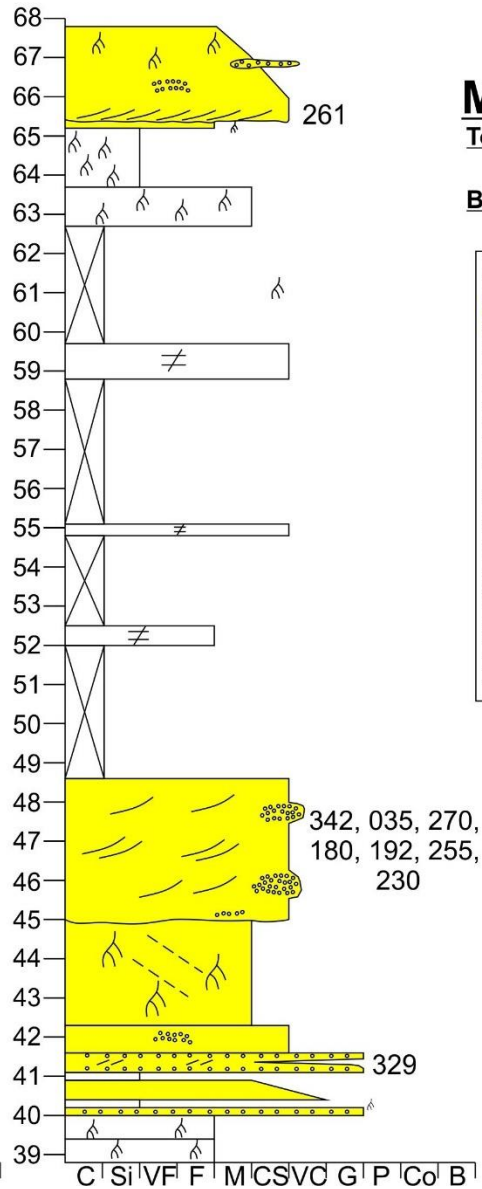
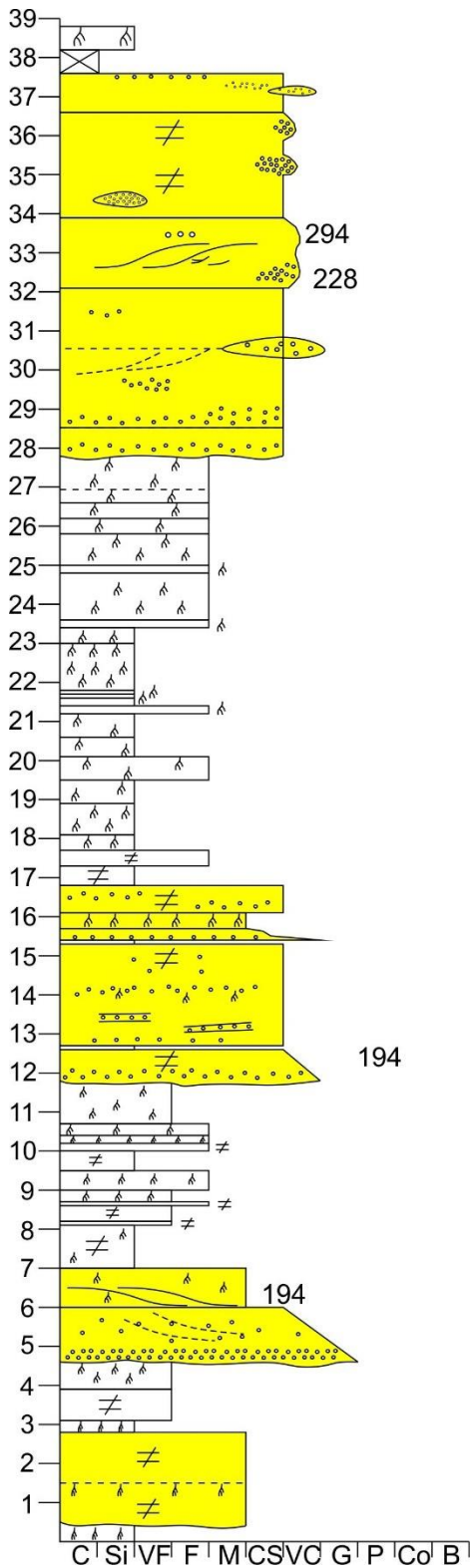


Pertusa Log

**Top GR: N:42.00144,
E:-000.13178**

**Base GR: N:42.00169,
E:-000.13077**

Key	
Channel Features	
	Channel Body
	Bar Bounding Surface
	Storey Surface
Sedimentary Structures	
	Lateral Accretion Surface
	Cross-bedding
	Inferred Cross-bedding
	High Angle Cross-Bedding
	Ripple lamination
	Wavy lamination
	Structureless
	Inferred
	Granular Lag
Secondary Structures	
	Vertical burrows
	Pedogenic alteration

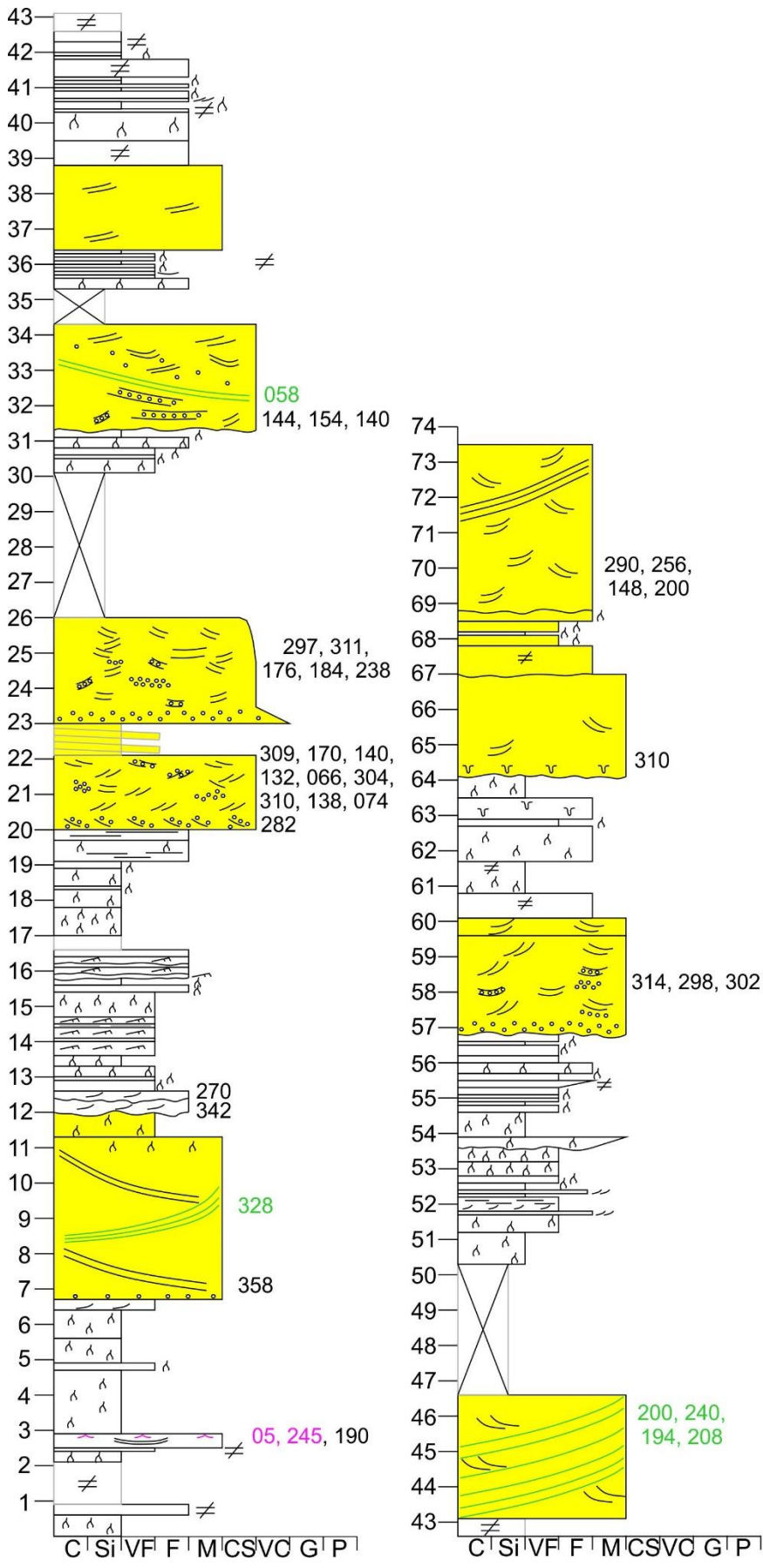


Monzon Log

Top GR: N:41.90445,
E:000.19210

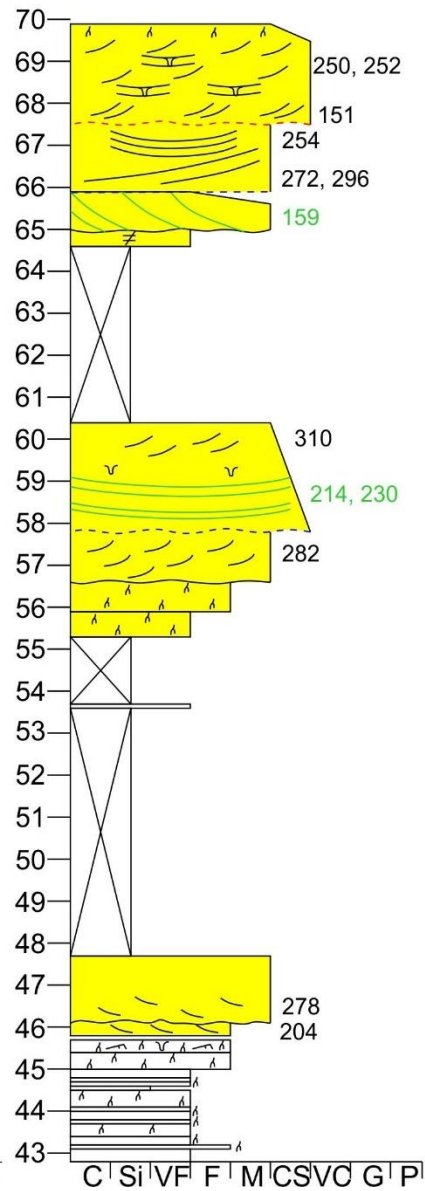
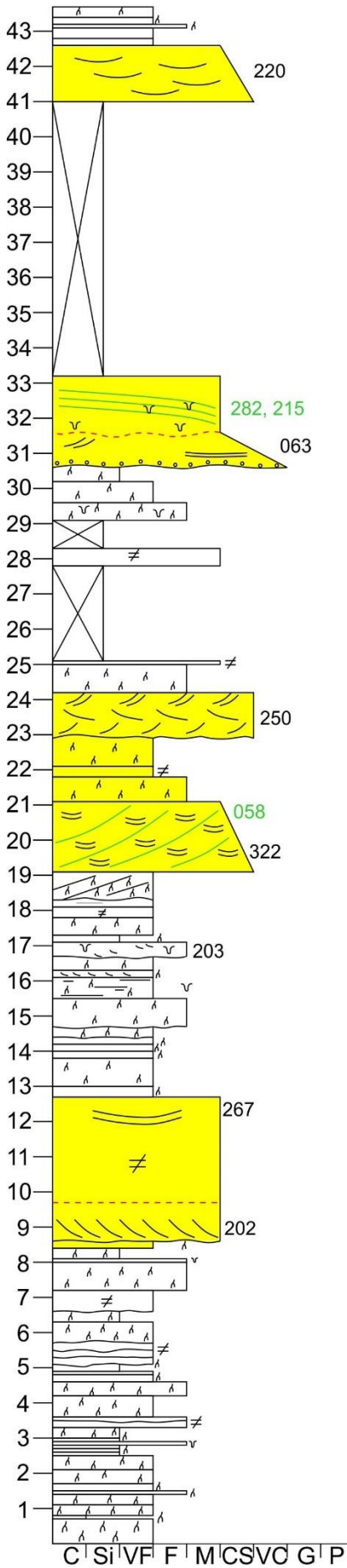
Base GR: N:41.90398,
E:000.19146

Key	
Channel Features	
	Channel Body
	Bar Bounding Surface
Sedimentary Structures	
	Lateral Accretion Surface
	Cross-bedding
	Inferred Cross-bedding
	Inferred High Angle Cross Bedding
	Ripple lamination
	Wavy lamination
	Structureless
	Inferred
	Granular Lag
Secondary Structures	
	Vertical burrows
	Pedogenic alteration



Piraces Log
 Top GR: N:42.01495,
 E:-000.31709
 Base GR: N:42.01284,
 E:-000.31614

Key	
Channel Features	
	Channel Body
	Bar Bounding Surface
	Storey Surface
Sedimentary Structures	
	Lateral Accretion Surface
	Cross-bedding
	Inferred Cross-bedding
	High Angle Cross-Bedding
	Ripple lamination
	Bi-directional Ripple lamination
	Wavy lamination
	Structureless
	Inferred
	Granular Lag
Secondary Structures	
	Vertical burrows
	Pedogenic alteration



Torrillon Log

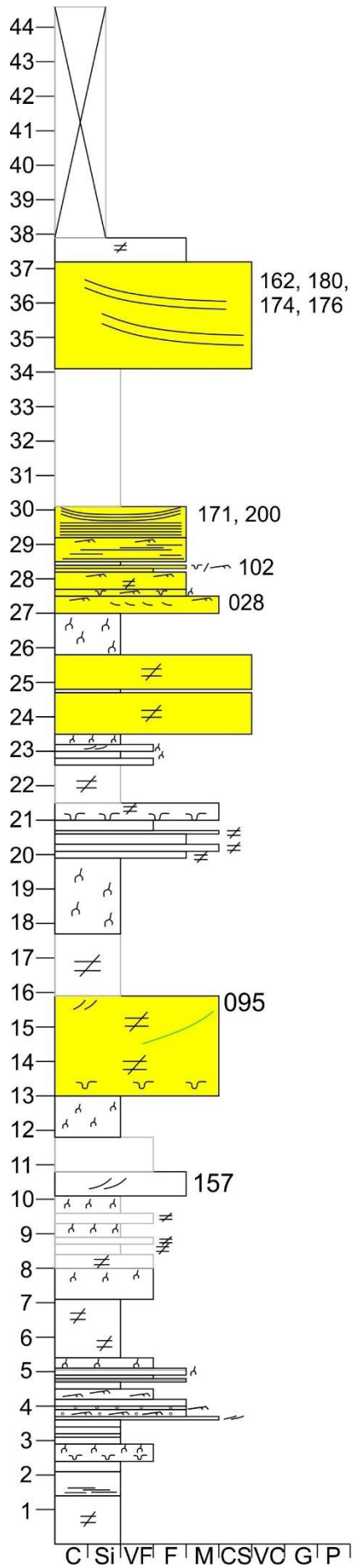
Top GR: N:41.92776,
E:-000.25668

Base GR: N:41.9268,
E:-000.25821

Key	
Channel Features	
	Channel Body
	Bar Bounding Surface
	Storey Surface
Sedimentary Structures	
	Lateral Accretion Surface
	Cross-bedding
	Inferred Cross-bedding
	High Angle Cross-Bedding
	Ripple lamination
	Bi-directional Ripple lamination
	Wavy lamination
	Structureless
	Inferred
	Granular Lag
Secondary Structures	
	Vertical burrows
	Pedogenic alteration

Castleflorite Log

Top GR: N:41.81384,
E:-000.01442
Base GR: N:41.81367,
E:-000.1285



Key

Channel Features

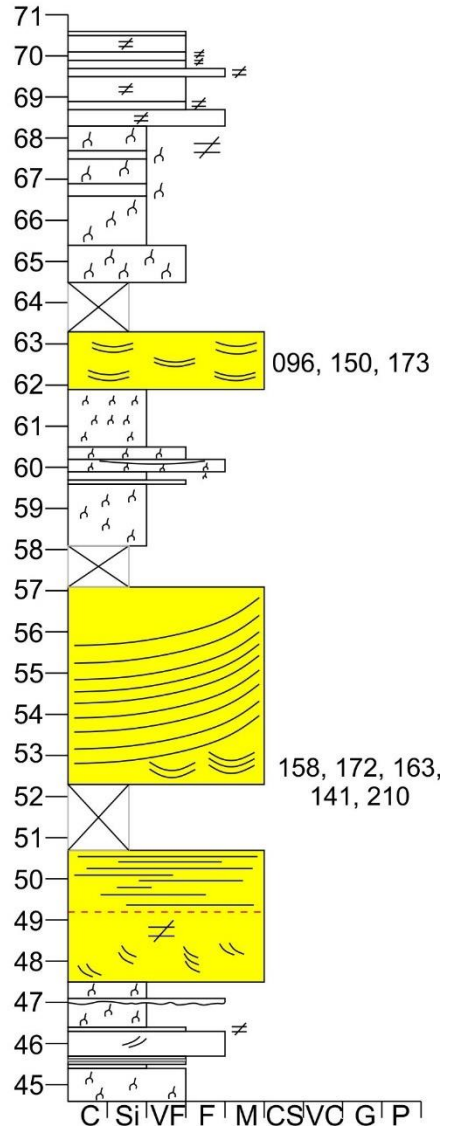
- Channel Body
- Bar Bounding Surface
- Storey Surface

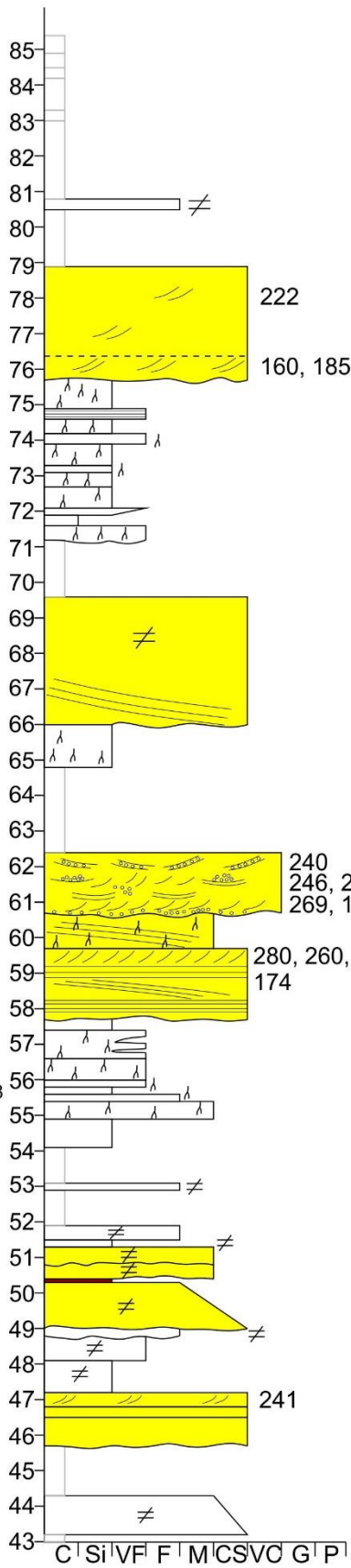
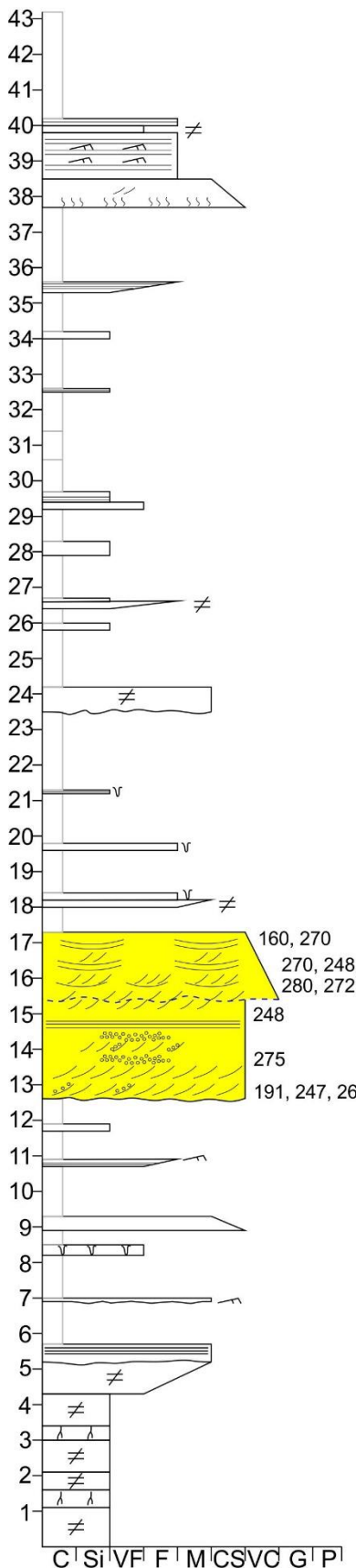
Sedimentary Structures

- Lateral Accretion Surface
- Cross-bedding
- Inferred Cross-bedding
- High Angle Cross-Bedding
- Ripple lamination
- Bi-directional
- Ripple lamination
- Wavy lamination
- Structureless
- Inferred
- Granular Lag

Secondary Structures

- Vertical burrows
- Pedogenic alteration



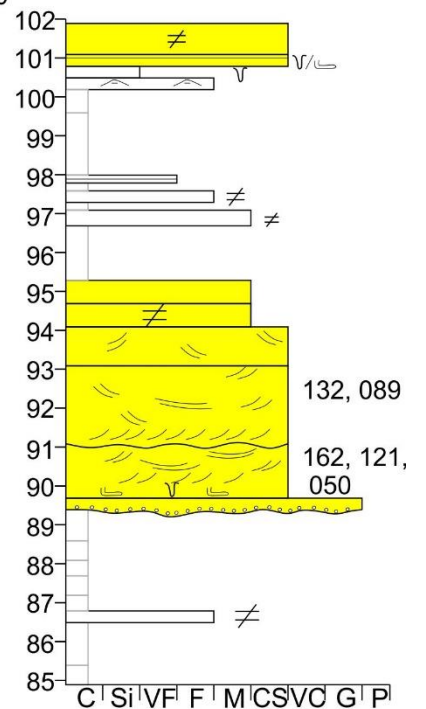


Monte Aragon Log

Top GR: N:42.15988,
E:-000.36035

Base GR: N:42.15775,
E:-000.36139

Key	
Channel Features	
	Channel Body
	Bar Bounding Surface
	Storey Surface
Sedimentary Structures	
	Lateral Accretion Surface
	Cross-bedding
	Inferred Cross-bedding
	High Angle Cross-Bedding
	Ripple lamination
	Wavy lamination
	Structureless
	Inferred
	Granular Lag
Secondary Structures	
	Vertical burrows
	Pedogenic alteration



Bolea Log

Top GR: N:42.25753,

E:-000.25668

Base GR: N:42.25665,

E:-000.15553

Key

- Channel Body
- Sedimentary Structures**
- Cross-bedding
- Ripple lamination
- Wavy lamination
- Structureless
- Inferred
- Secondary Structures**
- Vertical burrows
- Pedogenic alteration

